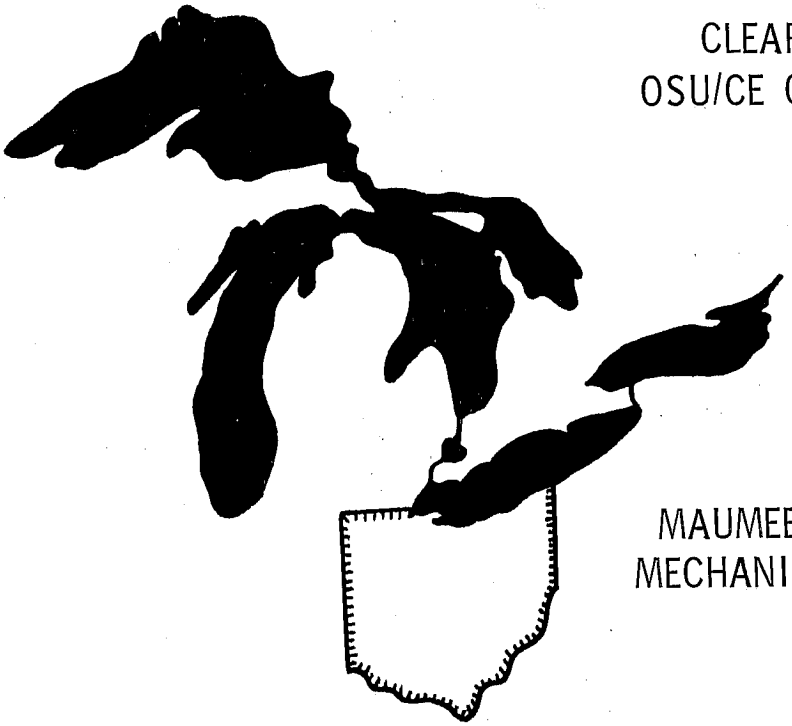

CLEAR TECHNICAL REPORT NO. 95
OSU/CE COASTAL ENGINEERING REPORT
SERIES NO. 1-78-1

MAUMEE BAY SEDIMENT TRANSPORT MECHANISMS DURING SPRING RUNOFF

by

Keith W. Bedford
and
Bipin C. Shah

Prepared for

U.S. Environmental Protection Agency
and
International Joint Commission
Pollution from Land Use Activities Reference Group, Task D
Grant No. R-804612

THE OHIO STATE UNIVERSITY
CENTER FOR LAKE ERIE AREA RESEARCH
COLUMBUS, OHIO

May 1978

ACKNOWLEDGMENTS

The work presented herein, in substantial part, was completed as partial fulfillment of the requirements for the Master of Science degree in Civil Engineering by Bipin C. Shah. His extensive work is gratefully appreciated. Substantial help was provided by Dr. John Paul of the EPA Grosse Ile laboratories, not only for introducing us to his model, but also for displaying patience for those frequent times when the authors failed to comprehend simple ideas. Thanks also to Dr. J. Zapotosky of CLEAR and the NASA staff for insight on the field data collected during the springs of 1975 and 1976. Finally, a special thanks to Dr. C.E. "Ed" Herdendorf of the Center for Lake Erie Area Research, for his mental and financial support of this brief project.

TABLE OF CONTENTS

Page

LIST OF FIGURES

LIST OF TABLES

NOMENCLATURE

A	linear differential operator;
A_H	horizontal eddy viscosity (L^2/T);
A_{ij}	eddy coefficients (L^2/T);
A_v	vertical eddy viscosity (L^2/T);
α	SGS eddy coefficients scaling parameter
B_H	horizontal eddy diffusivity (L^2/T)
B_v	vertical eddy diffusivity (L^2/T)
C	concentration (M/L^3)
c	Deardorff eddy coefficient scaling parameter;
C_f	reference concentration (M/L^3)
e_{ij}	Schumann SGS eddy coefficients (L^2/T)
e_s	eddy viscosity at surface (L^2/T)
e_b	eddy viscosity at bottom (L^2/T)
f	Coriolis parameter $(1/T)$
F_r	Froude number;
f1,f2	outer boundary conditions for u and v;
g	gravitational acceleration (L/T^2)
g1,g2	river outflow boundary condition for u and v;
h	bottom depth (L);
h_o	reference depth (L);
ℓ	time index;
n,m,k	space grid indices;
P	pressure (M/T^2L^2);
Ps	surface pressure (M/T^2L^2);

P_r	turbulent Prandtl number;
Re	Reynolds number;
Ro	Rossby number;
t	time (T);
u,v,w	velocity in x, y, and z directions (L/T);
u_o	reference velocity (L/T);
w_s	sinking velocity (L/T);
ρ	density (M/L^3);
σ	stretched vertical co-ordinate;
Ω	velocity in σ direction (1/T);
Ω_s	sinking velocity in σ direction (1/T);
τ_x, τ_y	surface wind stress in x and y directions (M/T^2L^2);
τ_{Bx}, τ_{By}	bottom stress in x and y directions (M/T^2L^2);
ω	relaxation parameter;
ω_{opt}	optimum ω;
$\Delta X, \Delta Y, \Delta Z, \Delta\sigma$	space increments (L);
ΔT	time increment (T)

CHAPTER ONE

INTRODUCTION AND STUDY OBJECTIVES

Under provisions of the Boundary Waters Treaty of 1909 the Governments of Canada and the United States in October 1964 requested the International Joint Commission (IJC) to examine the pollution problems of the Great Lakes resulting from the greater volumes of wastes discharges by industrial complexes and accompanying population growth. In 1970, the Commission recommended a long-term program of research to acquire scientific knowledge and understanding of the physical, chemical and biological behavior of the Great Lakes, particularly with respect to pollutants and their dispersal. As a partial result of this international effort, the IJC Pollution from Land Use Activities Reference Group (PLUARG) was established and a series of study tasks conceived.

One objective of study tasks B, C, and D was an intensive effort to determine the extent of lake degradation due to excessive spring time sediment runoff. These sediments, laden with heavy metals and toxic substances, are transferred into the lake by direct river or point source transport and by shoreline or nonpoint source activity. Because of their importance to each of the Great Lakes, five river basins were identified as pilot study areas and intensive field sampling and analyses were performed.

Maumee Bay, in the Western Basin of Lake Erie, was singled out for very intensive research on the spring sediment transport problem. The Bay and Basin are both very shallow, easily set into motion by meteorological events, and drain a heavily farmed region of the Great Lakes. Study groups for point source, nonpoint source, and Bay and Basin wide data collection were formed, and during the spring of 1976 were able to adequately monitor the runoff event. Bay and Basin data were collected on site by the Center for Lake Erie Area Research (CLEAR) with its HYDRA research vessel. These data were correlated with NASA-Lewis aerial photographs and imagery.

Two modeling efforts were conceived as a means of rationalizing the observed data. The primary effort by Drs. R. Gedney, P. Sheng, and W. Lick is a computer model of the entire Western Basin. The second study is the subject of this report and the objective is to, by mathematical modeling, determine, in Maumee Bay, the possible effect on plume paths of different transport mechanisms occuring during the spring runoff event.

Because the Bay is highly irregular and, in places, quite shallow the circulation is at times quite time variable and therefore a time varying three-dimensional code developed by Paul and Lick (1975) was modified and adapted to the problem. Attention is restricted to the physical transport of sediment and no attempt was made to include the effects of coagulation or biochemical alteration. Some effort is made to parameterize the turbulent transport as a function of grid sizes. This problem becomes acute as variable mesh spacings, required in this basin, will not allow adequate turbulent representation

by constant eddy viscosities.

This report is organized as follows: Chapter Two contains a site description and includes topography, climate, and design data on runoff and sediment; the space averaged mass balance and Navier Stokes equations are presented in Chapter Three along with the subgrid scale turbulence model the numberical formulation is presented in Chapter Four; design data and model inputs are explained in Chapter Five; Chapter Six delineates rudimentary Bay transport physics. The last Chapter is devoted to a discussion of the results, conclusions, and future study recommendations.

CHAPTER TWO

SITE DESCRIPTION

A. Bay Characteristics

Under a Level B planning study, Pinsak and Meyer (1976) have carried out an intensive study of Maumee Bay. Figure 1 which is taken from their work shows the area under consideration.

Maumee Bay is located in the southwestern corner of Lake Erie. As seen in the figure, Maumee Bay is separated from Lake Erie by a line joining the North Cape of the Woodtick Peninsula and Cedar Point. The surface area of Maumee Bay is 21 square miles and represents only 3% of the surface area of Lake Erie's Western Basin. Maumee River contributes the largest discharge to the Bay. Ottawa River and six creeks drain into the west end of the Bay but the southern portion is devoid of any tributaries. The western shore is highly irregular with many tiny islands but the southern shore is almost a smooth arc resembling a crenulate shaped shoreline. The geometry of the area is further complicated by the channel and the two disposal sites. The narrow long spit A (Figure 1) at the mouth of the Maumee River blocks most of the northern flow.

Herdendorf and Cooper (1975) have reported on Maumee Bay bathymetry (Figure 2). Except for the navigation channel and its surroundings the Bay is very shallow and the mean depth is 5 ft below Great Lakes

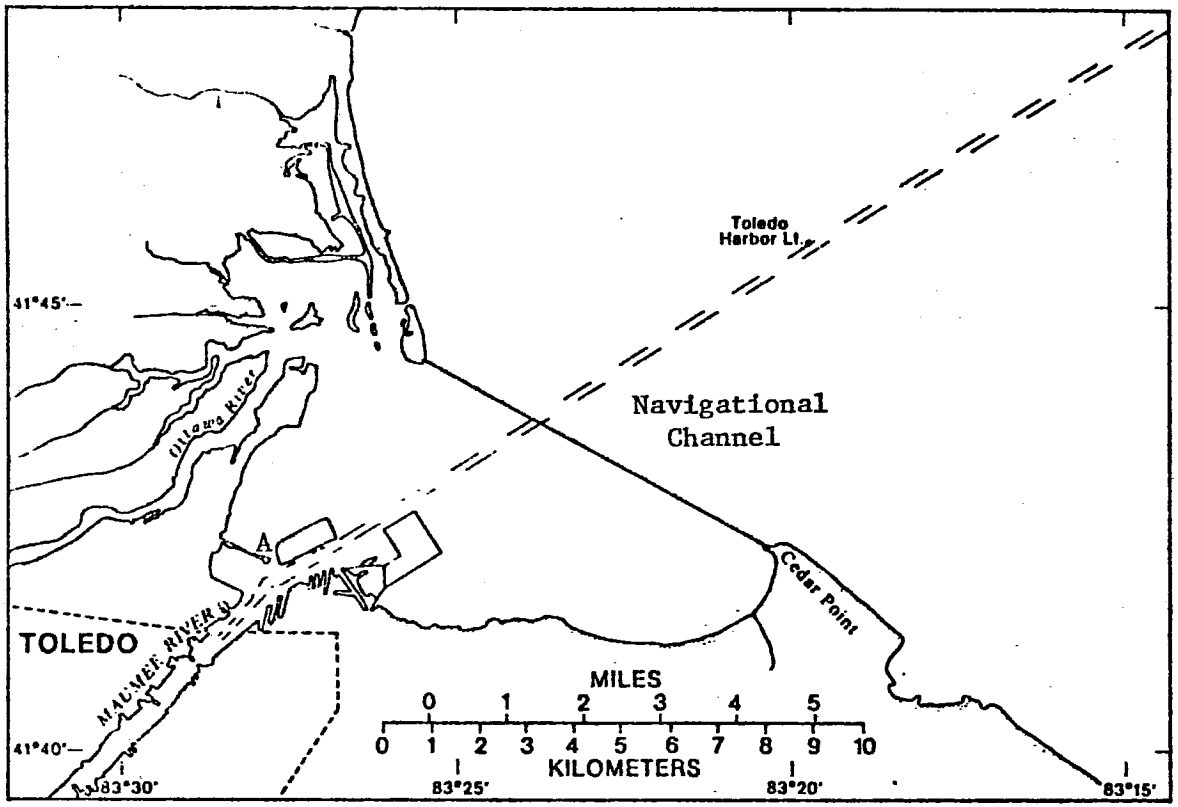

Figure 1. Maumee Bay (Pinsak and Meyer 1976).

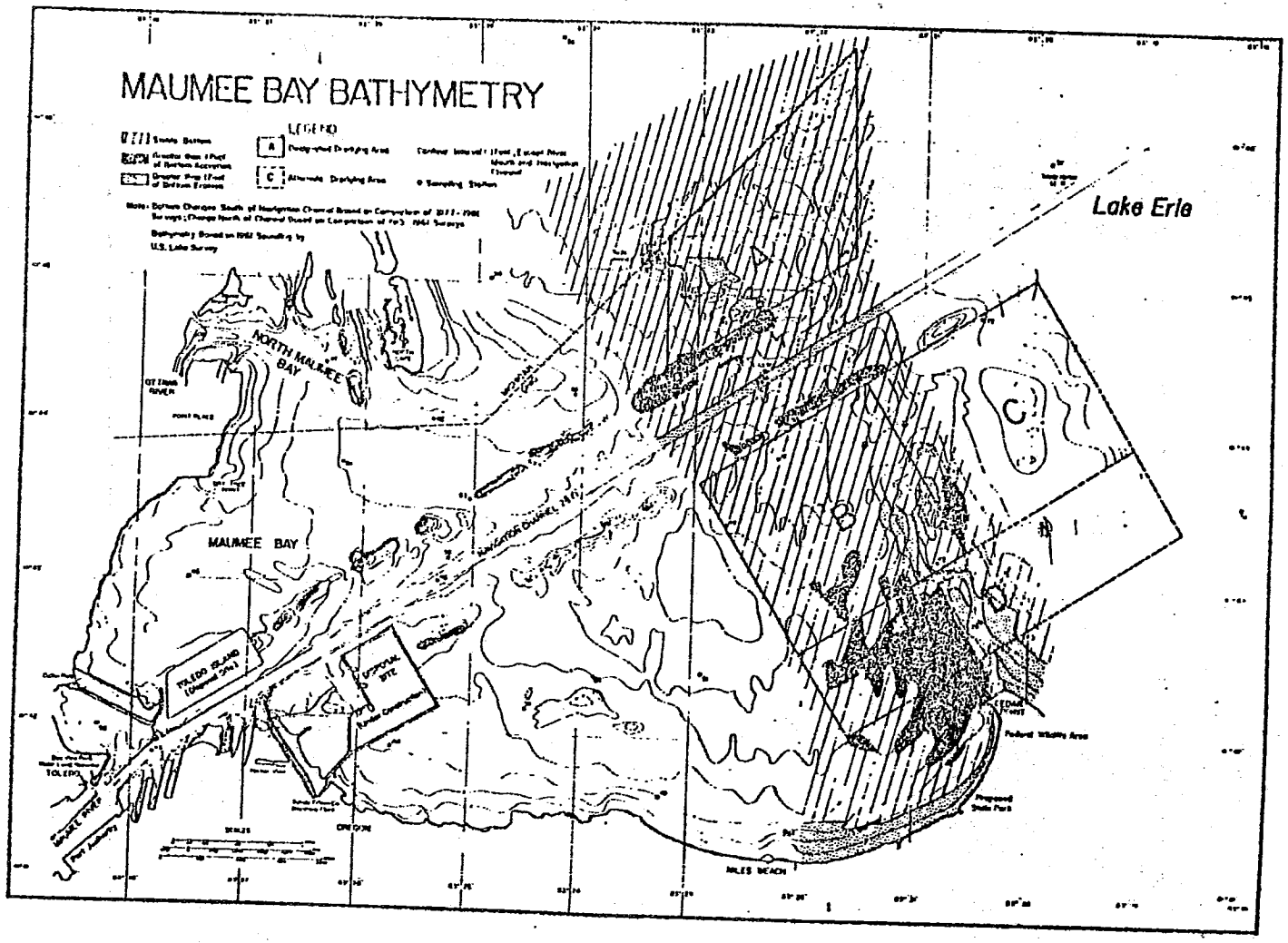

Figure 2. Maumee Bay Bathymetry (Herdendorf and Cooper 1975).

Low Water Datum (IGLD). The navigation channel divides the bay into approximately two equal parts (by area) and is 500 feet wide and 28 feet deep in the bay. About 2000 feet from either side of the channel shoals were formed by side dumping from channel dredging.

B. River Characteristics

Maumee River, 131 miles long has headwaters at Fort Wayne, Indiana where the St. Marys and St. Joseph rivers meet. The river drains about 6,750 sq miles, of which 92% is agricultural. Daily average discharge ranges from a high of 94,000 cfs to a low of 32 cfs (Pinsak and Meyer, 1975). Since the present study is restricted to short-term extreme flows, one-day extreme discharges versus their probability of occurrence were computed and plotted (Figure 3). It can be seen from the figure that average monthly flows temper these extremes.

At the mouth the direction of Maumee River flow depends upon wind stresses, seiche activity and river discharge. Reversals of flow due to fluctuations of water levels in the Bay have been measured and Figure 4, taken from Pinsak and Meyer (1975), shows the effect of river discharge on the flow direction. Below 200 m^3/s discharge, the current maintains its reversing characteristics. Above this discharge, the current does not reverse unless there is a rapid rise in the Bay water level. As pointed out by Pinsak and Meyer (1975) a 98% persistence in lakeward flow is maintained when the river discharge is above 800 m^3/s (28,000 cfs). For this study only peak flows of 60,000 cfs, occurring during spring runoff will be considered and therefore flow reversal effects will not be considered.

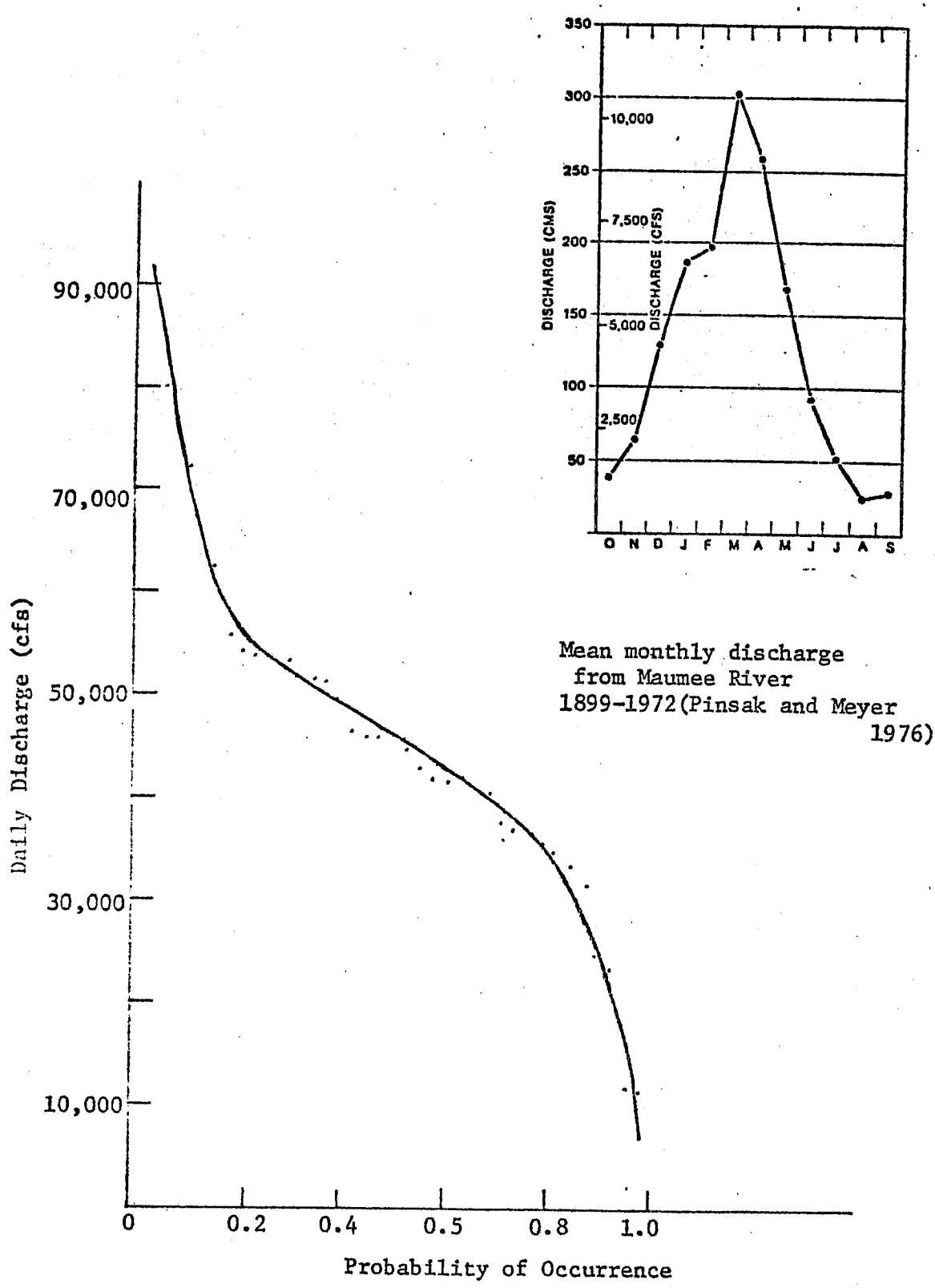

Figure 3. Flow Duration Curve of Maumee River. (Data analyzed by Kathy Stanton 1976).

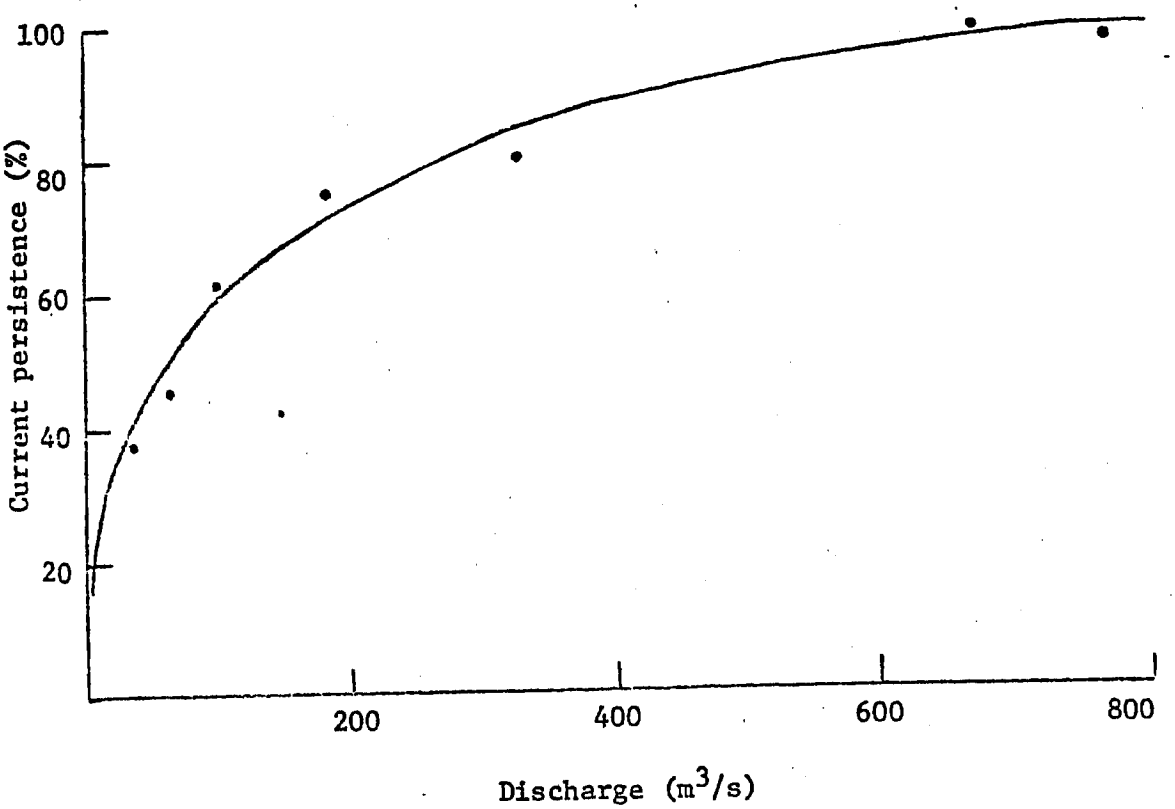

Figure 4. Current persistence at Maumee River mouth (Pinsak and Meyer 1975).

C. Climate of the Area

Since Maumee Bay is shallow it is extremely sensitive to meteorological changes.

For the month of March the maximum and minimum temperatures recorded were 44.7°F and 25.6°F and the predominant wind direction was WSW (Pinsak and Meyer 76). Figure 5, taken from Pinsak and Meyer (1976), shows the predominant wind directions for Toledo, Ohio. The northeasterly and southwesterly winds running parallel to the axis of the Bay together with the southeasterly winds will be considered for the present study.

D. Observed Sediment Distribution

The Maumee River is the primary factor in transport of sediment loads into the Bay. Herdendorf and Cooper (1975) indicated that Maumee River accounts for only 3% of the flow into the lake, but included in this discharge is 1.6 million metric tons of suspended solids, annually representing 6.0% of the total sediment load to the Lake. Table 1 shows the sediment input to the lake from various sources. Horowitz et. al. (1975) stated that at low flows sediment loads were often less than 5 tons/day, but at flood peaks, there was about a ton of sediment for each cfs discharge (Figure 6).

Figure 7 taken from Pinsak and Meyer (1976) gives an idea of net erosion and sedimentation occurring between 1844 and 1970. The only sand deposit of any significance lies north of the modified Cedar Point and is deposited by littoral currents. Herdendorf and Cooper (1975) pointed out that this deposit has been extensively studied and concluded that none of the sand could have come from Maumee River because the

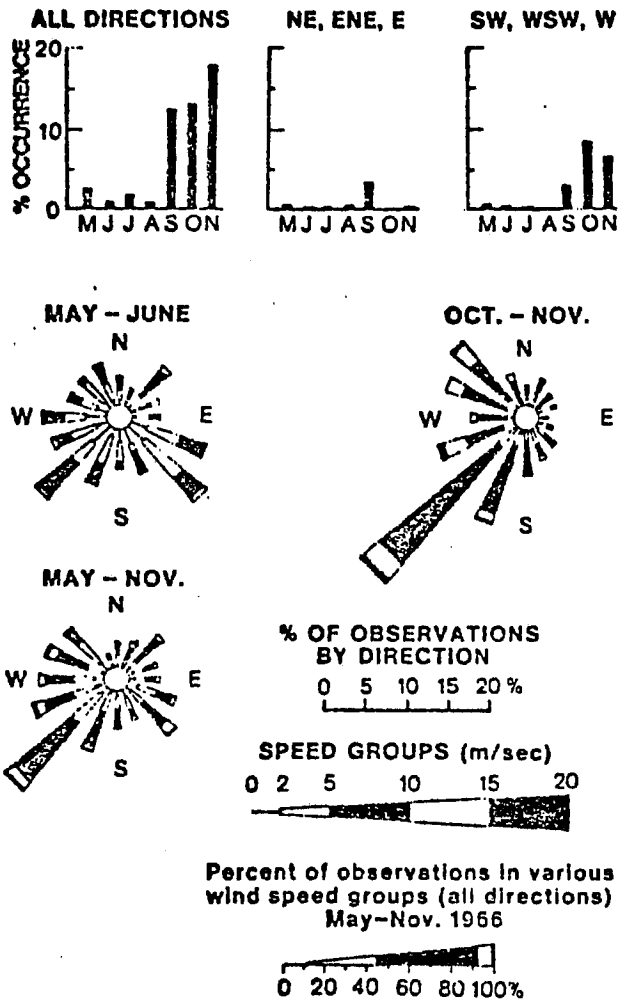

Figure 5. Wind roses and predominant wind directions for Toledo, Ohio (Pinsak and Meyer 1976).

Table 1. Estimated quantity of silt and clay sized sediment input from various sources (Kemp et. al. 1975).

Source	Zone	Yield of fine-grained material per annum (*Million metric tons*)
Shoreline erosion[a]	Detroit River — Point Pelee	0.4
	Point Pelee — Erieau	1.6
	Erieau — Long Point	21.2
	Long Point — Niagara River	0.2
	Detroit River — Maumee River	{<0.1}
	Maumee River — Sandusky	<0.1
	Sandusky — Ohio — Penn. Border	1.3
	Ohio — Penn. Border — Niagara River	{1.0}
	TOTAL	25.7
River inputs[b]	Detroit River	1.4
	Maumee River	1.8
	Other rivers	0.9
	TOTAL	4.1
Airborne particles[c]	Estimated range for the whole lake	0.2–3.3
Autochthonous organic matter[d]		1.0
Dredged spoils[e]	Whole lake	1.4

[a]Shoreline erosion data (Carter 1974; J. P. Coakley personal communication; W. S. Haras and J. Shaw personal communication). Bracketed quantities are our own estimates.
[b]Data from I.J.C. (1969).
[c]Whelpdale (1974 a, b).
[d]Decomposed residues of primary organic matter, see text for explanation.
[e]International Working Group Report (1974).

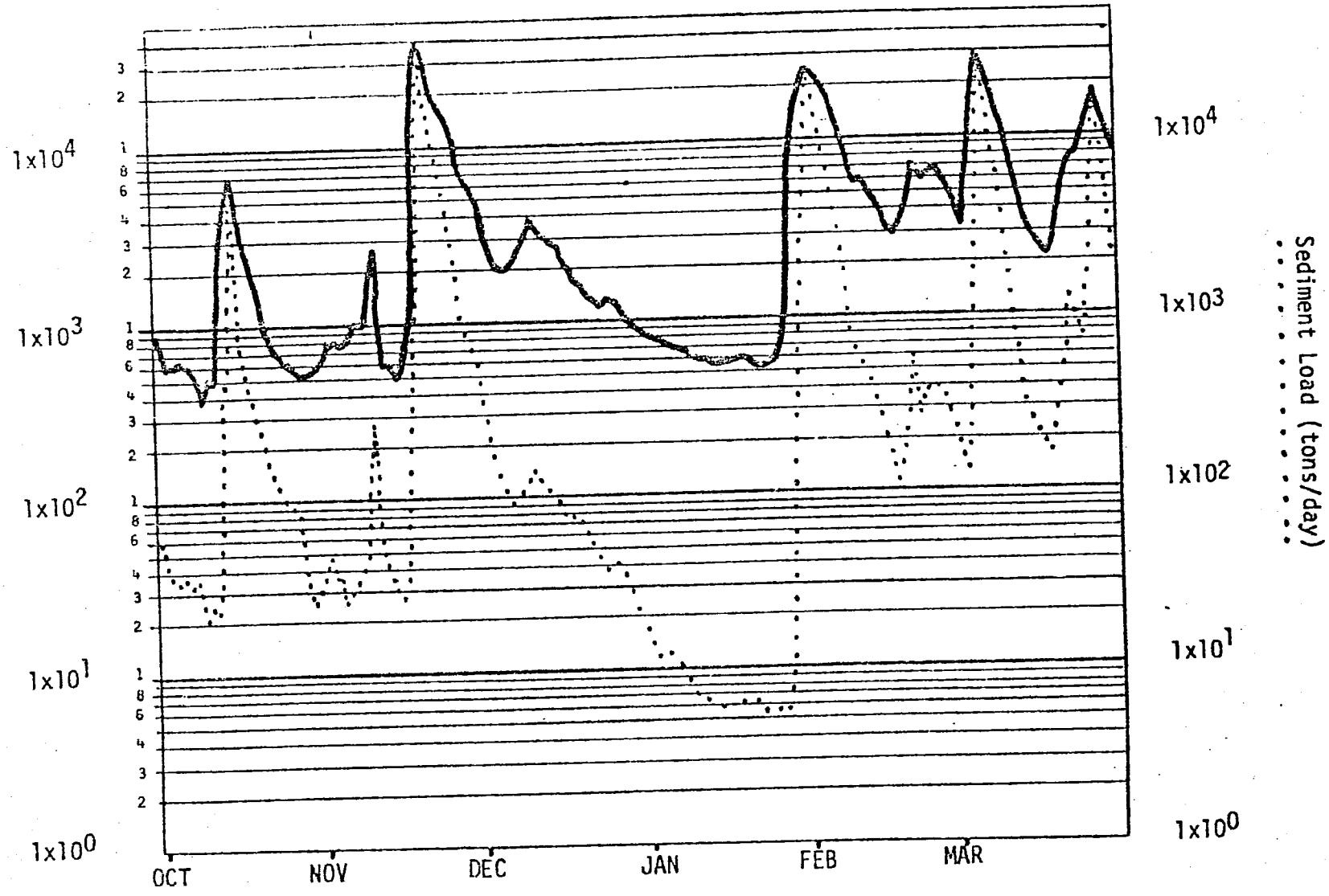

Figure 6. Flow and sediment loads at Waterville (USGS #04193500): October 29-March 70 (Horowitz et. al. 1975)

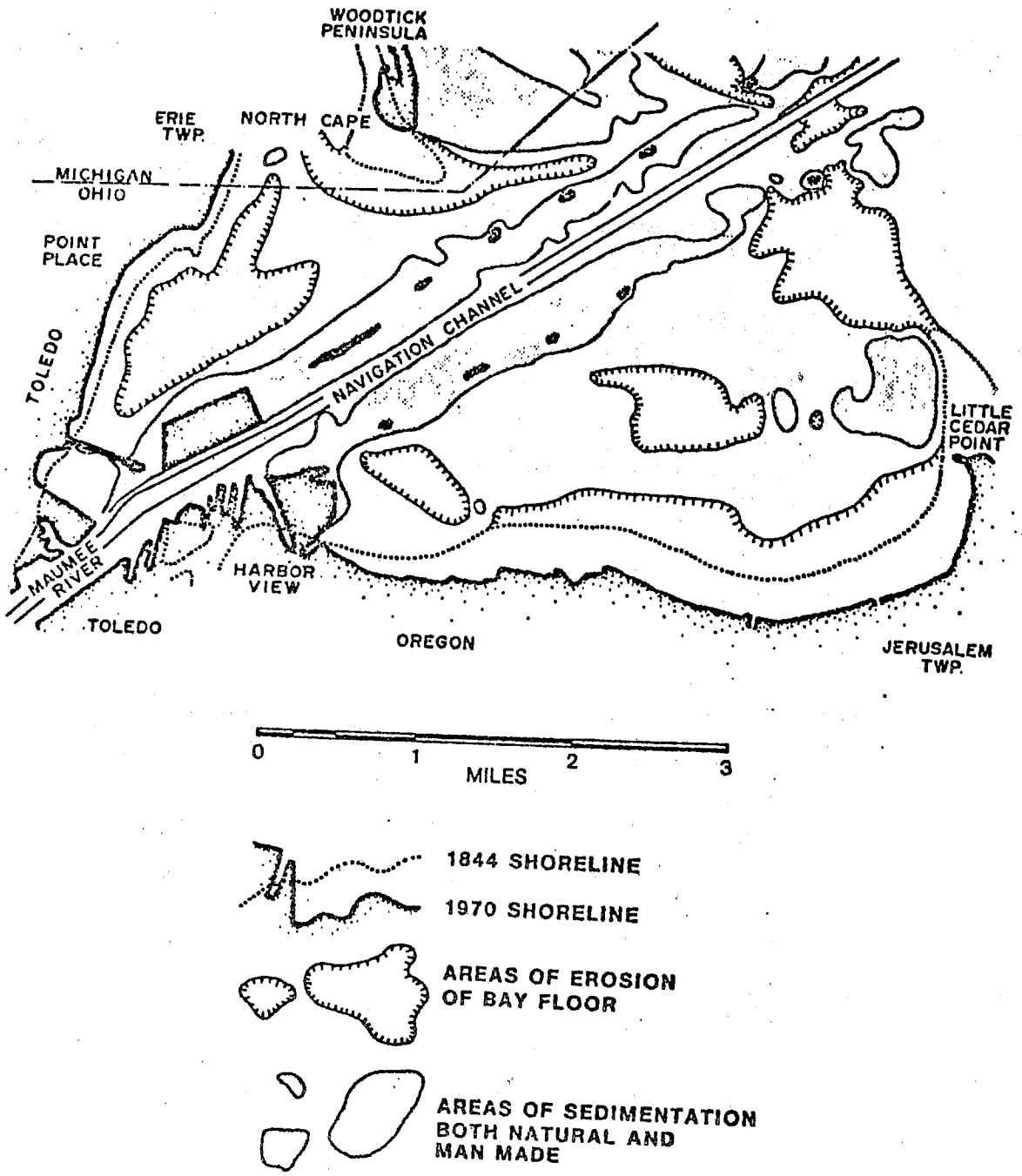

Figure 7.--Erosion and sedimentation in Maumee Bay, 1844-1970. (Pinsak and Meyer 1976).

river loses its sand carrying capacity near Perrysburg where the river rises above IGLD (Herdendorf 1970).

Suspended materials such as clay, and silt are the main constituents in turbid waters. Turbidity in Maumee Bay decreases from the mouth of the river to Lake Erie. The average of 41.5 hrs for 90% settling shows that a large percentage of the fine sediments remain suspended and carry into the main lake (Pinsak and Meyer 1976).

CHAPTER THREE

THE GOVERNING EQUATIONS

A. Background

Only one numerical technique has been developed by Pinsak and Meyer (1976))to predict circulation in Maumee Bay and western Lake Erie. The model does not incorporate advection or turbulent motion in the momentum equations. Vertical velocity was neglected and a constant eddy diffusivity was considered in the mass transport equation.

Gedney and Lick (1972), Sheng and Lick (1975), and Paul and Lick (1976, 1973) have developed three-dimensional circulation and contaminant dispersion models for Lake Erie. The present work is concerned with the modification and adaptation of the Paul and Lick model to the Maumee Bay area.

The original model was developed for variable temperature flow but converted to transport of pollutants for this study. The effects of wind, bottom characteristics, river inflow, earth's rotation, and shoreline configuration are taken into account. Also Deardorff's (1969) approach to subgrid scale (SGS) motions is applied.

By varying the model inputs this numerical technique could be used to evaluate what dominant transport mechanisms are operating in the Bay.

B. Notation

The notation used in this study is based on the cartesian index notation. A right handed cartesian coordinate system with axis X, Y, and Z is used. The X-axis represents the northeast direction as seen in Figure 8. u, v, w, and Ω are velocities in X, Y, Z, and vertically stretched σ directions respectively. The unit vectors are denoted as n, m, and k. Also the present time step is denoted by ℓ.

ΔX, ΔY, ΔZ, and $\Delta\sigma$ are the grid spaces in X, Y, Z, and σ directions. Whenever space and time indices occur as n, m, k, and ℓ they are omitted and simply implied.

C. Assumptions

The following assumptions are made:

1. The vertical momentum equation is reduced to the hydrostatic equation by the shallow water assumption which neglects all acceleration terms (both local and inertial) compared to gravity. The hydrostatic approximation has been extensively used in the modeling of lakes (Paul and Lick 1976, 1973, Liggett 1970, Leendertse 1970, Sheng and Lick 1975). Because of this approximation the order of the system of equations is reduced and hence greater computational speed is attained.

2. Sheng and Lick (1975) have pointed out that the western basin of Lake Erie is essentially homogeneous throughout the year including summer. Hence the lake is assumed to be homogeneous and the effect of temperature is not considered.

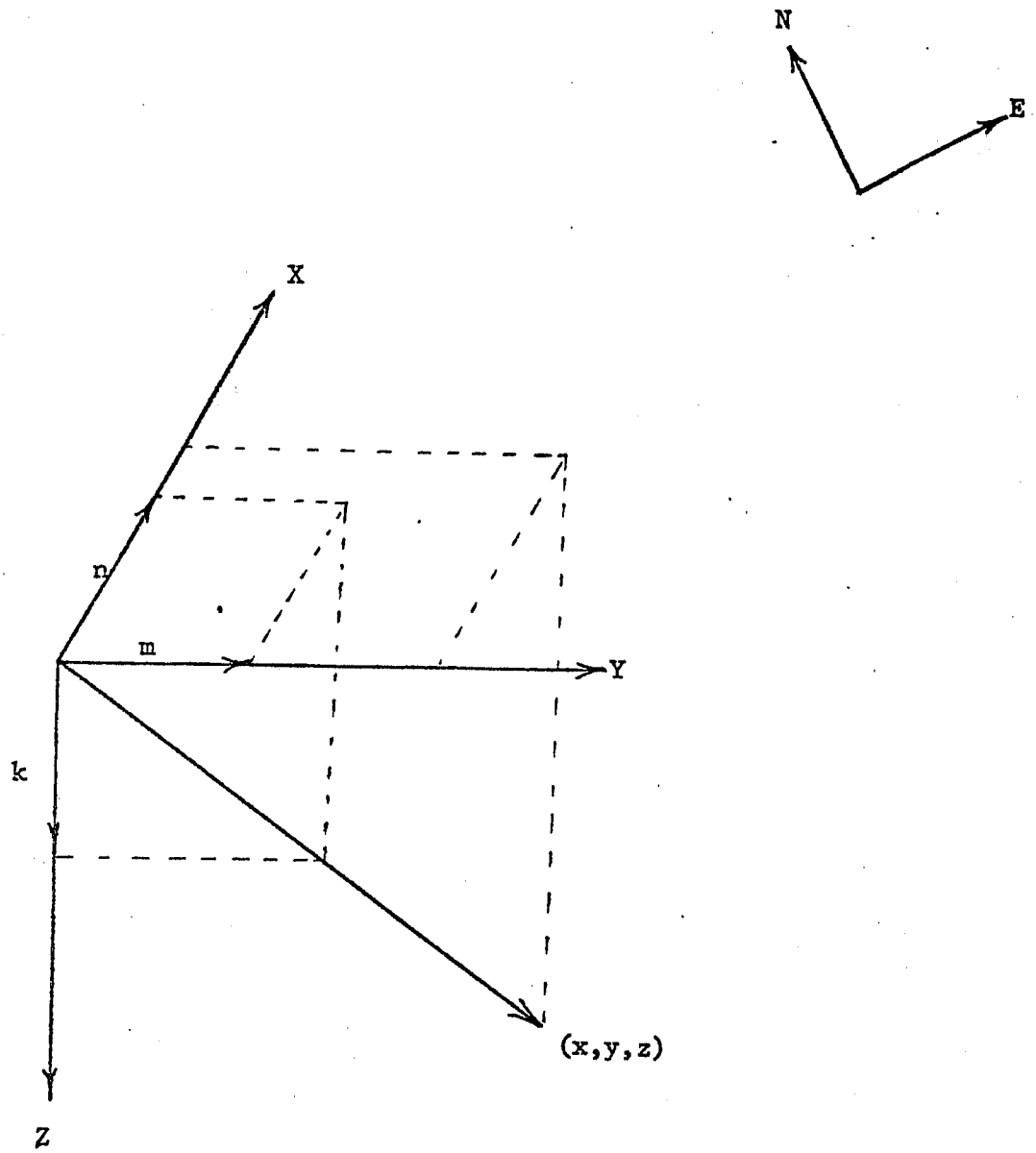

Figure 8. Notation definition.

3. The turbulent stresses far outweigh the molecular viscous components, hence the latter can be omitted with a good degree of approximation.

4. The rigid lid approximation, which sets the vertical velocity at the surface to zero, is made. The surface gravity waves are then damped out and the computational time step is increased. This approximation is valid during runoff because this study concentrates on the short-term peak flows which are generated during intense meterological events. Water level fluctuations are reduced during the passage of the event and only become large after the storm has moved off the lake. Since the sediment events often occur during storms it was felt that for the brief time periods and small space scales involved that a rigid lid approach was justified. Obviously this is also a more economical approach than the free surface model and, in light of the study objectives, will therefore allow a reasonably detailed description of the gross transport mechanisms.

5. The velocities in the mass balance equation are the velocities of the contaminant and not the velocities of the fluid. Therefore for small concentrations and small particles and if fluid particle accelerations are small in comparison with the gravitational acceleration, it can be assumed that the horizontal velocities of the fluid and the contaminant are the same while the vertical velocities are of the form

$$w = w_f + w_s$$

where w_s is the settling velocity of the contaminant relative to the fluid and w_f is the vertical velocity of the fluid (Sheng and Lick 1975).

Murray (1970) studied the effect of turbulence on the settling of sediment particles. He concluded that the settling velocity of a particle in a turbulent shearing condition can be reduced by as much as 30% below its terminal settling velocity in still water. However Sheng and Lick (1975) indicated that for small sediment particles of diameter less than 0.1 mm, with the settling velocity in the Stokes range, the eddy diffusion coefficient for the particle is nearly equal to that of the fluid and the shearing effects can be ignored.

D. Basic Equations

The basic shallow water equations for the numerical model are the Navier-Stokes equations and the mass conservation equation of fluid and contaminant. The three-dimensional equations of motion are derived in Schlicting (1968) and Bird et. al. (1964). After considering the assumptions stated in the previous section, the equations are of the following form:

Continuity:

$$\frac{\partial u}{\partial x} + \frac{\partial v}{\partial y} + \frac{\partial w}{\partial z} = 0 \qquad (3.1)$$

X-Momentum:

$$\frac{\partial u}{\partial t} + \frac{\partial (uu)}{\partial x} + \frac{\partial (uv)}{\partial y} + \frac{\partial (uw)}{\partial z} = -\frac{1}{\rho}\frac{\partial P}{\partial x} - fv \qquad (3.2)$$

Y-Momentum:

$$\frac{\partial v}{\partial t} + \frac{\partial (uv)}{\partial x} + \frac{\partial (vv)}{\partial y} + \frac{\partial (vw)}{\partial z} = -\frac{1}{\rho}\frac{\partial P}{\partial x} + fu \qquad (3.3)$$

Hydrostatic Pressure:

$$\frac{\partial P}{\partial z} = \rho g \qquad (3.4)$$

Contaminant Conservation:

$$\frac{\partial C}{\partial t} + \frac{\partial (uC)}{\partial x} + \frac{\partial (vC)}{\partial y} + \frac{\partial ((w + w_s)C)}{\partial z} = 0 \qquad (3.5)$$

where:

t = time;

u(x,y,z,t)= intantaneous velocity in x-direction;

v(x,y,z,t)= intantaneous velocity in y-direction;

w(x,y,z,t)= intantaneous velocity in z-direction;

P(x,y,z,t)= instantaneous pressure;

ρ= density;

C(x,y,z,t)= concentration; and

f= coriolis parameter.

E. Equation Analysis

1. Spatial Filtering of the Primitive Equations

An analytical solution of equations 3.1 to 3.5, together with boundary conditions, would yield instantaneous values of u, v, w, and C at every point in the system. As an analytical solution is not

possible, a numerical model must be developed which would yield values of each parameter at finite number of discrete points in the flow region.

The discrete calculation of turbulent flows requires grid spacings which preclude the rational prediction of turbulent modes with wave numbers less than twice the largest grid spacing. Therefore filtering and averaging is necessary in order to separate the deterministic modes from the subgrid scale motion. The averaging is applied over the grid volume to filter out subgrid scale motions. The resulting equations are solved for the filtered variables after an assumption is made for the SGS Reynolds stresses arising from the averaging process.

Deardorff (1969) uses the following scheme for averaging. The instantaneous parameters (u, v, w, and C) are expressed in terms of a filtered variable and a SGS component α'.

$$\alpha = \bar{\alpha} + \alpha'$$

$$\text{and } \bar{\alpha}(x,y,z,t) = \frac{1}{\Delta X \Delta Y \Delta Z} \int_{x-1/2\Delta X}^{x+1/2\Delta X} \int_{y-1/2\Delta Y}^{y+1/2\Delta Y} \int_{z-1/2\Delta Z}^{z+1/2\Delta Z} \alpha(x,y,z,t)\,dx\,dy\,dz$$

where the overbar indicates a spatial average over grid volume and ΔX, ΔY and ΔZ are grid spacings in the numerical model.

Substituting $u = \bar{u} + u'$; $v = \bar{v} + v'$; $w = \bar{w} + w'$; $P = \bar{P} + P'$; $C = \bar{C} + C'$ into equations 3.1 to 3.5 and averaging as indicated above yields the following set of equations for the filtered variables.

$$\frac{\partial \bar{u}}{\partial x} + \frac{\partial \bar{v}}{\partial y} + \frac{\partial \bar{w}}{\partial z} = 0 \tag{3.6}$$

$$\frac{\partial \bar{u}}{\partial t} + \frac{\partial (\overline{uu})}{\partial x} + \frac{\partial (\overline{uv})}{\partial y} + \frac{\partial (\overline{uw})}{\partial z} = -\frac{1}{\rho}\frac{\partial P}{\partial x} - fv$$

$$-\frac{\partial (\overline{u'u'})}{\partial x} - \frac{\partial (\overline{u'v'})}{\partial y} - \frac{\partial (\overline{u'w'})}{\partial z} \tag{3.7}$$

$$\frac{\partial \bar{v}}{\partial t} + \frac{\partial (\overline{uv})}{\partial x} + \frac{\partial (\overline{vv})}{\partial y} + \frac{\partial (\overline{vw})}{\partial z} = -\frac{1}{\rho}\frac{\partial P}{\partial y} + fu$$

$$-\frac{\partial (\overline{u'v'})}{\partial x} - \frac{\partial (\overline{v'v'})}{\partial y} - \frac{\partial (\overline{v'w'})}{\partial z} \tag{3.8}$$

$$\frac{\partial P}{\partial z} = \rho g \tag{3.9}$$

$$\frac{\partial \bar{C}}{\partial t} + \frac{\partial (\overline{uC})}{\partial x} + \frac{\partial (\overline{vC})}{\partial y} + \frac{\partial (\overline{(w + w_s)C})}{\partial z} = -\frac{\partial (\overline{u'C'})}{\partial x}$$

$$-\frac{\partial (\overline{v'C'})}{\partial y} - \frac{\partial (\overline{(w + w_s)'C'})}{\partial x} \tag{3.10}$$

The ensemble average of u' is zero but the ensemble average of the cross products $u'v'$ are not zero.

2. Stretched Coordinate System

A standard numerical procedure to take care of variable depth is to vary the number of grid points in the mesh according to the local depth. But in the present study the vertical coordinate is stretched according to:

$$\sigma = z/h(x,y)$$

where σ is the new vertical coordinate and h is the local depth. Phillips (1957) used this technique originally for numerical forecasting. Also Paul and Lick (1976) used it for their model.

The equations to be solved are more complicated looking, but they are solved for a basin of constant depth in the transformed system. This greatly reduces the programming complexities of the model and makes the inclusion of depth variations simpler.

The resulting system of equations, after Eqs. 3.6 - 3.10 are vertically stretched and the bars dropped, are as follows:

$$\frac{1}{h}\frac{\partial (hu)}{\partial x} + \frac{1}{h}\frac{\partial (hv)}{\partial y} + \frac{\partial \Omega}{\partial \sigma} = 0 \qquad (3.11)$$

$$\frac{\partial u}{\partial t} + \frac{1}{h}\frac{\partial (hu^2)}{\partial x} + \frac{1}{h}\frac{\partial (huv)}{\partial y} + \frac{\partial (\Omega u)}{\partial \sigma} = -\frac{1}{\rho}\frac{\partial P}{\partial x}$$

$$- fv - \frac{1}{h}\frac{\partial (hu'u')}{\partial x} - \frac{1}{h}\frac{\partial (hu'v')}{\partial y} - \frac{\partial (u'\Omega')}{\partial \sigma} \qquad (3.12)$$

$$\frac{\partial v}{\partial t} + \frac{1}{h}\frac{\partial}{\partial x}(huv) + \frac{1}{h}\frac{\partial}{\partial y}(hv^2) + \frac{\partial}{\partial \sigma}(\Omega v) = -\frac{1}{\rho}\frac{\partial P}{\partial y}$$

$$+ fu - \frac{1}{h}\frac{\partial}{\partial x}(hu'v') - \frac{1}{h}\frac{\partial}{\partial y}(hv'v') - \frac{\partial}{\partial \sigma}(v'\Omega') \qquad (3.13)$$

$$\frac{1}{h}\frac{\partial P}{\partial \sigma} = \rho g \qquad (3.14)$$

$$\frac{\partial C}{\partial t} + \frac{1}{h}\frac{\partial}{\partial x}(huC) + \frac{1}{h}\frac{\partial}{\partial y}(hvC) + \frac{\partial}{\partial \sigma}((\Omega+\Omega_s)C) = -\frac{1}{h}\frac{\partial}{\partial x}(hu'C') - \frac{1}{h}\frac{\partial}{\partial y}(hv'C')$$

$$- \frac{\partial}{\partial \sigma}((\Omega+\Omega_s)'C') \qquad (3.15)$$

where Ω is the vertical velocity in stretched coordinates and is defined as:

$$\Omega = \frac{1}{h}(w - \sigma(u\frac{\partial h}{\partial x} + v\frac{\partial h}{\partial y})) = \frac{\partial \sigma}{\partial t} \qquad (3.16)$$

In obtaining the above set of transformed equations it was assumed that the depth varies gradually. The transformed diffusion terms involve cross-derivatives of the spatial coordinates. The terms containing the derivatives of the depth are neglected with respect to those terms containing only the depth. Phillips (1957), Smagorinsky et. al. (1965), and Sheng and Lick (1975) have used this approximation. This approximation was tested for Maumee Bay, especially for the navigational channel. Maumee Bay slopes gently downwards towards the northeast. Various cross sectional profiles were plotted to look at

the slopes near the navigational channel (Figures 10 and 11). Figure 9 (Chart No. 370, U.S. Department of Commerce) shows the position of these cross-sections in the Bay. Though the slopes look steep (because of the small horizontal scale) it can be seen from Table 2 that the derivatives of the depth are small compared to the depth. Hence, terms derived from the vertical stretching which contain first derivatives and squares of the first derivative of h are neglected.

3. Nondimensional Analysis

The following variables are used to nondimensionalize Eqs. 3.11 to 3.15.

$$u^* = \frac{u}{u_o}; \quad v^* = \frac{v}{u_o}; \quad \Omega^* = \frac{b_o \Omega}{u_o}$$

$$x^* = \frac{x}{b_o}; \quad y^* = \frac{y}{b_o}; \quad h^* = \frac{h}{h_o}$$

$$t^* = \frac{t A_H}{b_o^2}; \quad p^* = \frac{b_o p}{\rho_o u_o A_H} \quad C^* = \frac{C}{C_f}$$

where:

u_o = reference velocity;

b_o = horizontal reference length;

h_o = vertical reference lenth;

C_f = reference concentration; and

A_H = horizontal eddy viscosity.

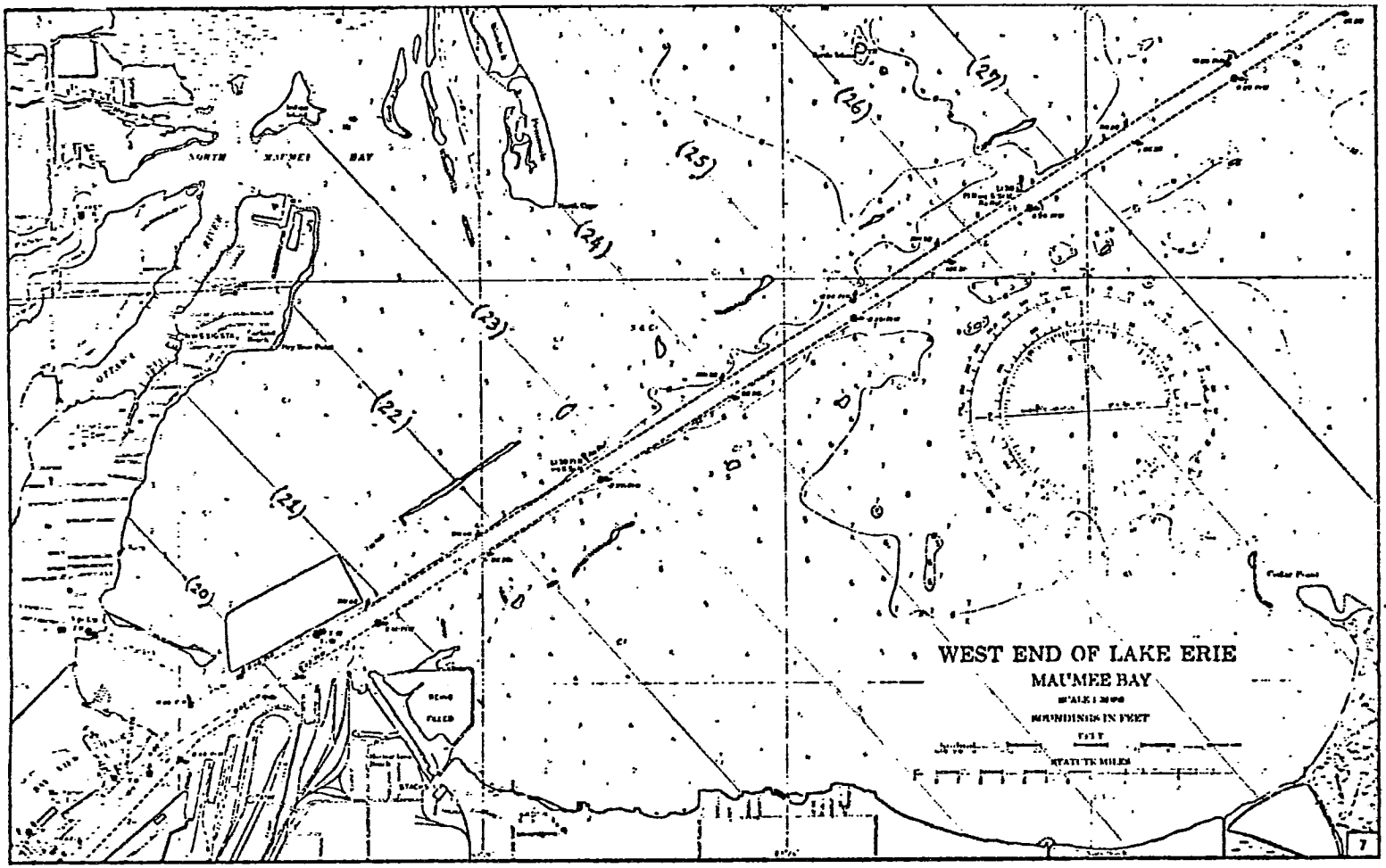

Figure 9. Location of the cross-sectional profiles (U.S. Department of Commerce).

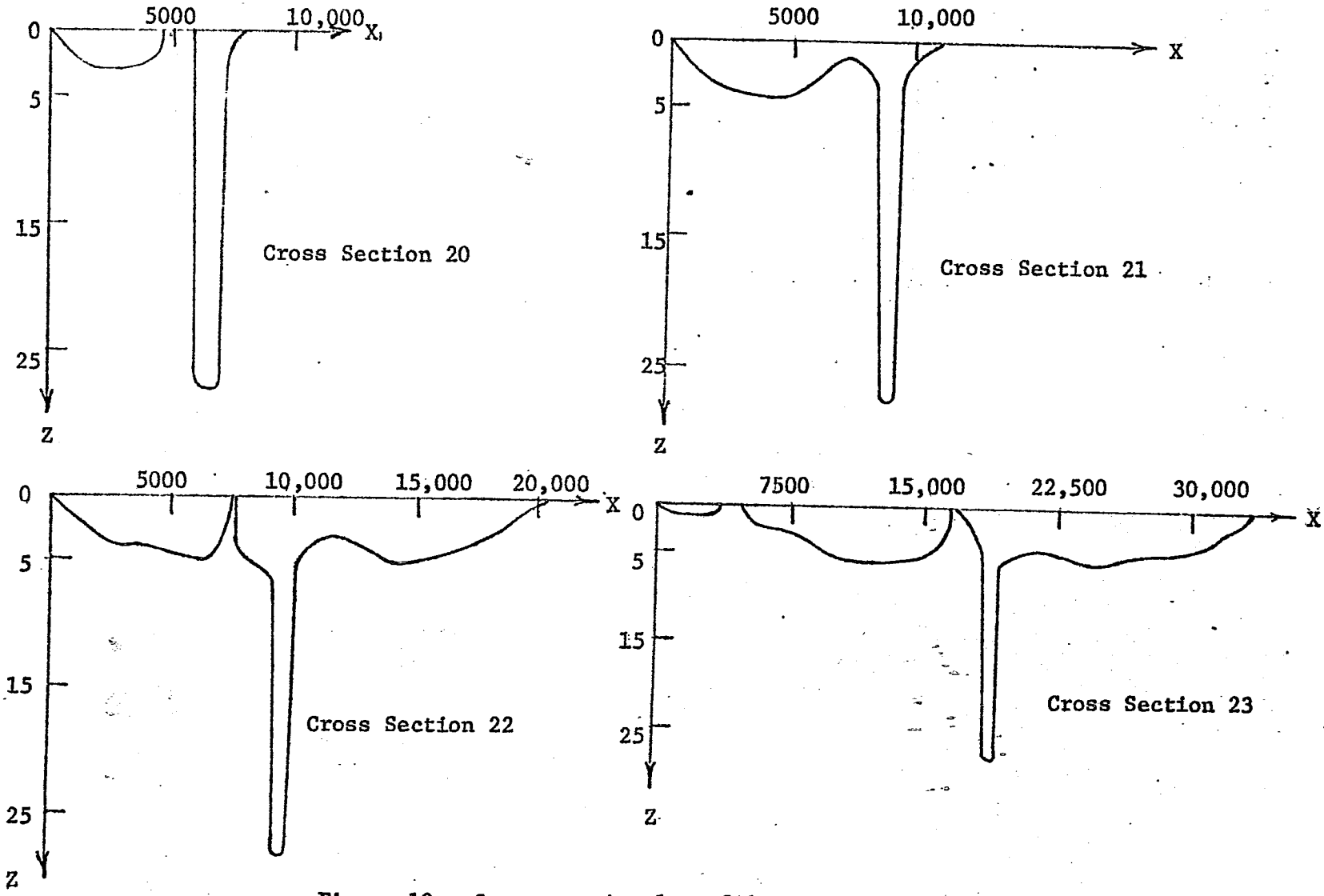

Figure 10. Cross-sectional profiles of Maumee Bay.

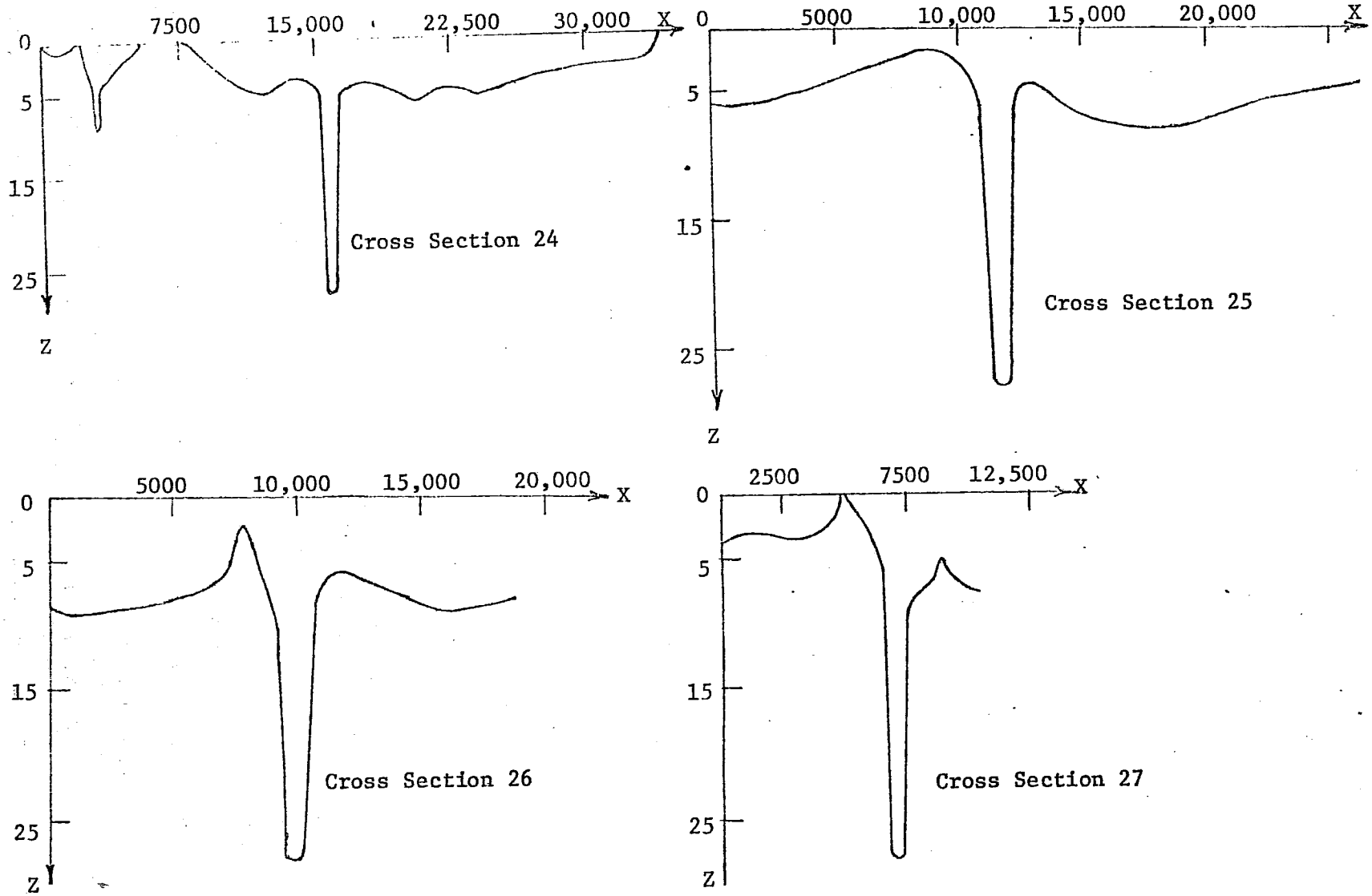

Figure 11. Cro-s-sectional profile of Maumee Bay.

Table 2. The depth and their derivatives in the channel at different cross-sections.

Cross Section	Depth	Derivatives
20	28	0.112
21	28	0.096
22	28	0.096
23	28	0.088
24	28	0.088
25	28	0.088
26	28	0.072
27	28	0.088

After Eqs. 3.11 to 3.15 are rendered dimensionless by introducing the above variables and dropping the asterisks, the following set of equations are obtained:

$$\frac{1}{h}\frac{\partial (hu)}{\partial x} + \frac{1}{h}\frac{\partial (hv)}{\partial y} + \frac{\partial \Omega}{\partial \sigma} = 0; \tag{3.17}$$

$$\frac{\partial u}{\partial t} + R_e\left[\frac{1}{h}\frac{\partial (hu^2)}{\partial x} + \frac{1}{h}\frac{\partial (huv)}{\partial y} + \frac{\partial (\Omega u)}{\partial \sigma}\right] + R_o v = -\frac{\partial P}{\partial x}$$

$$- R_e\left[\frac{1}{h}\frac{\partial (hu'u')}{\partial x} + \frac{1}{h}\frac{\partial (hu'v')}{\partial y} + \frac{\partial (u'\Omega)}{\partial \sigma}\right]; \tag{3.18}$$

$$\frac{\partial v}{\partial t} + R_e\left[\frac{1}{h}\frac{\partial (huv)}{\partial x} + \frac{1}{h}\frac{\partial (hv^2)}{\partial y} + \frac{\partial (\Omega v)}{\partial \sigma}\right] - R_o u$$

$$= -\frac{\partial P}{\partial y} - R_e\left[\frac{1}{h}\frac{\partial (hu'v')}{\partial x} + \frac{1}{h}\frac{\partial (v'v')}{\partial y} + \frac{\partial (v'\Omega')}{\partial \sigma}\right]; \tag{3.19}$$

$$\frac{1}{h}\frac{\partial P}{\partial \sigma} = \frac{R_e}{F_r^2} \quad ; \quad \text{and} \tag{3.20}$$

$$\frac{\partial C}{\partial t} + R_e\left(\frac{1}{h}\frac{\partial (huC)}{\partial x} + \frac{1}{h}\frac{\partial (hvC)}{\partial y} + \frac{\partial}{\partial \sigma}\left((\Omega + \Omega_s)C\right)\right)$$

$$= R_e\left(\frac{1}{h}\frac{\partial (hu'C')}{\partial x} + \frac{1}{h}\frac{\partial (hv'C')}{\partial y} + \frac{\partial}{\partial \sigma}\left((\Omega + \Omega_s)'C'\right)\right) \tag{3.21}$$

$$\frac{1}{h}\frac{\partial (hu)}{\partial x} + \frac{1}{h}\frac{\partial (hv)}{\partial y} + \frac{\partial \Omega}{\partial \sigma} = 0; \tag{3.25}$$

$$\frac{\partial u}{\partial t} + R_e\left[\frac{1}{h}\frac{\partial (hu^2)}{\partial x} + \frac{1}{h}\frac{\partial (huv)}{\partial y} + \frac{\partial}{\partial \sigma}(\Omega u)\right] + R_o v$$

$$= -\frac{\partial P}{\partial x} + R_e\left[\frac{1}{h}\frac{\partial}{\partial x}\left(2e_{xx}h\frac{\partial u}{\partial x}\right) + \frac{1}{h}\frac{\partial}{\partial y}\left(he_{xy}\left(\frac{\partial u}{\partial y} + \frac{\partial v}{\partial x}\right)\right)\right.$$

$$\left. + \left(\frac{b_o}{h_o}\right)^2 \frac{1}{h^2}\frac{\partial}{\partial \sigma}\left(e_{xz}\frac{\partial u}{\partial \sigma}\right)\right]; \tag{3.26}$$

$$\frac{\partial v}{\partial t} + R_e\left[\frac{1}{h}\frac{\partial (huv)}{\partial x} + \frac{1}{h}\frac{\partial (hv^2)}{\partial y} + \frac{\partial}{\partial \sigma}(\Omega v)\right] - R_o u$$

$$= -\frac{\partial P}{\partial y} + R_e\left[\frac{1}{h}\frac{\partial}{\partial x}\left(he_{yx}\left(\frac{\partial v}{\partial x} + \frac{\partial u}{\partial y}\right)\right) + \frac{1}{h}\frac{\partial}{\partial y}\left(2e_{yy}\frac{h\partial u}{\partial y}\right.\right.$$

$$\left.\left. + \left(\frac{b_o}{h_o}\right)^2 \frac{1}{h^2}\frac{\partial}{\partial \sigma}\left(e_{yz}\frac{\partial v}{\partial \sigma}\right)\right)\right] \tag{3.27}$$

$$\frac{\partial C}{\partial t} + \bar{R}_e\left[\frac{1}{h}\frac{\partial (huC)}{\partial x} + \frac{1}{h}\frac{\partial (hvC)}{\partial y} + \frac{\partial}{\partial \sigma}\left((\Omega + \Omega_s)C\right)\right]$$

$$= R_e\left[\frac{1}{h}\frac{\partial}{\partial x}\left(hP_r e_{xx}\frac{\partial C}{\partial x}\right) + \frac{1}{h}\frac{\partial}{\partial y}\left(hP_r e_{yy}\frac{\partial C}{\partial y}\right)\right.$$

$$\left. + \left(\frac{b_o}{h_o}\right)^2 \frac{1}{h^2}\frac{\partial}{\partial \sigma}\left(P_r e_{zz}\frac{\partial C}{\partial \sigma}\right)\right]; \text{ and} \tag{3.28}$$

$$\frac{1}{h}\frac{\partial P}{\partial \sigma} = \frac{R_e}{F_r 2} \tag{3.29}$$

where e_{ij} = SGS eddy coefficients.

5. Time Splitting and the Formulation of the Pressure Equation.

The use of stretched coordinates requires a different formulation of the rigid lid pressure equation $P_s(x,y)$. For shallow regions the vertical mesh spacings can be quite small and therefore the time steps used in the explicit time marching are severely limited, often being as small as seconds. A remedy for this malady, one which allows larger time steps is a splitting procedure similar to the simplified Marker and Cell method of the Los Alamos Group.

As formulated by Paul and Lick the pressure equation is derived as follows. Eqs. 3.26 and 3.27 are written in a different form as follows:

$$\frac{\partial u}{\partial t} - R_e \left(\frac{b_o}{h_o}\right)^2 \frac{1}{h^2} \frac{\partial}{\partial \sigma}\left(e_{xz} \frac{\partial u}{\partial \sigma}\right) = g(u) - \frac{\partial P_s}{\partial x} ; \tag{3.30}$$

$$\text{and} \quad \frac{\partial v}{\partial t} - R_e \left(\frac{b_o}{h_o}\right)^2 \frac{1}{h^2} \frac{\partial}{\partial \sigma}\left(e_{yz} \frac{\partial v}{\partial \sigma}\right) = f(v) - \frac{\partial P_s}{\partial y} \tag{3.31}$$

g(u) and f(v) contain the rest of the terms in x and y directions respectively. The left hand sides of Eqs. 3.30 and 3.31 are to be solved implicitly (for values at time $\ell + 1$) for each set of vertical nodes located at planform nodal location (M,N). The equations are linearized by evaluating the nonlinear inertial terms with the previous time step information.

The pressure equation is derived by taking the divergence of the vertically integrated Eqs. 3.30 and 3.31, and using the vertically integrated continuity equation. The resulting equation is as follows:

$$\nabla \cdot (h\nabla Ps) = -\frac{\partial D}{\partial t} + \frac{\partial}{\partial x}(e_s \tau_x^{\ell+1} - e_b \tau_{Bx}^{\ell+1}) + \frac{\partial}{\partial y}(e_s \tau_y^{\ell+1} - e_b \tau_{BY}^{\ell+1})$$

$$+ \frac{\partial}{\partial x}(h\bar{G}) + \frac{\partial}{\partial y}(h\bar{F}) \qquad (3.32)$$

in which e_s and e_b represent the eddy viscosities at the surface and bottom, respectively. The bars indicate averages according to

$$(\overline{\quad}) = \int_1^0 (\quad)\, \partial\sigma .$$

τ_x and τ_y represents the wind stresses, while τ_{BX} and τ_{BY} are the bottom stresses and

$$D = \frac{\partial}{\partial x}(h\bar{u}) + \frac{\partial}{\partial y}(h\bar{v})$$

Equation 3.32 requires $\tau_{BX}^{\ell+1}$ and $\tau_{BY}^{\ell+1}$ which are unknown. A proper approach to this problem is to seek a solution of the form

$$u = g_1 (y,z) \qquad (3.33)$$

and

$$v = g_2 (y,z) \qquad (3.34)$$

Eqs. 3.30 and 3.31 are splitup by using Eqs. 3.33 and 3.34. The finite difference form is:

$$Au_Q = G + u \tag{3.35}$$

$$Au_P = - I \frac{\partial Ps}{\partial x} \tag{3.36}$$

$$Av_Q = F + v \tag{3.37}$$

$$Av_P = - I \frac{\partial Ps}{\partial y} \tag{3.38}$$

where A is a tridiagonal matrix (Eq. 4.3) and I is the identity matrix.

The formal solution to Eqs. 3.36 and 3.38 is:

$$u_P = - \lambda \frac{\partial Ps}{\partial x} \text{ ; and } v_P = - \lambda \frac{\partial Ps}{\partial y}$$

where λ satisfies the equation $A\lambda = I$.

An equation for $\tau_{BX}^{\ell+1}$ and $\tau_{BY}^{\ell+1}$ is formulated by vertically integrating Eqs. 3.35 and 3.37, taking the divergence and requiring the sum to satisfy the vertically integrated continuity equation. The result is:

$$\frac{\partial D_Q}{\partial t} - \frac{\partial D}{\partial t} + \frac{\partial}{\partial x}(e_s \tau_{xQ}^{\ell+1} - e_b \tau_{BXQ}^{\ell+1}) + \frac{\partial}{\partial y}(e_s \tau_{yQ}^{\ell+1} - e_b \tau_{BYQ}^{\ell+1})$$

$$+ \frac{\partial}{\partial x}(h\bar{G}) + \frac{\partial}{\partial y}(h\bar{F}) = 0 \tag{3.39}$$

Equation 3.39 is now subtracted from 3.32 and the result is a suitable pressure equation in terms of known variables

$$-\frac{\partial D_Q}{\partial t} + \frac{\partial}{\partial x}\left(e_s \tau_{xP}^{\ell+1} - e_b \tau_{BXP}^{\ell+1}\right) + \frac{\partial}{\partial y}\left(e_s \tau_{YP}^{\ell+1} - e_b \tau_{BYP}^{\ell+1}\right)$$

$$= \nabla \cdot (h \nabla Ps) \qquad (3.40)$$

Expressions for τ_{BXP} and τ_{BYP} are formed from equations 3.36 and 3.38.

$$\tau_{BXP}^{\ell+1} = -\frac{1}{h}\frac{\partial \lambda_b}{\partial \sigma}\frac{\partial Ps}{\partial x} \quad \text{and} \quad \tau_{BYP}^{\ell+1} = -\frac{1}{h}\frac{\partial \lambda_b}{\partial \sigma}\frac{\partial Ps}{\partial y}$$

Upon substitution into Eq. 3.40 a second order elliptic equation for Ps(x,y) results

$$\frac{\partial}{\partial x}\left[\left(h - \frac{e_b}{h}\frac{\partial \lambda_b}{\partial \sigma}\right)\frac{\partial Ps}{\partial x}\right] + \frac{\partial}{\partial y}\left[\left(h - \frac{e_b}{h}\frac{\partial \lambda_b}{\partial \sigma}\right)\frac{\partial Ps}{\partial y}\right]$$

$$= -\frac{\partial D_Q}{\partial t} + \frac{\partial}{\partial x}\left(e_s \tau_{XP}^{\ell+1}\right) + \frac{\partial}{\partial y}\left(e_s \tau_{YP}^{\ell+1}\right) \qquad (3.41)$$

F. Boundary Conditions

1. Sediment Transport Equation

Sheng and Lick (1975) have neatly summarized the general boundary condition for concentration, indicated by Monin and Yaglom (1971), as follows:

$$- w_s C + \frac{Av}{h} \frac{\partial C}{\partial \sigma} = \beta C - E$$

The first term represents the flux to the boundary due to gravitational settling while the second term represents the flux to the boundary due to vertical turbulent diffusion. On the right-hand-side, the first term depends on the porosity or stickiness of the wall. The case $\beta = 0$ corresponds to perfect reflection of the substance from the boundary while the case $\beta \longrightarrow \infty$ corresponds to perfect absorption at the boundary. For $0 < \beta < \infty$, partial reflection and absorption occurs. The second term on the right-hand-side is due to entrainment.

At the surface a zero flux or $\frac{\partial C}{\partial \sigma} = KhC$ condition is considered. At the bottom a perfectly absorbing $C = 0$ and perfectly reflecting $\frac{\partial C}{\partial \sigma} = KhC$ conditions with no entrainment are used. The concentration profile is specified at the inlet. At the outer boundaries either the normal derivatives are zero or concentrations are specified.

2. Momentum Equations

The following boundary conditions are used with the momentum equations:

$$u = g_1 (y,z)$$

River outflow

$$v = g_2(y,z)$$

At the surface wind dependent stresses are imposed:

$$\left.\frac{\partial u}{\partial \sigma}\right|_{\sigma = 0} = h\,\tau_x$$

$$\left.\frac{\partial v}{\partial \sigma}\right|_{\sigma = 0} = h\,\tau_y$$

The bottom and shore are taken as no slip, impermeable surfaces:

Bottom

$u = 0$
$v = 0$; and at the
$w = 0$

Shore

$u = 0$
$v = 0$.

At the outer boundary either

$$\frac{\partial u}{\partial n} = 0 \text{ or } u = f_1;$$

and $\frac{\partial v}{\partial n} = 0$ or $v = f_2$.

CHAPTER FOUR

THE NUMERICAL REPRESENTATION

In this chapter a numerical model to solve the mathematical model outlined in Chapter Three is presented. The model is an adaptation of the Paul and Lick plume model (1976, 1973) and therefore extensive documentation is available within their reports.

A. Grid Definitions and Spatial Differencing Schemes

The general arrangements of the variables in the grid system is shown in Figure 12. The horizontal velocities are defined at nodal points, the concentrations are defined at half nodal points in the horizontal and at nodal points in the vertical, and the surface pressure is defined at half nodal points in the horizontal.

As indicated earlier the finite difference approximations to the filtered equations represent solutions for cell averaged variables. Typical nodal cells are indicated in Figure 13. Part of the rationale behind the arrangement of the variables is to provide cells which lend themselves to the use of a consistent integration procedure. In the derivation of the finite difference equations, variables are sometimes required at points where they are not defined. In these circumstances, the undefined quantity is taken as the simple average of the neighboring values.

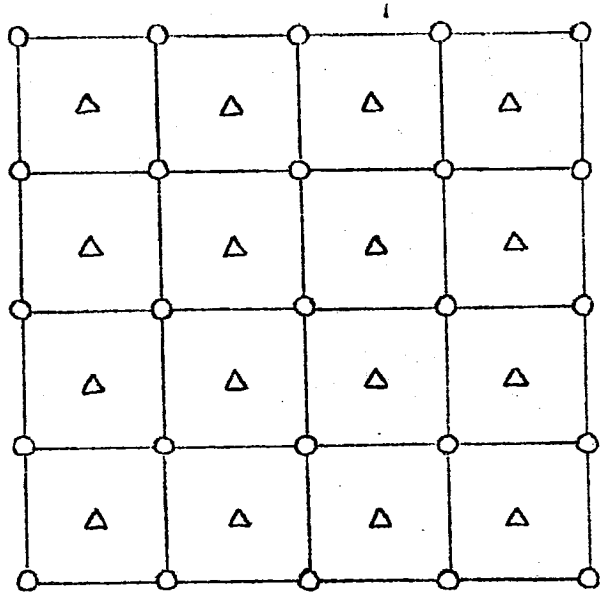

Horizontal plane

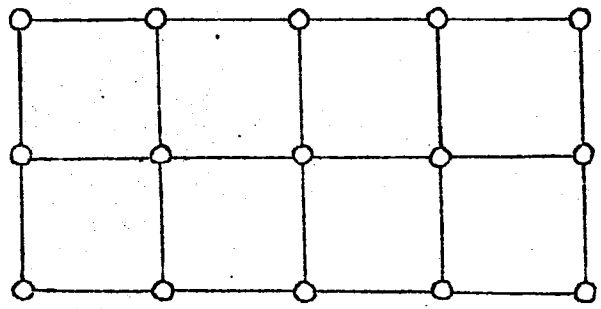

Vertical plane at nodal section

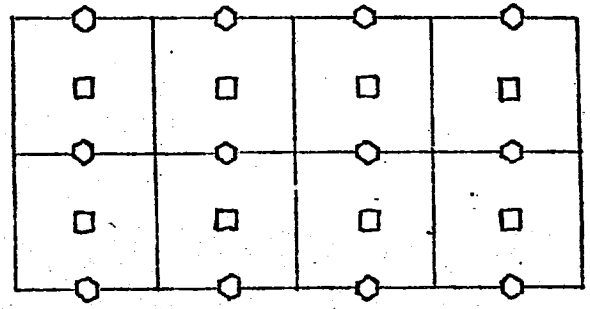

Vertical plane at half nodal section

O - u, v

Δ - C, Ps, Ω

⬡ - C

□ - Ω

Figure 12. Arrangement of variables in grid sections (Paul and Lick 1976).

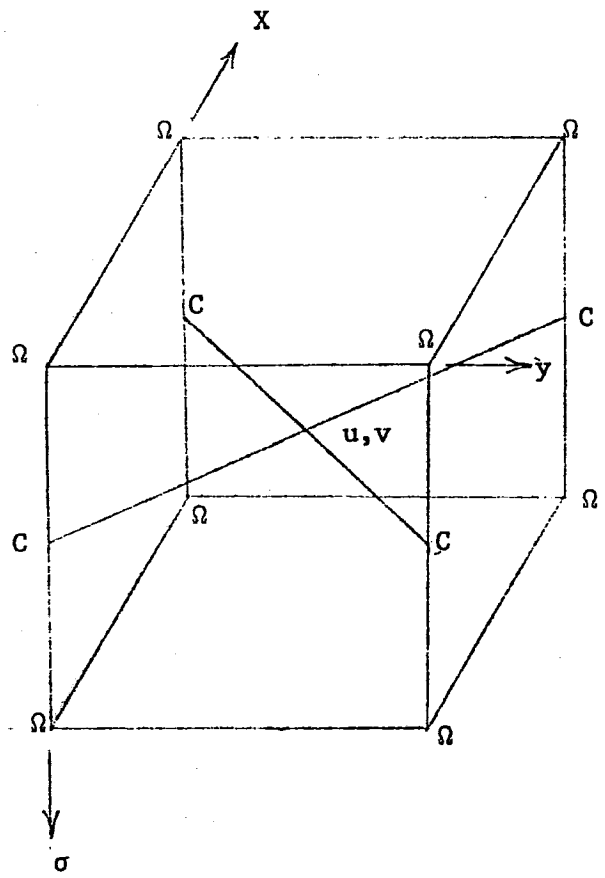

Typical nodal cell for u

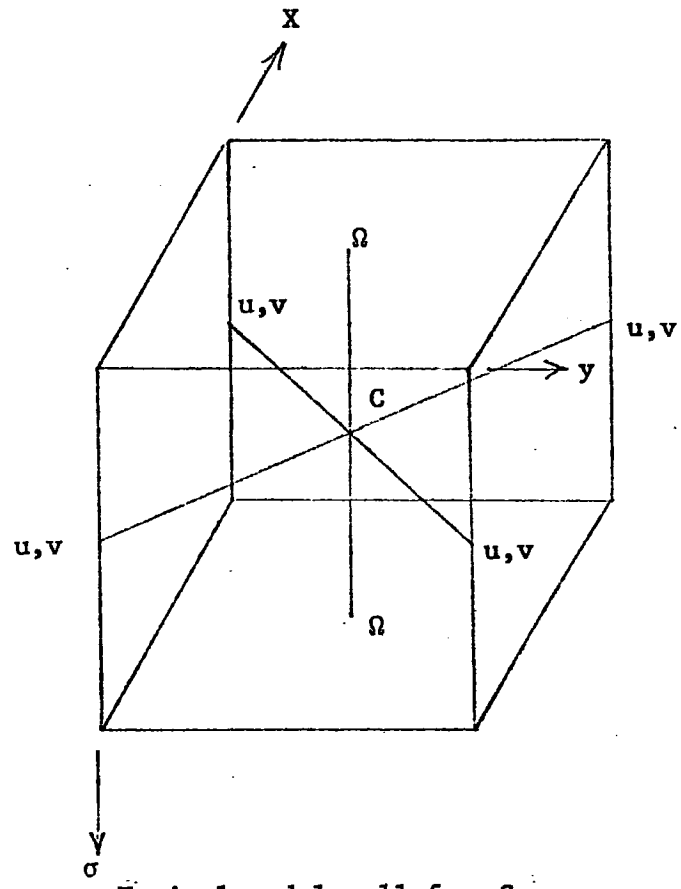

Typical nodal cell for C

Figure 13. Typical nodal cells for the grid system (Paul and Lick 1976).

For illustration purposes consider Equation 3.30

$$\frac{\partial u}{\partial t} - R_e \left(\frac{b_o}{h_o}\right)^2 \frac{1}{h^2} \frac{\partial e_{xz}}{\partial \sigma} \frac{\partial u}{\partial \sigma} = g(u) - \frac{\partial Ps}{\partial x} \tag{4.1}$$

where:

$$g(u) = R_e\left[\frac{1}{h} \frac{\partial}{\partial x}\left(2e_{xx} h \frac{\partial u}{\partial x}\right) + \frac{1}{h} \frac{\partial}{\partial y}\left(h e_{xy}\left(\frac{\partial u}{\partial y} + \frac{\partial v}{\partial x}\right)\right)\right.$$

$$\left. - \frac{1}{h} \frac{\partial}{\partial x}(hu^2) - \frac{1}{h} \frac{\partial}{\partial y}(huv) - \frac{\partial}{\partial \sigma}(\Omega u)\right] - R_o v$$

The finite difference scheme for g(u) which contains the horizontal viscous and nonlinear convection terms is:

$$\frac{4 R_e}{h(\Delta X_{n+1} + \Delta X)} \left[(e_{xx})_{n+1/2} \cdot h_{n+1/2} \left(\frac{u_{n+1} - u}{\Delta X_{n+1}}\right) - (e_{xx})_{n-1/2} h_{n-1/2}\right.$$

$$\left.\left(\frac{u - u_{n-1}}{\Delta x}\right)\right] + \frac{2R_e}{h(\Delta Y_{m+1} + \Delta Y)} \left[(e_{xy})_{m+1/2} h_{m+1/2} \left[\left(\frac{u_{m+1} - u}{\Delta y_{m+1}}\right) + \right.\right.$$

$$\left.\left. 2\left(\frac{v_{n+1/2,\, m+1/2} - v_{n-1/2,\, m+1/2}}{\Delta X_{n+1} + \Delta X}\right)\right] - (e_{xy})_{m-1/2} h_{m-1/2} \left[\left(\frac{u - u_{m-1}}{\Delta Y}\right)\right.\right.$$

$$\left.\left. + 2\left(\frac{v_{n+1/2,\, m-1/2} - v_{n-1/2,\, m-1/2}}{\Delta X + \Delta X_{n+1}}\right)\right]\right] - \frac{R_e}{h \Delta X} \left[h_{n+1/2} u^2_{n+1/2}\right.$$

$$\left. - h_{n-1/2} u^2_{n-1/2}\right] - \frac{R_e}{h \Delta y} \left[h_{m+1/2} u_{m+1/2} v_{m+1/2} - h_{m-1/2} u_{m-1/2} v_{m-1/2}\right]$$

$$- \frac{Re}{\Delta\sigma} [\Omega_{k+1/2} \, u_{k+1/2} - \Omega_{k-1/2} \, u_{k-1/2}] - Rov$$

The forward in time and centered in space (FTCS) scheme used for the convection terms was found to be inadequate, in some cases, for the transport equation. The first and second upwind-differencing methods, which possess the transportive property are outlined by Roache (1972). The second upwind differencing scheme which was used at times in the present study is defined as:

$$\frac{C^{\ell+1} - C}{\Delta t} = -\left(\frac{u_R C_R - u_L C_L}{\Delta X}\right)$$

where $$u_R = \left(\frac{u_{n+1} + u}{2}\right)$$

$$u_L = \left(\frac{u + u_{n-1}}{2}\right)$$

$C_R = C$ for $u_R > 0$, $C_R = C_{n+1}$ for $u_R < 0$

$C_L = C_{n-1}$ for $u_L > 0$, $C_R = C$ for $u_L < 0$

This method retains something of the second-order accuracy of centered space schemes. It is slower than FTCS method since the direction of the velocity components must be sensed during each calculation.

Equation 4.1 is solved explicitly at horizontal nodal points (N,M). The finite difference form is:

$$\frac{u^{\ell+1} - u}{\Delta t} - \left(\frac{b_o}{h_o}\right)^2 \frac{1}{h^2(\Delta\sigma)^2} \left[(e_{xz})_{k+1/2}(u_{k+1}^{\ell+1} - u^{\ell+1}) - (e_{xz})_{k-1/2}\right.$$

$$\left.(u^{\ell+1} - u_{k-1}^{\ell+1})\right] = g(u) - \frac{\partial Ps}{\partial x}$$

which is simplified to tridiagonal form for each vertical string of nodes

$$- \left(\frac{b_o}{h_o}\right)^2 \frac{1}{h^2(\Delta\sigma)^2} (e_{xz})_{k-1/2}\, u_{k-1}^{\ell+1} + \left(\frac{1}{\Delta t} + \left(\frac{b_o}{h_o}\right)^2 \frac{1}{h^2(\Delta\sigma)^2} [(e_{xz})_{k+1/2}\right.$$

$$\left. + (e_{xz})_{k-1/2}\right] u^{\ell+1} - \left(\frac{b_o}{h_o}\right)^2 \frac{1}{h^2(\Delta\sigma)^2} (e_{xz})_{k+1/2}\, u_{k+1}^{\ell+1} = g(u) + \frac{u}{\Delta t}$$

$$- \frac{\partial Ps}{\partial x} \qquad (4.2)$$

which can be written as:

$$A\bar{u} = \bar{G} + \bar{V} - \bar{I}\, \frac{\partial Ps}{\partial x} \qquad (4.3)$$

B. The Time Marching Procedure

The solution of the numerical model proceeds as follows for each time step.

1. It is assumed that values from the previous time step are available.
2. The concentrations are calculated by the horizontal explicit scheme with implicit vertical diffusion calculation.
3. The convective and horizontal viscous terms (G) are calculated for the momentum equation.
4. The u_Q and v_Q velocities are calculated explicitly at each nodal point in the horizontal plane (Eqs. 3.35 and 3.37).
5. The pressure field is solved.
6. u_P and v_P velocities are calculated (Eqs. 3.36 and 3.38) and hence the horizontal velocities (Eqs. 3.33 and 3.34).
7. The vertical velocity is calculated by vertically integrating the continuity equation.
8. The present time step is now complete.

C. Pressure Solution Technique

The Poisson equation stated in Chapter 3 is not directly used to derive finite difference approximations. The elliptic equation is solved by an iterative technique called successive overrelaxation (SOR).

$$Pnew = P^{\ell} + \omega(P^{\ell} - P^{\ell-1})$$

For convergence, it is required to find an optimum value of the relaxation factor ω. The optimum value depends on the mesh, the shape of the domain, and the type of boundary conditions (Roache 1976). ω must be determined experimentally since analytic evaluation exists for only a few problems. The experimental determination of ω is almost always worthwhile, since the Poisson equation must be solved at every iteration of the equation. It is usually best to slightly overestimate ω than to underestimate it (Carnahan et. al. 1969, Roache 1976).

Rather than assuming a constant ω a technique called Accelerated Successive Overrelaxation (ASOR) is available (Bedford and Rai) which estimates an optimal ω every three iterations.

$$\omega_{opt} = \frac{P^{\ell+1} - P^{\ell}}{2P^{\ell} - P^{\ell+1} - P^{\ell+1}}$$

$$\text{and Pnew} = P^{\ell} + \frac{(P^{\ell} - P^{\ell-1})^2}{2P^{\ell-1} - P^{\ell} - P^{\ell-2}}$$

The forcing term in the Poisson equation for the surface pressure involves a time derivative of the vertical velocity at the surface. The rigid lid condition is that this velocity is zero. However, by the numerical vertical integration of the continuity equation, some non-zero value for the vertical velocity at the surface is obtained. This deviation from zero is an indication that the continuity equation is not satisfied exactly by the difference solution. To avoid a significant accumulation of this error, it is generally necessary to use a very fine convergence criterion for the iteration

process. Usually, the required computing time increases rapidly with the increase in the fineness of the convergence criterion.

Hirt and Harlow (1967), suggested a technique that permits the use of a coarse convergence criterion by prohibiting the usual accumulation of error. The procedure involves the term $\frac{\partial \Omega}{\partial t}\Big|\sigma = 0$. This term is written as a simple backward time difference

$$\frac{\partial \Omega}{\partial t} = \frac{\Omega - \Omega^{\ell-1}}{\Delta t}\Big|\sigma = 0$$

Ω is set to zero because of the rigid lid approximation and $\Omega^{\ell-1}$ is set to the value calculated from the previous time step. This technique was successfully used by Paul and Lick (1973, 1976).

D. Solution Flow Chart

The following is the general flowchart for the computer program used to numerically solve equations 3.25 to 3.29.

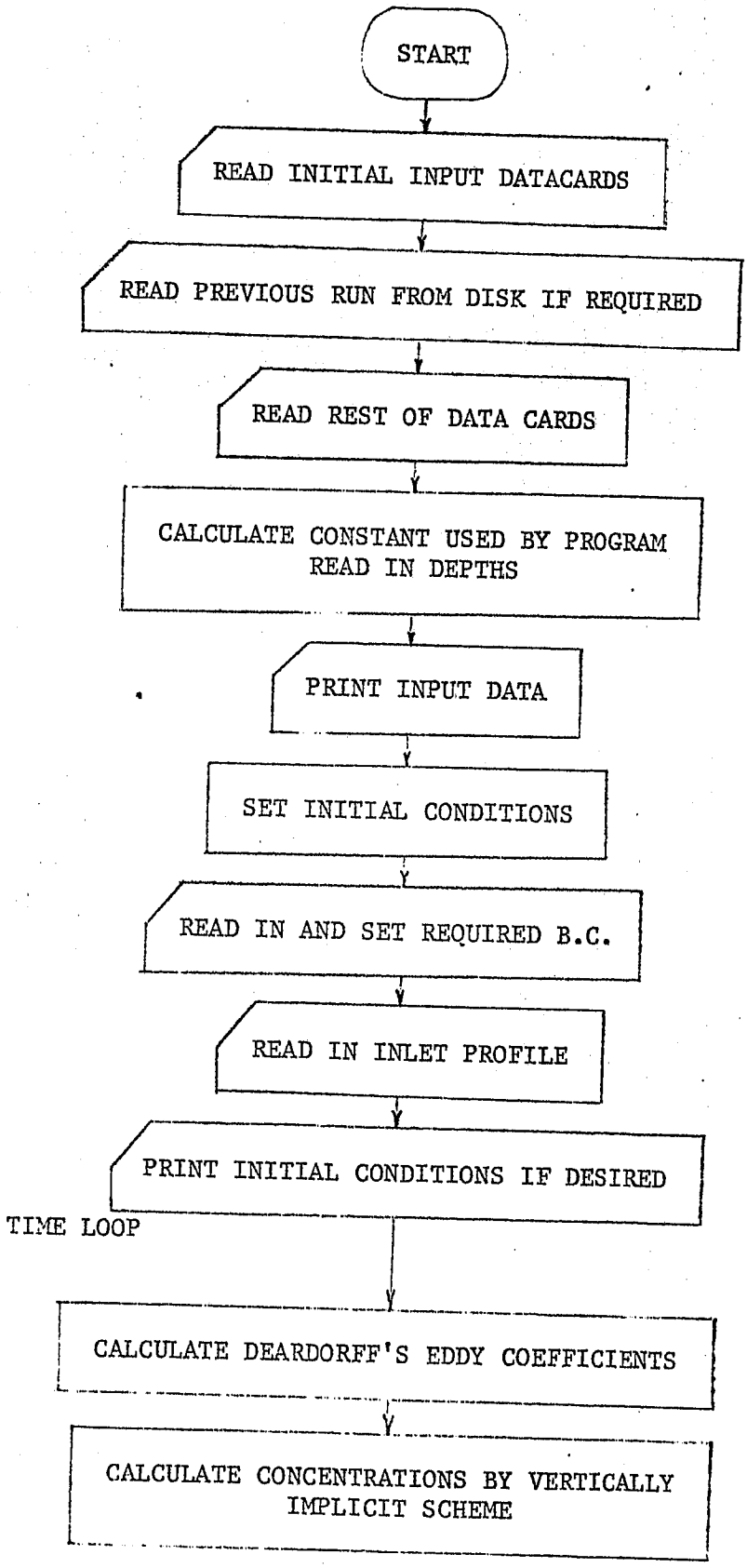
START
READ INITIAL INPUT DATACARDS
READ PREVIOUS RUN FROM DISK IF REQUIRED
READ REST OF DATA CARDS
CALCULATE CONSTANT USED BY PROGRAM
READ IN DEPTHS
PRINT INPUT DATA
SET INITIAL CONDITIONS
READ IN AND SET REQUIRED B.C.
READ IN INLET PROFILE
PRINT INITIAL CONDITIONS IF DESIRED
TIME LOOP
CALCULATE DEARDORFF'S EDDY COEFFICIENTS
CALCULATE CONCENTRATIONS BY VERTICALLY
IMPLICIT SCHEME

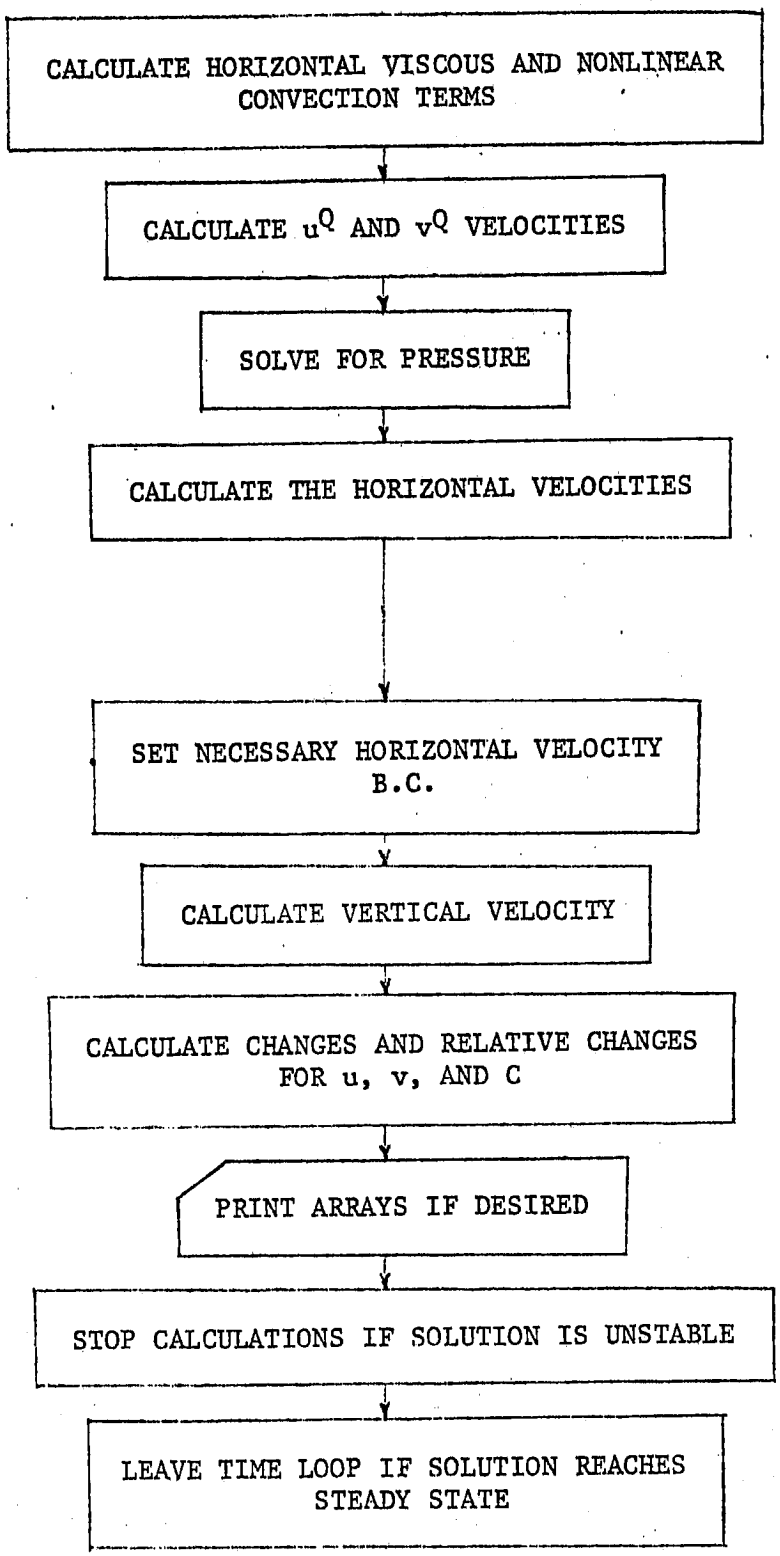

END OF TIME STEP

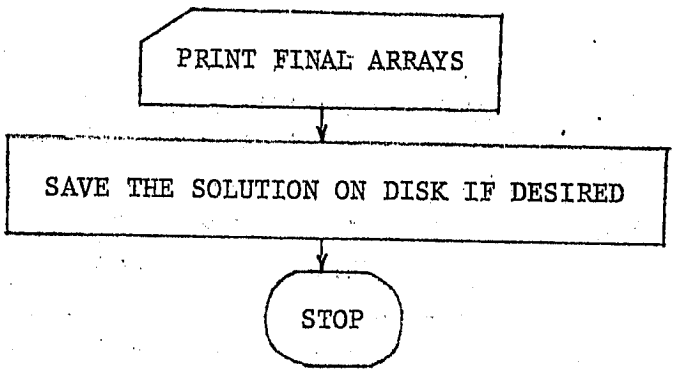
PRINT FINAL ARRAYS
SAVE THE SOLUTION ON DISK IF DESIRED
STOP

CHAPTER FIVE

PARAMETERS USED IN THE APPLICATION OF THE MODEL

A. Reference Length Scales and the Geometry of the Bay

The horizontal grid layout used for the Maumee Bay is shown in Figure 14. The basin was resolved with a 19 x 18 x 7 finite difference grid. The grid spacings in vertical direction were equal because of stretched coordinates. The nondimensional grid spacings in the horizontal directions are shown in Table 3. The reference length scale b_o in the horizontal direction was taken to be 1.09×10^6 cm, whereas the reference length h_o in the vertical direction was 915 cm.

All physical processes smaller than this grid size are approximately accounted for, handled, treated, by the SGS stresses. The molecular viscous stresses are neglected as mentioned earlier.

The nondimensional bottom topography is shown in Table 4. The shoals which appear on either sides of the channel have been explicitly taken care of. Unfortunately the geometry of Maumee Bay cannot be exactly represented by the grid. The finer the grid, the more accurately the geometry can be represented. But finer grids restrict the time step considerably, and therefore increase the computer storage and execution time. Smaller grid spacings were used at the mouth of Maumee River and the channel for better resolution.

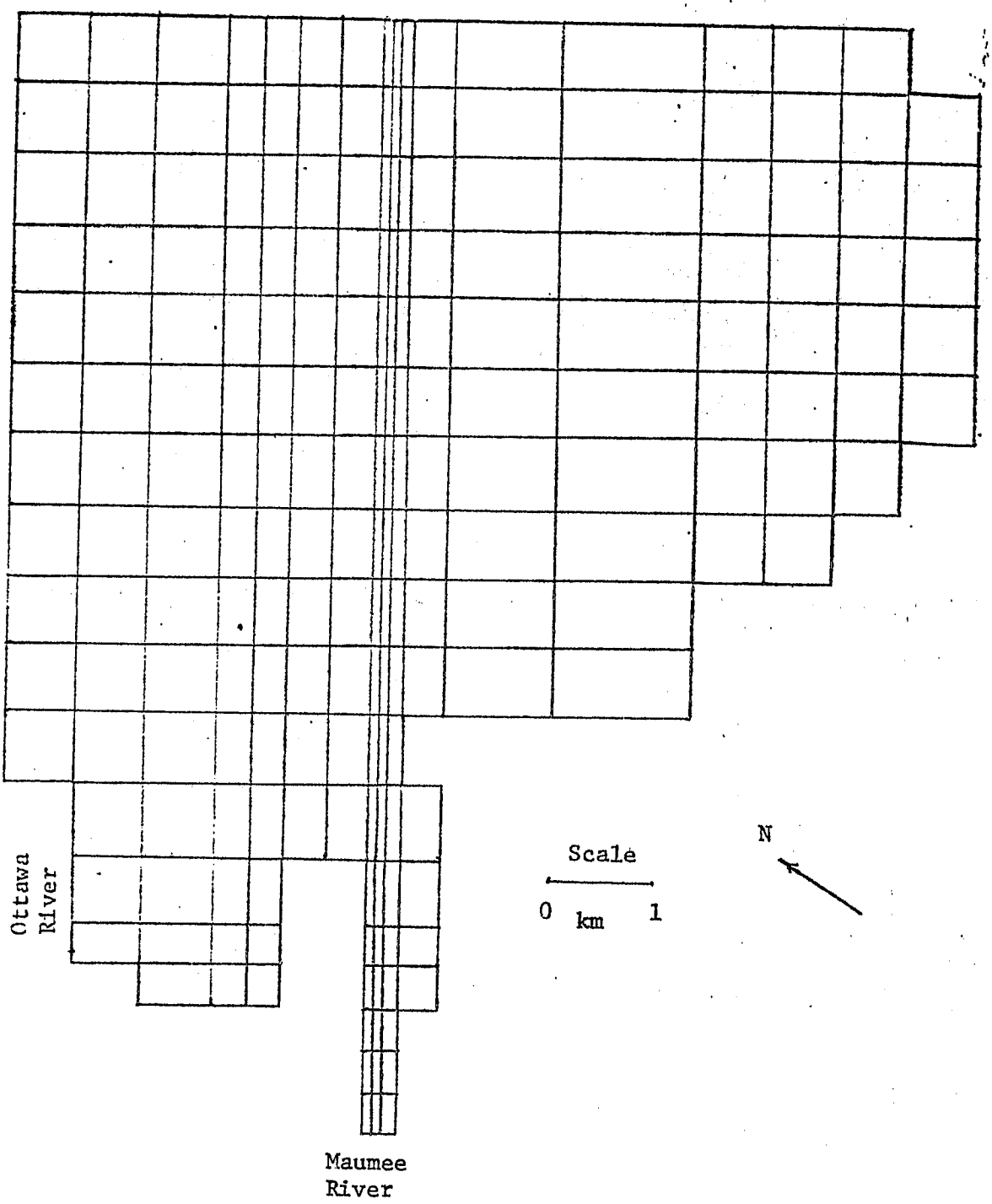

Figure 14. Horizontal grid layout for Maumee Bay.

Table 3. The nondimensional grid spacings for Maumee Bay.

```
X(N) =
 0.361000E-01 0.723000E-01 0.108400E+00 0.144600E+00 0.180700E+00 0.216900E+00 0.277100E+00 0.337300E+00 0.397600E+00 0.457800E+00
 0.513100E+00 0.578300E+00 0.638600E+00 0.698800E+00 0.759000E+00 0.819300E+00 0.879500E+00 0.939800E+00 0.100000E+01

Y(N) =
 0.0          0.602000E-01 0.120500E+00 0.180700E+00 0.210800E+00 0.241000E+00 0.277100E+00 0.313330E+00 0.319330E+00 0.325300E+00
 0.337300E+00 0.373500E+00 0.469900E+00 0.590400E+00 0.650600E+00 0.710800E+00 0.771100E+00 0.831300E+00
```

Table 4. The nondimensional bottom topography for Maumee Bay.

```
BOTTOM TOPOGRAPHY IS:
 1  0.333300E-01 0.333300E-01 0.333300E-01 0.333300E-01 0.333300E-01 0.333300E-01 0.333300E-01 0.333300E-01 0.933330E+00
    0.933330E+00 0.333300E-01 0.333300E-01 0.333300E-01 0.333300E-01 0.333300E-01 0.333300E-01 0.333300E-01 0.333300E-01
 2  0.333300E-01 0.333300E-01 0.333300E-01 0.333300E-01 0.333300E-01 0.333300E-01 0.333300E-01 0.333300E-01 0.933330E+00
    0.933330E+00 0.333300E-01 0.333300E-01 0.333300E-01 0.333300E-01 0.333300E-01 0.333300E-01 0.333300E-01 0.333300E-01
 3  0.333300E-01 0.333300E-01 0.333300E-01 0.333300E-01 0.333300E-01 0.333300E-01 0.333300E-01 0.333300E-01 0.933330E+00
    0.933330E+00 0.333300E-01 0.333300E-01 0.333300E-01 0.333300E-01 0.333300E-01 0.333300E-01 0.333300E-01 0.333300E-01
 4  0.333300E-01 0.333300E-01 0.333300E-01 0.333300E-01 0.333300E-01 0.333300E-01 0.333300E-01 0.333300E-01 0.933330E+00
    0.933330E+00 0.333300E-01 0.333300E-01 0.333300E-01 0.333300E-01 0.333300E-01 0.333300E-01 0.333300E-01 0.333300E-01
 5  0.333300E-01 0.333300E-01 0.333300E-01 0.140000E+00 0.133330E+00 0.333000E-01 0.333300E-01 0.333300E-01 0.933330E+00
    0.933330E+00 0.600000E+00 0.333300E-01 0.333300E-01 0.333300E-01 0.333300E-01 0.333300E-01 0.333300E-01 0.333300E-01
 6  0.333300E-01 0.333300E-01 0.126660E+00 0.150000E+00 0.140000E+00 0.333200E-01 0.333300E-01 0.333300E-01 0.933330E+00
    0.933330E+00 0.500000E+00 0.333300E-01 0.333300E-01 0.333300E-01 0.333300E-01 0.333300E-01 0.333300E-01 0.333300E-01
 7  0.333300E-01 0.333300E-01 0.140000E+00 0.150000E+00 0.150000E+00 0.333300E-01 0.333300E-01 0.333300E-01 0.933330E+00
    0.933330E+00 0.150000E+00 0.333300E-01 0.333300E-01 0.333300E-01 0.333300E-01 0.333300E-01 0.333300E-01 0.333300E-01
 8  0.333300E-01 0.333300E-01 0.120000E+00 0.150000E+00 0.150000E+00 0.166670E+00 0.116670E+00 0.200000E+00 0.933330E+00
    0.933330E+00 0.333300E-01 0.333300E-01 0.333300E-01 0.333300E-01 0.333300E-01 0.333300E-01 0.333300E-01 0.333300E-01
 9  0.666700E-01 0.116670E+00 0.173330E+00 0.166670E+00 0.193330E+00 0.173330E+00 0.133330E+00 0.233330E+00 0.933330E+00
    0.933330E+00 0.333300E-01 0.333300E-01 0.333300E-01 0.333300E-01 0.333300E-01 0.333300E-01 0.333300E-01 0.333300E-01
10  0.150000E+00 0.176670E+00 0.206670E+00 0.210000E+00 0.200000E+00 0.193330E+00 0.173330E+00 0.233330E+00 0.933330E+00
    0.933330E+00 0.333300E+00 0.160000E+00 0.173330E+00 0.333300E-01 0.333300E-01 0.333300E-01 0.333300E-01 0.333300E-01
11  0.150000E+00 0.176670E+00 0.156670E+00 0.206670E+00 0.200000E+00 0.210000E+00 0.193330E+00 0.226670E+00 0.933330E+00
    0.933330E+00 0.933330E+00 0.216670E+00 0.183330E+00 0.333300E-01 0.333300E-01 0.333300E-01 0.333300E-01 0.333300E-01
12  0.106670E+00 0.126670E+00 0.600000E-01 0.200000E+00 0.160000E+00 0.216670E+00 0.200000E+00 0.233330E+00 0.933330E+00
    0.933330E+00 0.933330E+00 0.216670E+00 0.240000E+00 0.173330E+00 0.173330E+00 0.333300E-01 0.333300E-01 0.333300E-01
13  0.106670E+00 0.126670E+00 0.126670E+00 0.140000E+00 0.166670E+00 0.183330E+00 0.200000E+00 0.233330E+00 0.933330E+00
    0.933330E+00 0.933330E+00 0.166670E+00 0.250000E+00 0.223330E+00 0.206670E+00 0.176670E+00 0.333300E-01 0.333300E-01
14  0.240000E+00 0.250000E+00 0.216670E+00 0.173330E+00 0.166670E+00 0.160000E+00 0.200000E+00 0.260000E+00 0.933330E+00
    0.933330E+00 0.933330E+00 0.133330E+00 0.280000E+00 0.243330E+00 0.216670E+00 0.190000E+00 0.176670E+00 0.333300E-01
15  0.303000E+00 0.293330E+00 0.276670E+00 0.246670E+00 0.233330E+00 0.233330E+00 0.216670E+00 0.260000E+00 0.933330E+00
    0.933330E+00 0.933330E+00 0.226670E+00 0.290000E+00 0.240000E+00 0.226670E+00 0.210000E+00 0.176670E+00 0.333300E-01
16  0.316670E+00 0.326670E+00 0.310000E+00 0.280000E+00 0.233330E+00 0.243330E+00 0.233330E+00 0.260000E+00 0.933330E+00
    0.933330E+00 0.933330E+00 0.226670E+00 0.303330E+00 0.250000E+00 0.226670E+00 0.210000E+00 0.180000E+00 0.333300E-01
17  0.350000E+00 0.350000E+00 0.250000E+00 0.206670E+00 0.233330E+00 0.243330E+00 0.250000E+00 0.293330E+00 0.933330E+00
    0.933330E+00 0.933330E+00 0.313330E+00 0.313330E+00 0.240000E+00 0.213330E+00 0.216670E+00 0.166670E+00 0.333300E-01
18  0.366670E+00 0.350000E+00 0.296670E+00 0.133330E+00 0.133330E+00 0.126670E+00 0.173330E+00 0.256670E+00 0.933330E+00
    0.933330E+00 0.933330E+00 0.226670E+00 0.243330E+00 0.140000E+00 0.113330E+00 0.106670E+00 0.333300E-01
19  0.366670E+00 0.333330E+00 0.276670E+00 0.246670E+00 0.213330E+00 0.213330E+00 0.200000E+00 0.300000E+00 0.933330E+00
    0.933330E+00 0.933330E+00 0.250000E+00 0.233330E+00 0.166670E+00 0.216670E+00 0.216670E+00 0.150000E+00 0.333300E-01
```

The spit A, mentioned in Chapter 2, was difficult to represent and the flow between Toledo Island and the spit was completely cut off. Also the area SW of the spit was considered to be too shallow and not included in the calculations. The subsequent calculations incorporating this field justified this assumption. Toledo Island and the Disposal Site were included in the grid layout.

The shoreline used in the model is determined by where the water depths become less than 2 feet. Zero depth could not be used the shoreline because the stretched coordinate transformation used becomes singular at zero depths. This approximation is not a restriction on the model because an extremely small amount of area is neglected compared to the total area modeled.

Table 5 shows the typical values for the Coriolis parameter, horizontal and vertical diffusivities, and the characteristic horizontal velocity for Lake Erie (Gedney and Lick, 1972).

Table 5. Typical values for characteristic parameters.

Reference Quantity	Maximum Value	Minimum Value
f, sec^{-1}	1.0×10^4	1.0×10^4
A_v, cm^2/sec	200	20
A_h, cm^2/sec	5×10^5	
u_o, cm/sec	15	

A vertical diffusion coefficient of 16.8 cm^2/sec was used for the constant eddy coefficient model.

Using the above reference parameters the Reynolds, Rossby, Froude, and turbulent Prandtl numbers were calculated as follows:

$$Re = \frac{u_o b_o}{A_H} = \frac{15 \times 1.09 \times 10^6}{5 \times 10^5} = 32.7$$

$$R_o = \frac{f b_o^2}{A_H} = \frac{10^{-4} \times (1.09 \times 10^6)^2}{5 \times 10^5} = 238.7$$

$$F_r = \frac{u_o}{\sqrt{g h_o}} = \frac{15}{(980 \times 915)^{1/2}} = 0.01568$$

$$P_r = \frac{AH}{B_H} = 1.0$$

B. Settling Velocity

Although other materials besides quartz may be present in appreciable quantities, the average specific gravity of sediment is very close to that of quartz, i.e., 2.65 and this value will be used for all calculations.

The particles are assumed to be spherical and small enough to obey Stokes Law. A standard formula (Yalin 1977, Graf 1973, V. Vanoni 1975) is used for the settling velocity:

$$w_s = 0.056(\gamma_s - \gamma)D^2/\mu;$$

where: γ_s = specific weight of sediment particles;

D = sphere diameter;

μ = absolute viscosity; and

γ = specific weight of fluid.

A design particle size of 1/64 mm was considered, with both larger (1/8 mm) and smaller (1/256 mm) sizes used for delimiting calculations. Hence $w_s = 0.056 \times 1.65 \left(\frac{1}{640}\right)^2 + \left(\frac{980}{1.79 \times 10^{-2}}\right) = 0.0123$ cm/sec.

C. Wind Calculations

It is necessary to know the horizontal shear stress imposed as a boundary condition at the surface of the bay. This stress is due to wind action. The relation of this stress to the wind speed is very difficult to determine from theoretical considerations and its value is usually based on semi-empirical formulas and on observations. Lick (1976) stated a general relationship between the wind speed and stress

$$\tau = \rho_a C_d \left| W_a^{n-1} \right| W_a;$$

where: C_d = drag coefficient;

ρ_a = density of air;

W_a = wind velocity 10 m above the water surface; and

n = empirically determined exponent not necessarily an integer.

Wilson (1960) has analyzed data from many different sources and has given a best fit (Figure 15). According to him:

$\tau = 0.00237\rho_a W_a^2$ for strong winds and $\tau = 0.00166\ \rho_a W_a^2$ for light winds.

The wind speeds have to be measured over the lake at a specified height. Gedney and Lick (1972) observed that winds over the lake may be higher than those measured on land by as much as a factor of 1.48.

A wind speed of 1m/sec, corresponds to a stress of 2.2×10^{-2} dynes/cm^2. The nondimensional stress is $h_o\tau = h_o\left(\frac{\tau\ Re}{\rho_o g h_o Fr^2}\right) = 3.0$.

D. Scaling Parameter (α) for SGS Eddy Coefficients

The c of Deardorff (1969) (Eq. 3.23) is approximately equal to $2^{1/4}\alpha^{1/2}$. Lilly (1967) suggested c = 0.17 while Deardorff (1969) choose c = 0.10 for his numerical model. Back calculating α should be between 0.0204 and 0.0071.

Spraggs and Street (1975) used $\alpha = 1.0 \times 10^{-2}$ for their approximate SGS model, but concluded that $\alpha = 0.000354$, for the complete model, produces most reasonable results.

For the present study α was taken to be 0.000354. There is considerable speculation about the applicability of a constant α. The above value of α was assumed to be appropriate for all ΔX, ΔY, and $\Delta\sigma$.

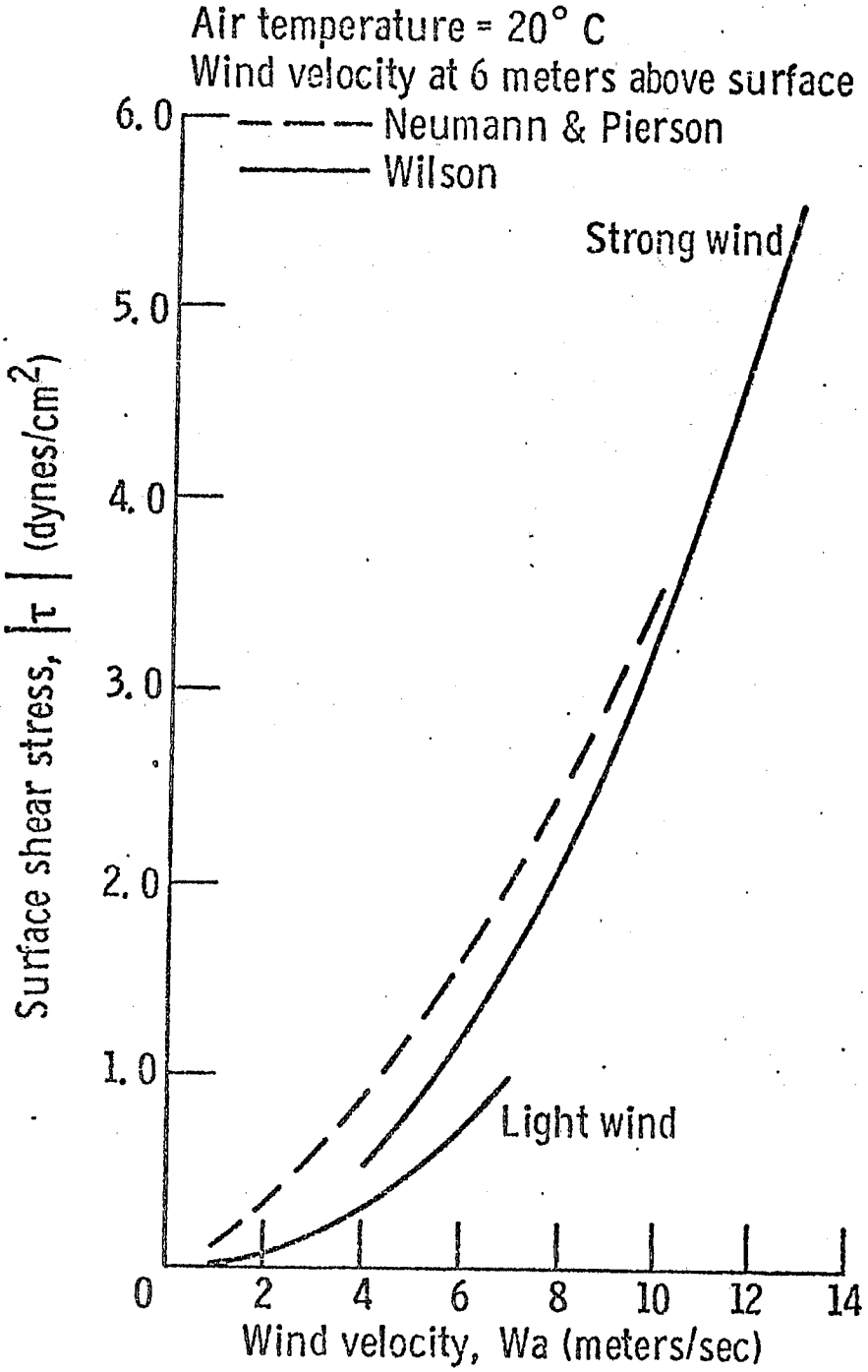

Figure 15. Wind shear stress relation (Lick 1976).

CHAPTER SIX

RESULTS

All the results for the three-dimensional model of Maumee Bay presented in this chapter were obtained on a IBM 370/168 computer. The results are presented to indicate the qualitative effects of introducing sediment from the Maumee River into the Bay. The mechanisms of sediment transport within the Bay are studied but actual simulation, with specified open water boundary conditions, was not carried out.

As seen in Figure 3, 15% of the time the maximum discharge (in a year) of Maumee River was equal to or greater than 60,000 cfs. This study concentrates on peak flows during February and March when the sediment loading into the Bay is the highest, hence a design discharge of 60,000 cfs is considered for all the results. Herdendorff and Zapotosky (1977) indicated a 301 mg/l concentration for the total suspended solids in Maumee River for 1976. The concentration is nondimensionalized by C/C_{ref}, hence a dimensionless concentration of 1.0 was used at the mouth of the Maumee Bay. By choosing an appropriate C_{ref} the actual concentration can be obtained by simple multiplication. All the concentration contours are plotted for this nondimensional inlet. The model was run with the specified inlet velocities, concentrations and with the boundary conditions and the relevant

parameters indicated in Chapter five until a quasi-steady state was reached. For a small bay such as the Maumee, the Coriolis force was found to be negligible.

This chapter is organized as follows. Section A explains the pressure solution; the effects of horizontal viscosities together with SGS model results are explained in Section B; Section C delineates the sediment transport mechanisms within the Basin; the Ottawa River influence is presented in Section D; Section E deals with the wind effects; and the last Section gives some estimates of the computational costs involved.

A. Pressure Solution

As explained in previous sections two iterative techniques were used to solve the pressure equation. Tests were carried out to establish the optimum SOR parameter ω. As seen in Figure 16 a value of 0.3 for ω gave the best rate of convergence. Unfortunately the ASOR method was not found to be as effective as SOR method when the optimum ω was used. Hence for all further calculations the SOR method, with ω equal to 0.3, was used.

B. Effect of Horizontal Viscosities

The effect of varying the horizontal eddy viscosities on the flow field was studied. The horizontal viscosities in the two directions were taken to be equal since the length scales involved are the same in both directions as seen in Figure 14. In this section, only the flushing of Maumee River outflow into the Bay was considered. Ottawa River inlet, wind and sediment concentrations were not taken

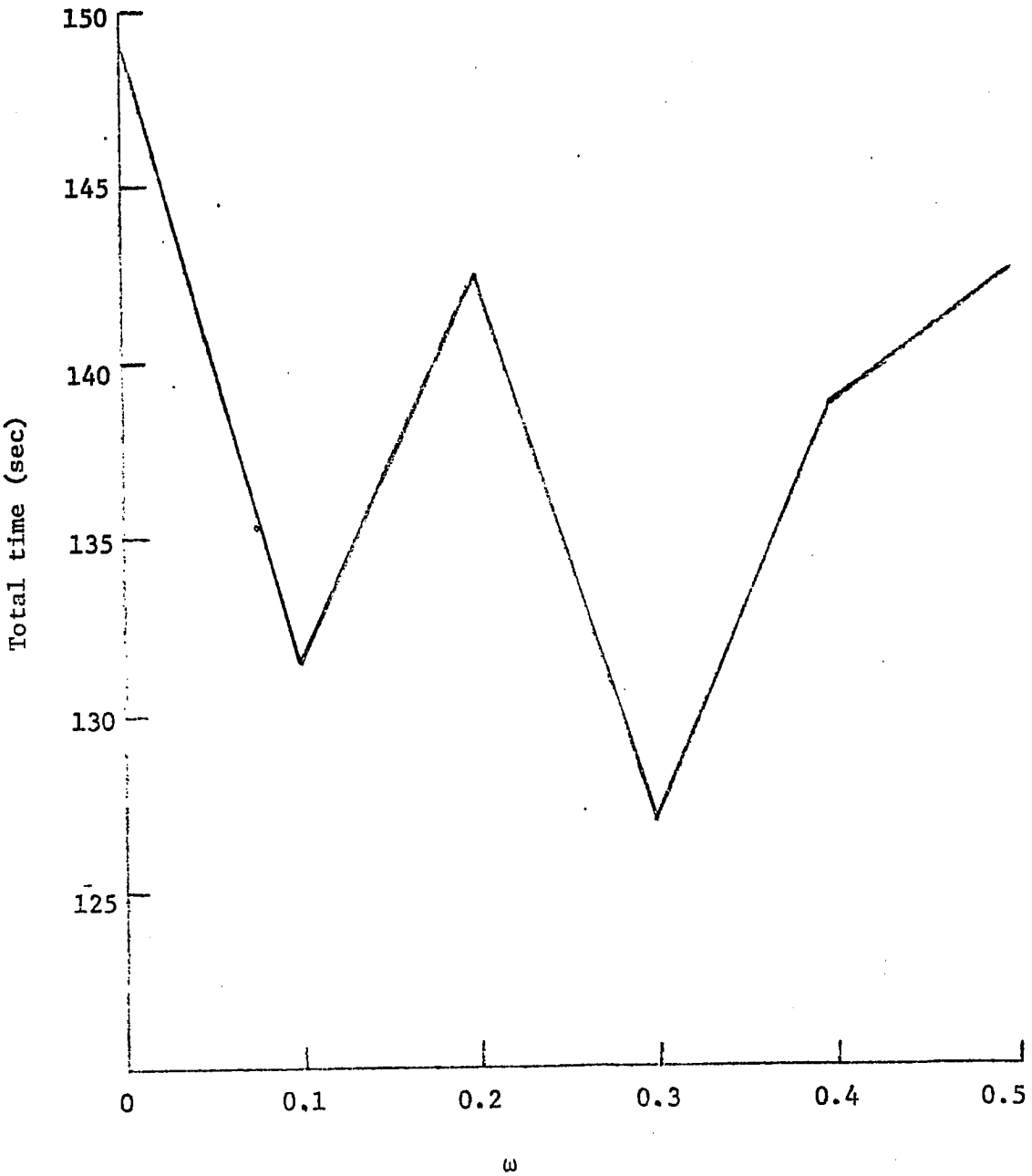

Figure 16. SOR Convergence testing.

into account.

The velocities in the vicinity of the Maumee River inlet were large compared to the other velocities in the Bay. Figure 17 shows a typical profile of the velocities near the inlet on a large scale for 1000 cm^2/s viscosity. Since all future plots were on a smaller scale the velocities near the inlet were not plotted.

The velocity profiles for 1000; 10,000; 50,000; and 500,000 cm^2/s viscosities at the surface and 15.0 ft depth are shown in Figures 18 to 25. Stronger currents close to the channel and greater circulation patterns were obtained as the viscosities were increased. The horizontal viscosities introduced a flux opposing the convection due to the shoreline configuration.

The velocity profiles for the SGS viscosity model at the surface and 15.0 ft depth are shown in Figures 26 and 27. Because they are proportioned to the local velocity deformation, the SGS viscosities vary a great deal over the flow field, however, they are approximately 1000 cm^2/s. The shoals on either side of the channel were represented implicitly in the model by using the appropriate bottom topography. These spoil banks exert a great influence on the characteristics of the Bay and its effect was depicted by the SGS viscosity model. Even when the flow convects more (for low viscosities) and there is less damping the constant viscosity model did not show the same effect.

In all cases it was found that there was a stronger flow north along the Michigan shore compared to the flow east along the Ohio shore.

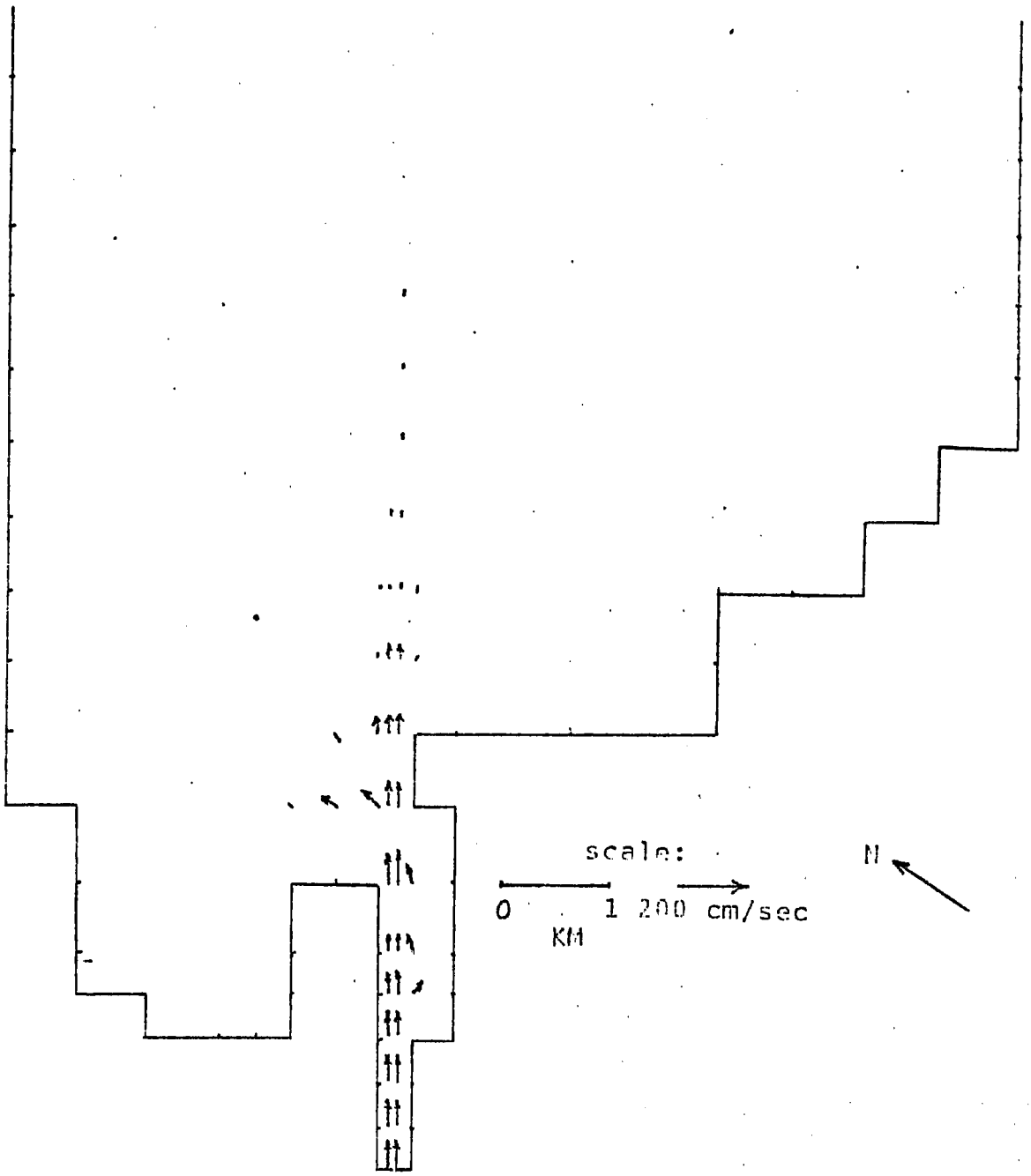

Figure 17. Velocity profile at inlet.

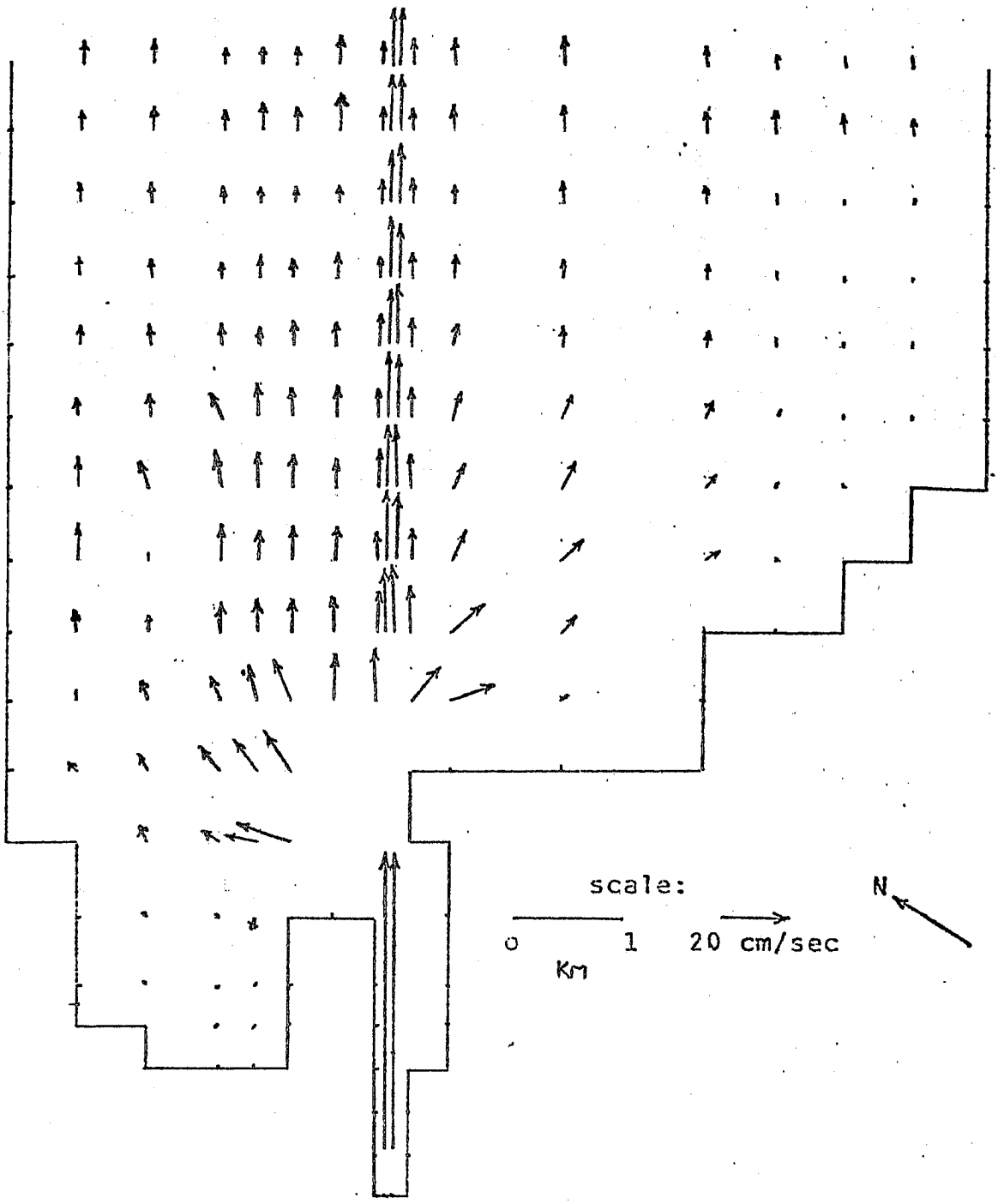

Figure 18. Surface velocities for 1000 cm^2/s viscosity.

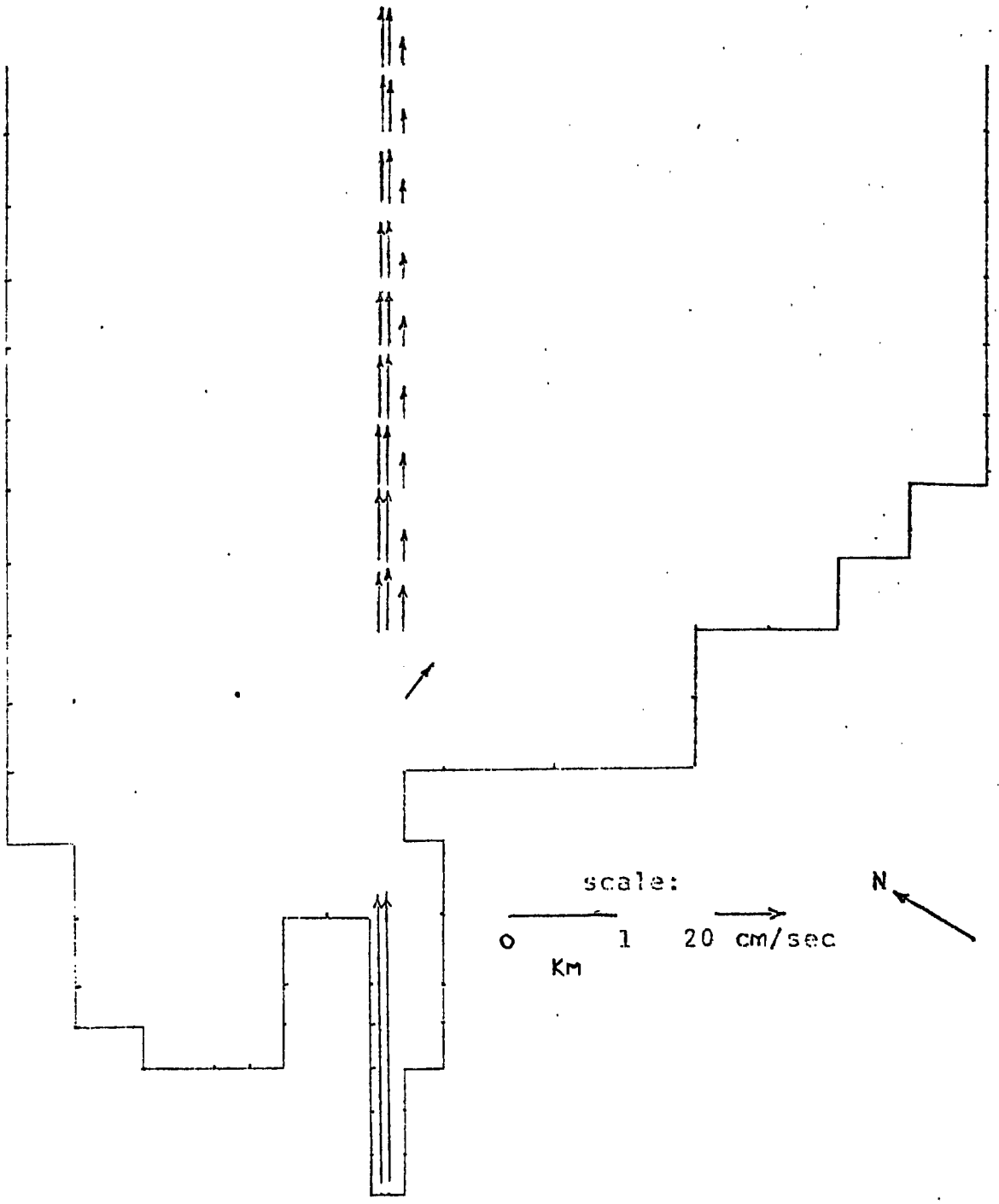

Figure 19. Velocities at 15.0 ft for 1000 cm^2/s viscosity.

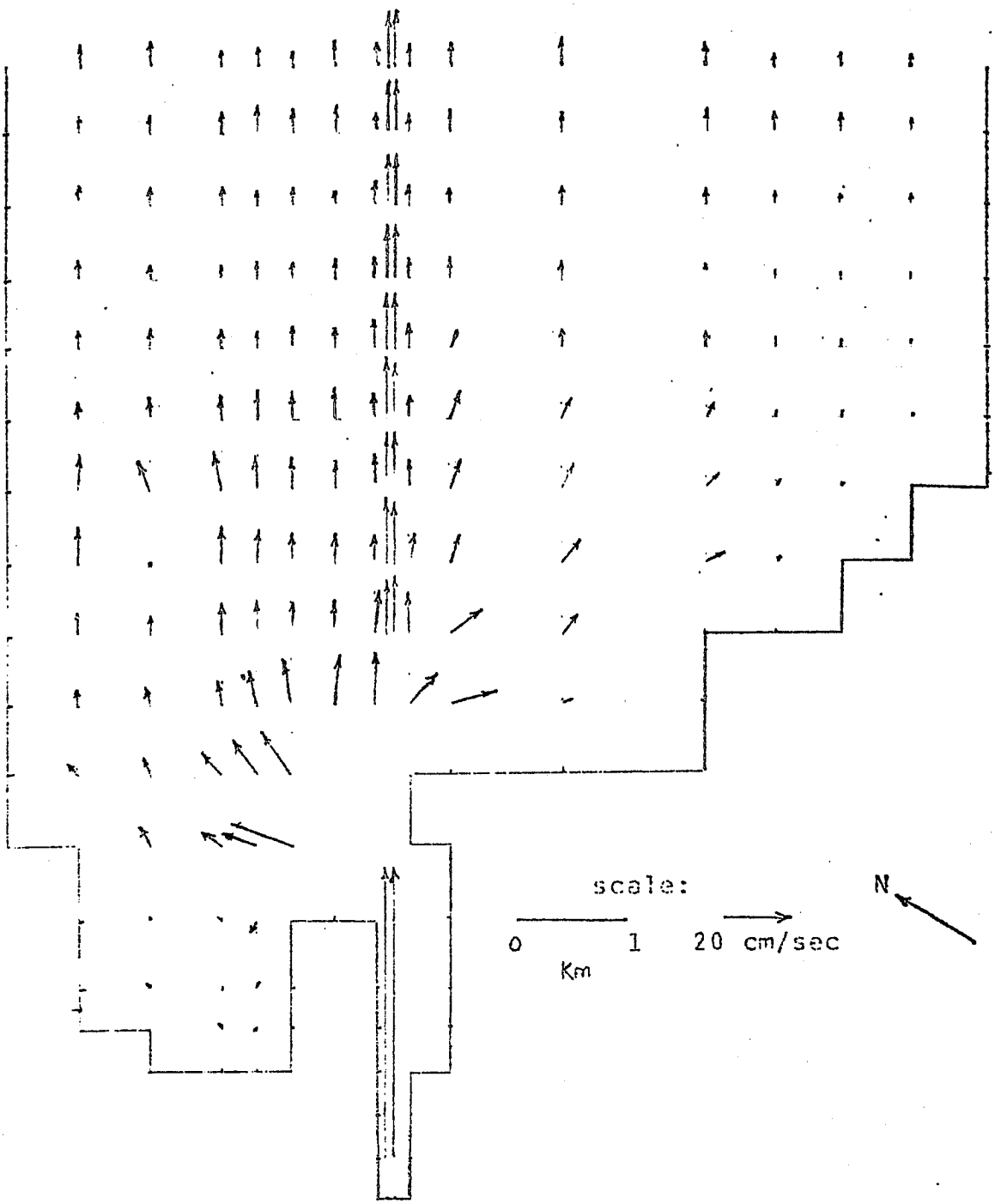

Figure 20. Surface velocities for 10,000 cm^2/s viscosity.

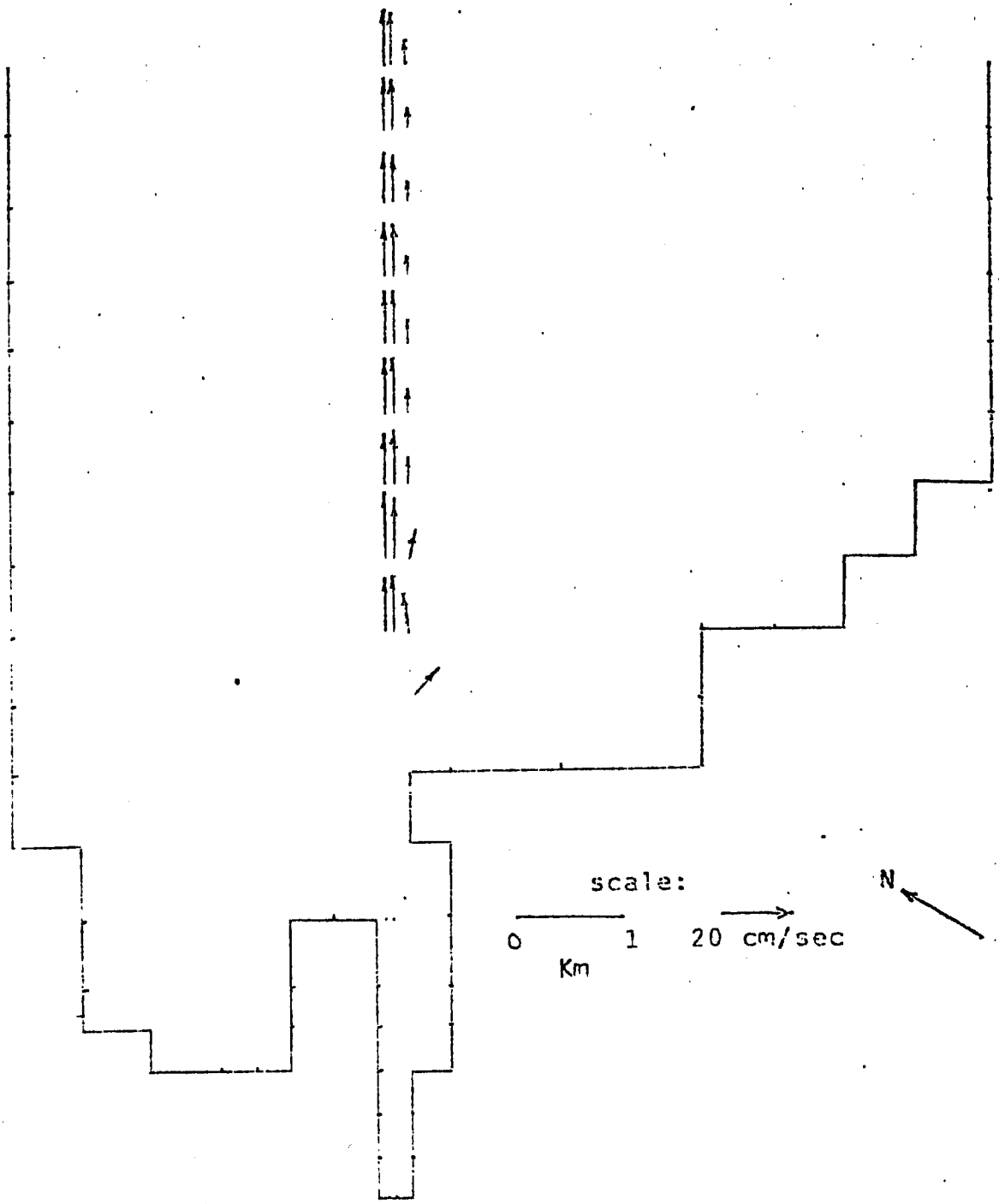

Figure 21. Velocities at 15.0 ft for 10,000 cm^2/s viscosity.

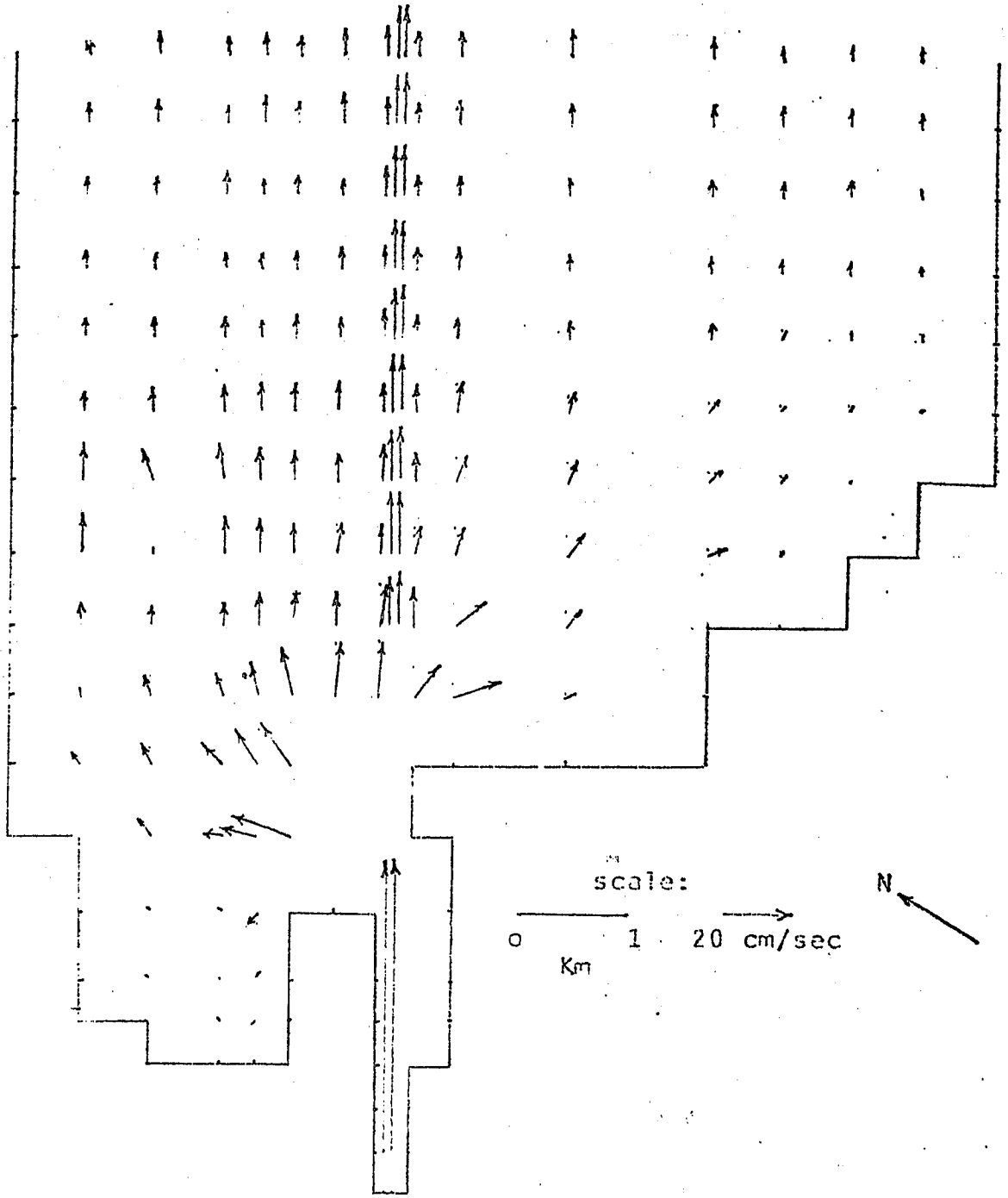

Figure 22. Surface velocities for 50,000 cm^2/s viscosity.

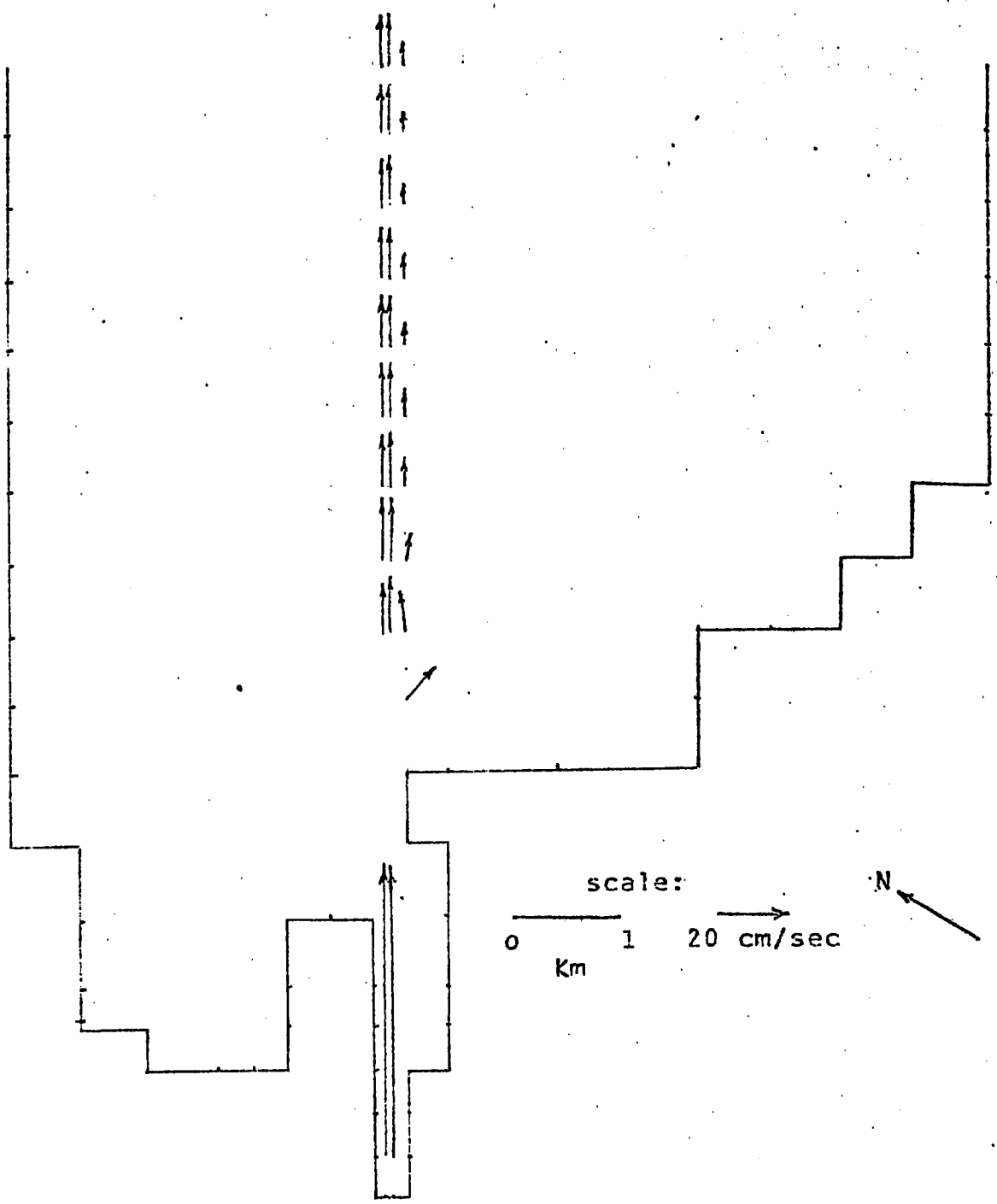

Figure 23. Velocities at 15.0 ft for 50,000 cm^2/s viscosity.

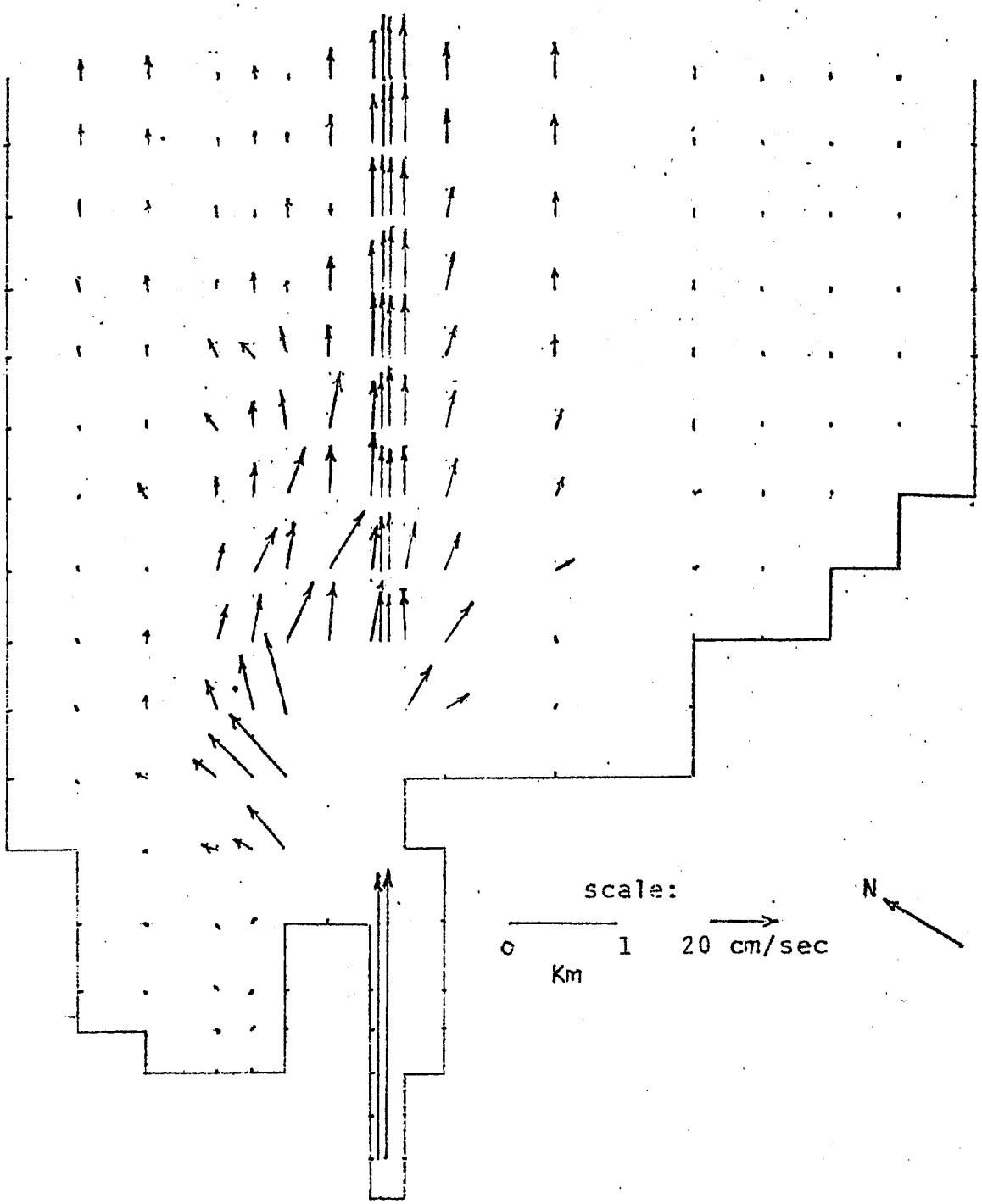

Figure 24. Surface velocities for 500,000 cm^2/s viscosity.

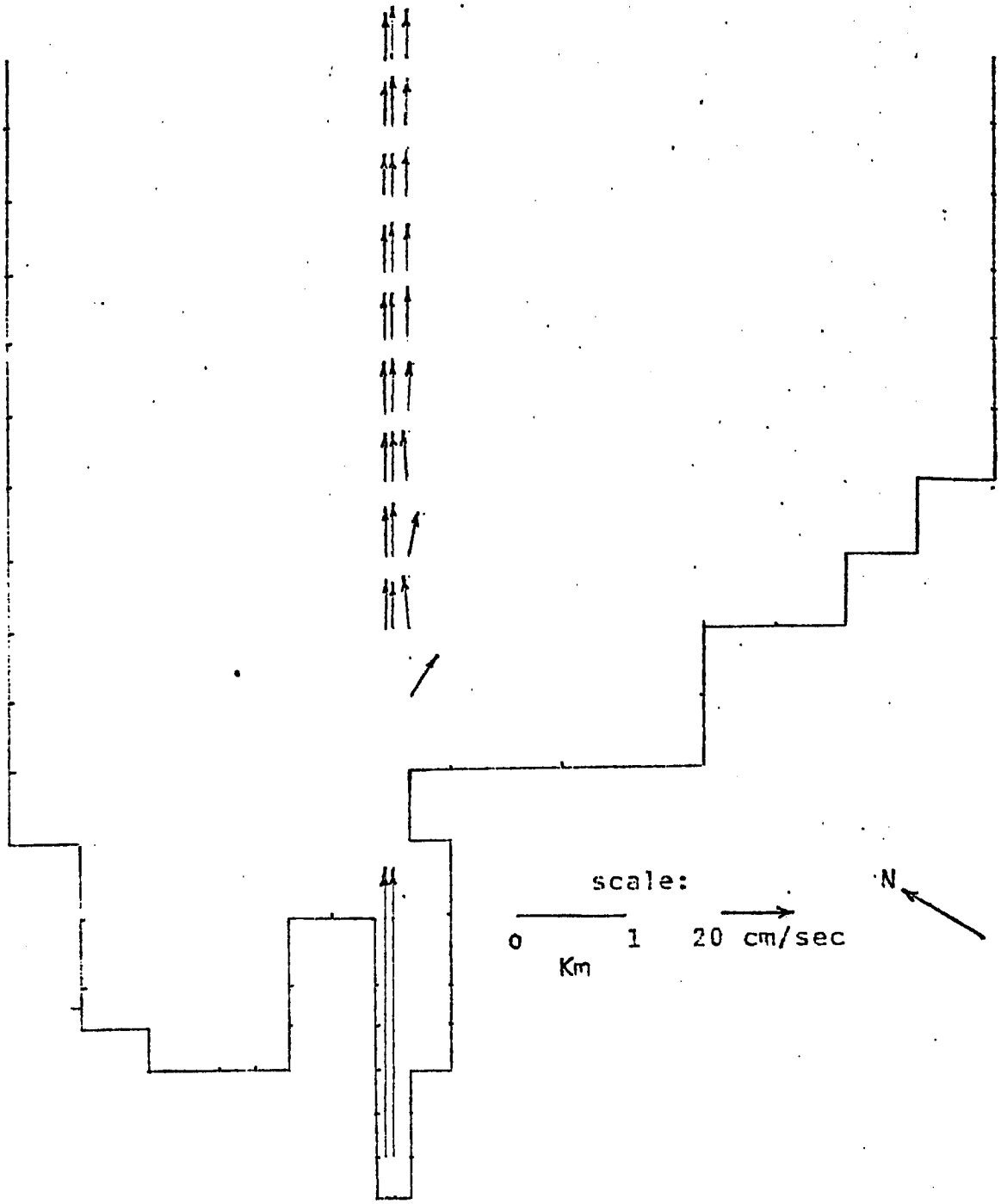

Figure 25. Velocities at 15.0 ft for 500,000 cm^2/s viscosity.

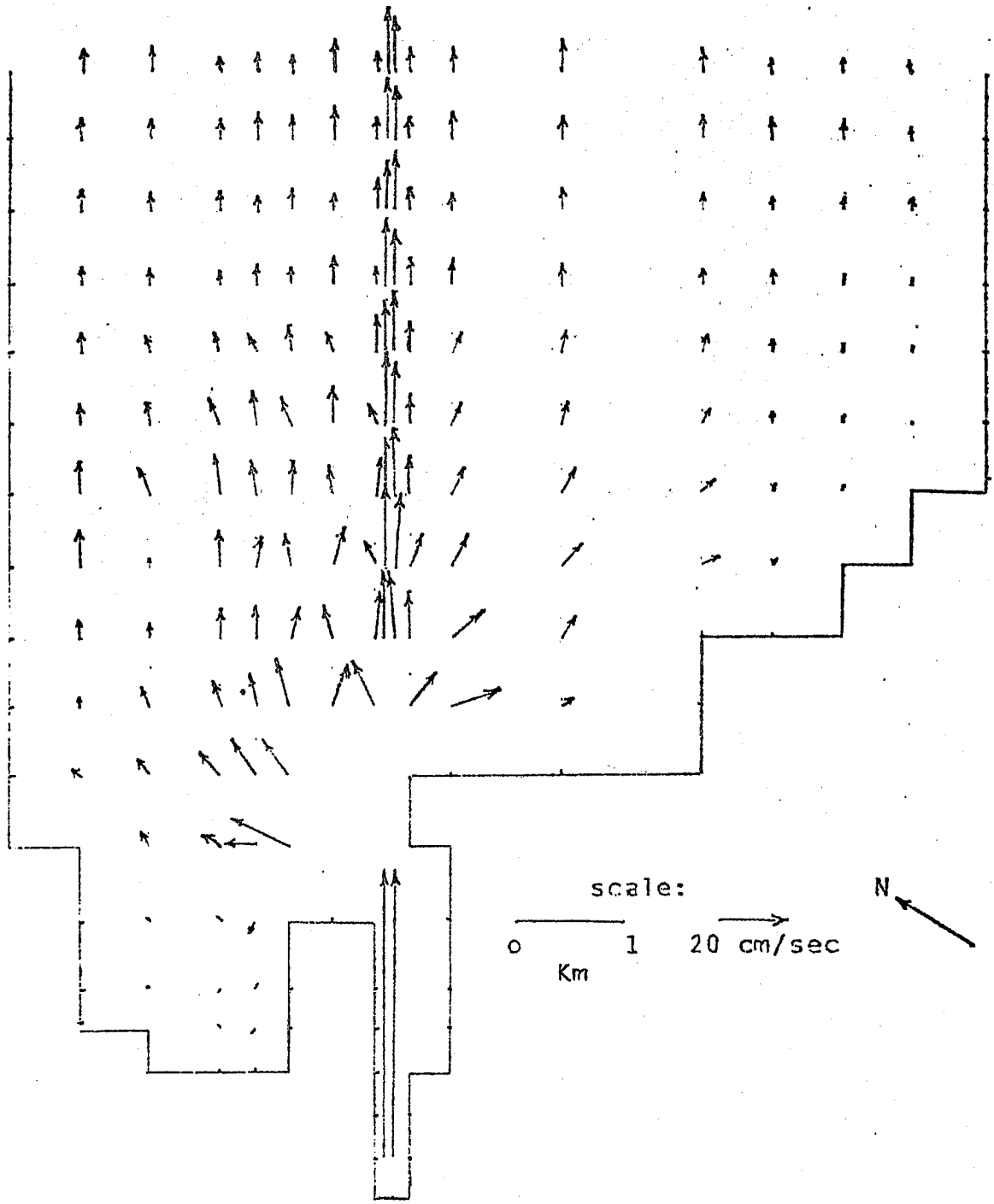

Figure 26. Surface velocities for SGS eddy coefficients.

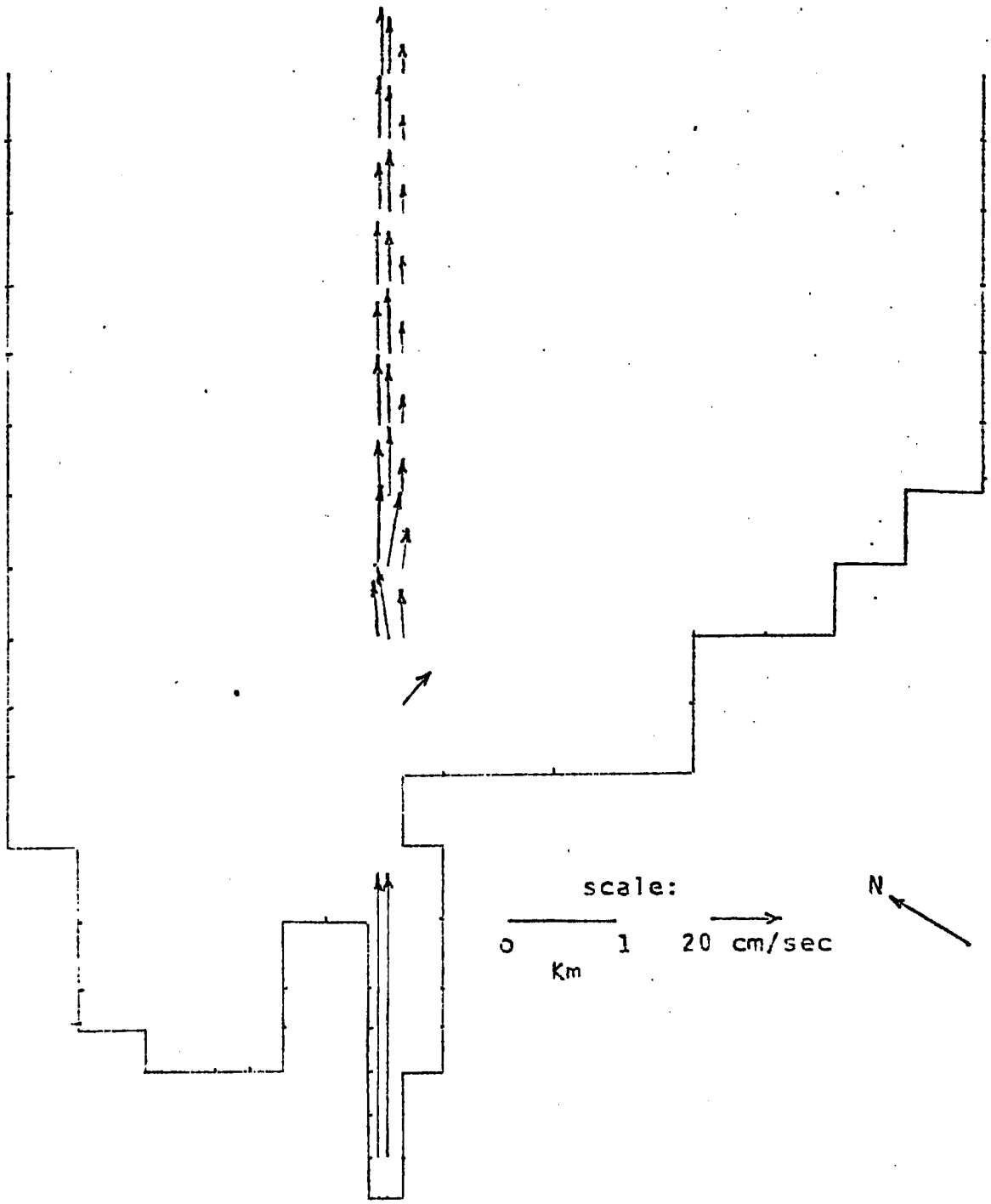

Figure 27. Velocities at 15.0 ft for SGS eddy coefficients.

The vertical velocities were found to be significant only close to the channel. Ignoring the local effects there was a general upwelling on the left side and downwelling on the right edge of the channel. Also it can be seen from the figures that the horizontal velocities at the surface and 15.0 ft depth vary considerably indicating a boundary layer effect. By considering vertically averaged velocities the accuracy of the results is lost, hence a three-dimensional model is essential.

C. Sediment Transport Mechanisms

All the sediment transport results were obtained with the SGS viscosity model and the effect of Ottawa River and wind was not considered.

A scheme was set up to obtain and compare the total mass/sec inflow and outflow from the Bay. This was done by multiplying the concentration and discharge for each cell at the inlet and outlet and summing over the total area of the two boundaries.

In the following section, Section 1, the effect of two boundary conditions on the sediment distributions is investigated. Section 2 deals with the particle size and Section 3 details the effects of horizontal viscosities.

1. Boundary Conditions.

The concentration distributions were calculated with two bottom boundary conditions, (1) a reflective bottom and (2) a perfectly absorbing bottom as explained in the previous sections.

Figures 28 and 29 show the concentration contours for a particle sinking velocity of 0.0123 cm/s and the two bottom boundary conditions. Steady state is reached 21.53 hrs after the sediment is introduced. It can be seen from the figures that for a perfectly absorbing bottom most of the sediment is deposited within a short distance from the inlet, hence very little is transported into Lake Erie. Only 2% of the sediment introduced into the Bay is transported out of it and the rest of it is deposited in the Bay. Whereas for a reflective bottom condition about 85% of the sediment introduced into the Bay is transported out of it.

The vertical concentration contours at four horizontal locations (9,1), (9,18), (4,9), and (14,17) for the two boundary conditions are shown in Figures 30 and 31. The first two locations are in the channel and the other two are on either side of it. Note that the vertical scales used are different since the depths vary considerably. The concentration was found to increase with depth at all points for the reflective bottom condition but the concentration was fairly uniform from the surface to near bottom for the absorbing bottom condition.

2. Particle Size.

Two extreme particle sizes of 1/8 mm and 1/256 mm with a sinking velocity of 0.788 cm/s and 0.0008 cm/s where considered to study the effect of gravitational settling. The concentration profiles for the two particle sizes and the bottom boundary conditions are shown in Figures 32 to 35. The lighter particle should take longer to settle down and hence it has more chance of being carried out of the

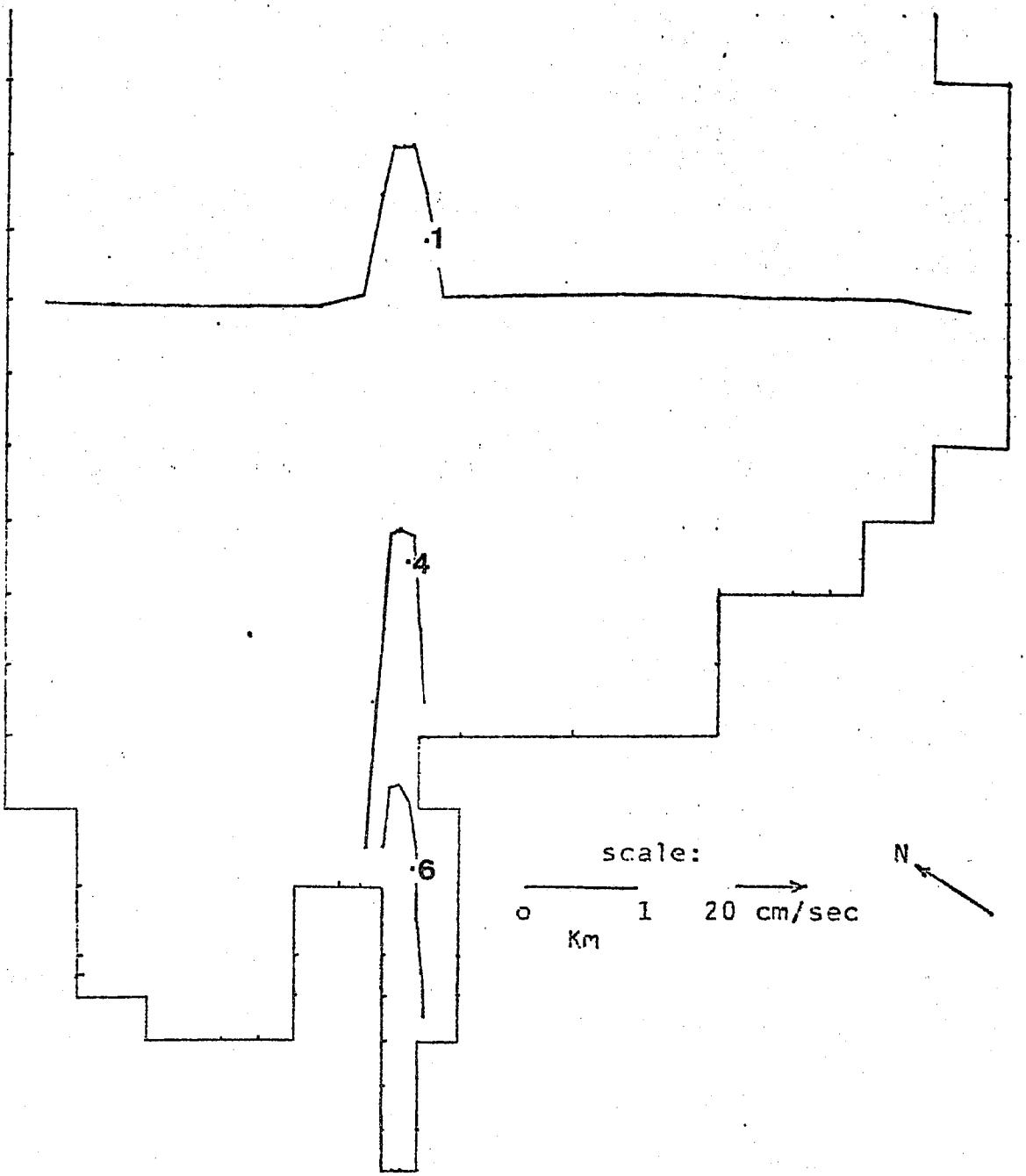

Figure 28. SGS model concentration contours for absorbing bottom and particle sinking velocity of 0.0123 cm/s.

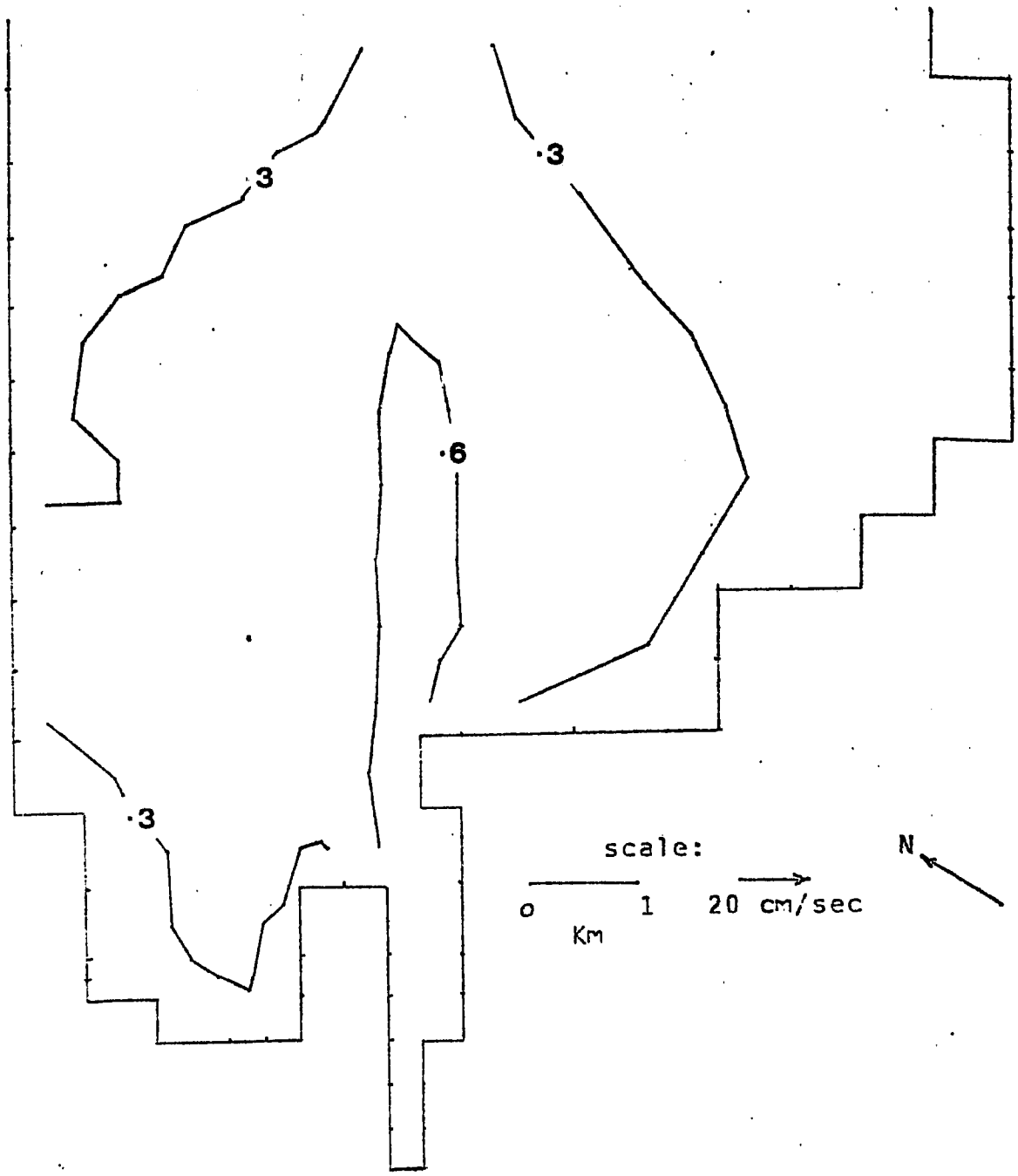

Figure 29. SGS model concentration contours for reflecting bottom and particle sinking velocity of 0.0123 cm/s.

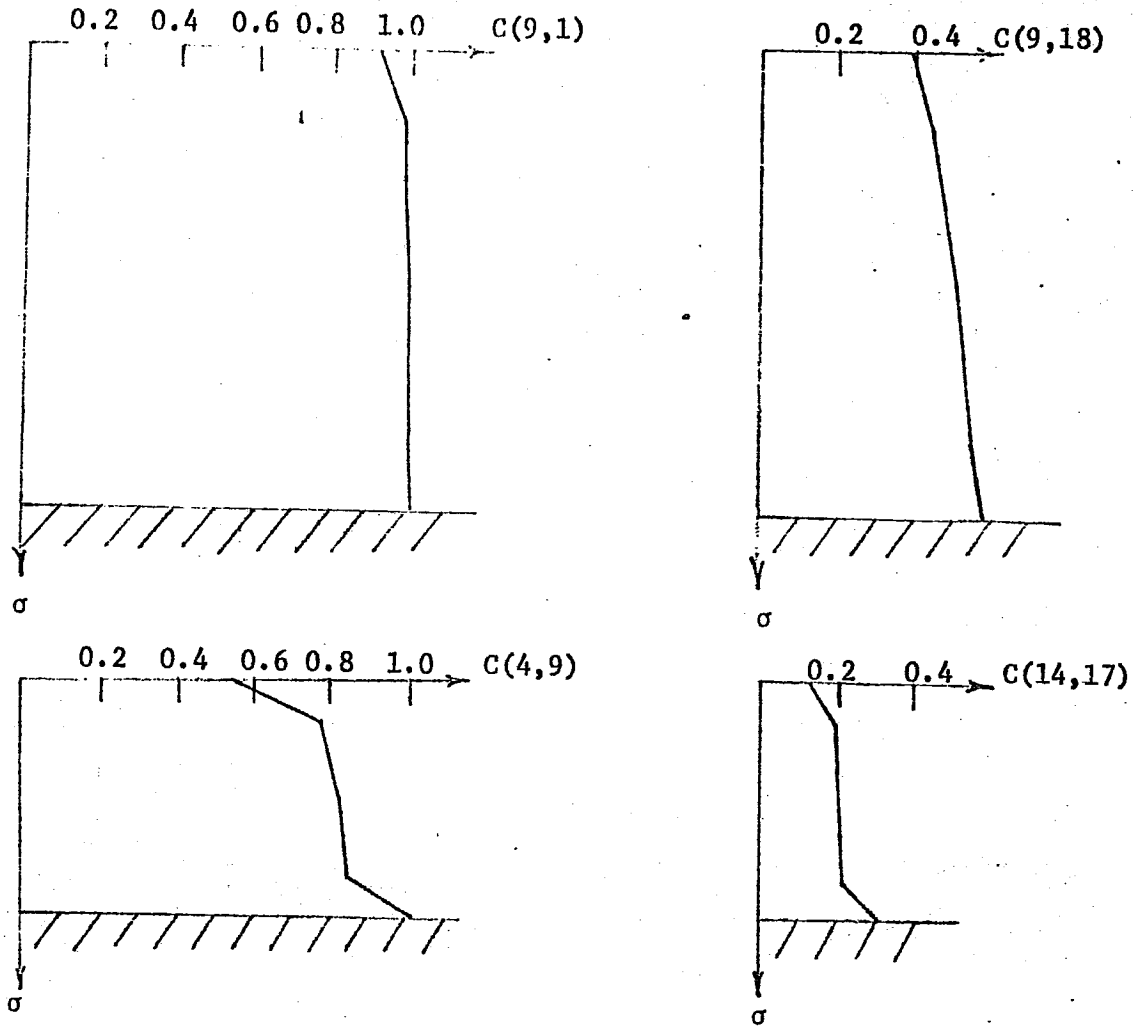

Figure 30. Vertical profiles of concentration at (M,N) = (9,1), (9,18), (4,9) and (14,17) for reflecting bottom.

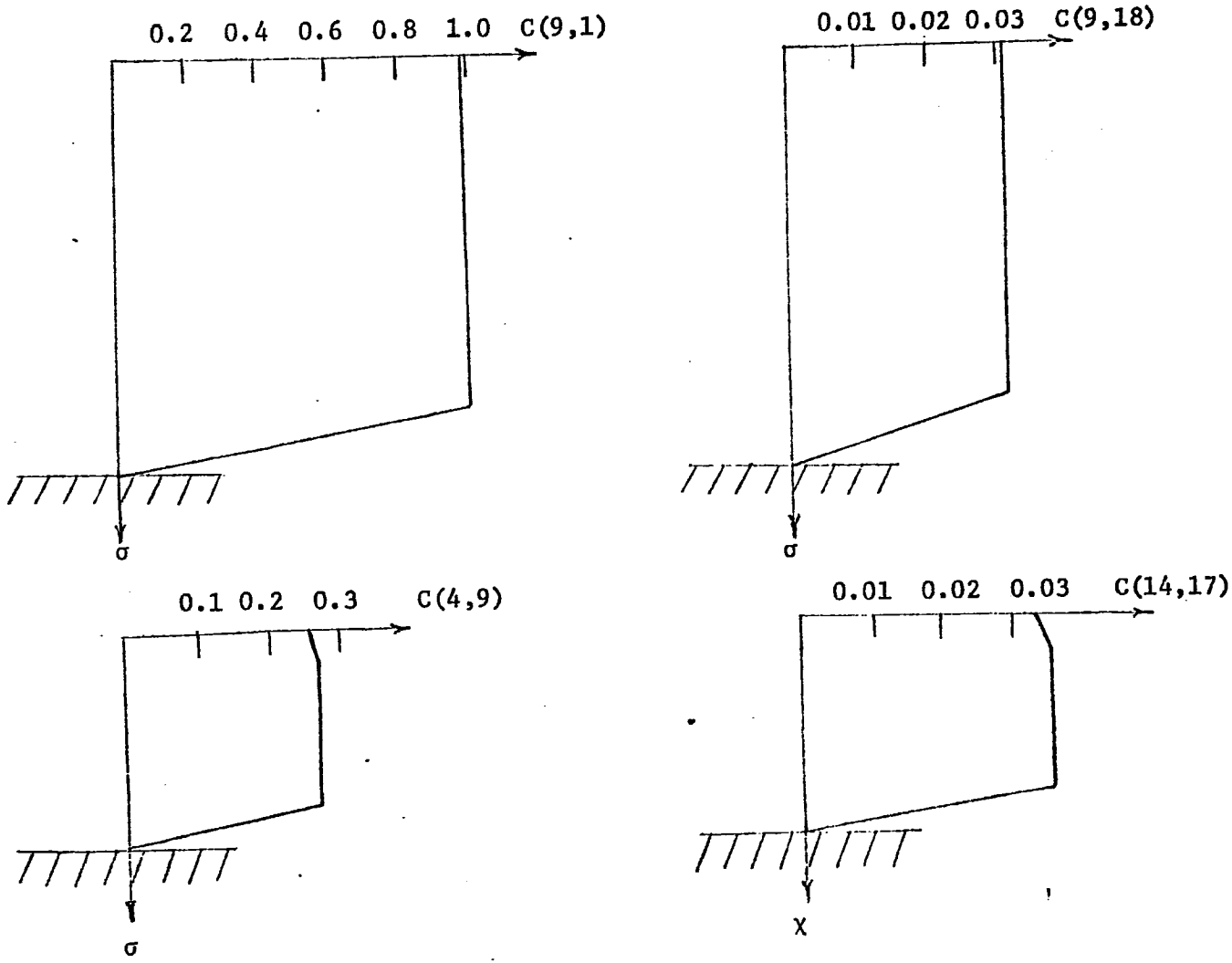

Figure 31. Vertical profiles of concentration at (M,N) = (9,1), (9,18), (4,9) and (14,17) for absorbing bottom.

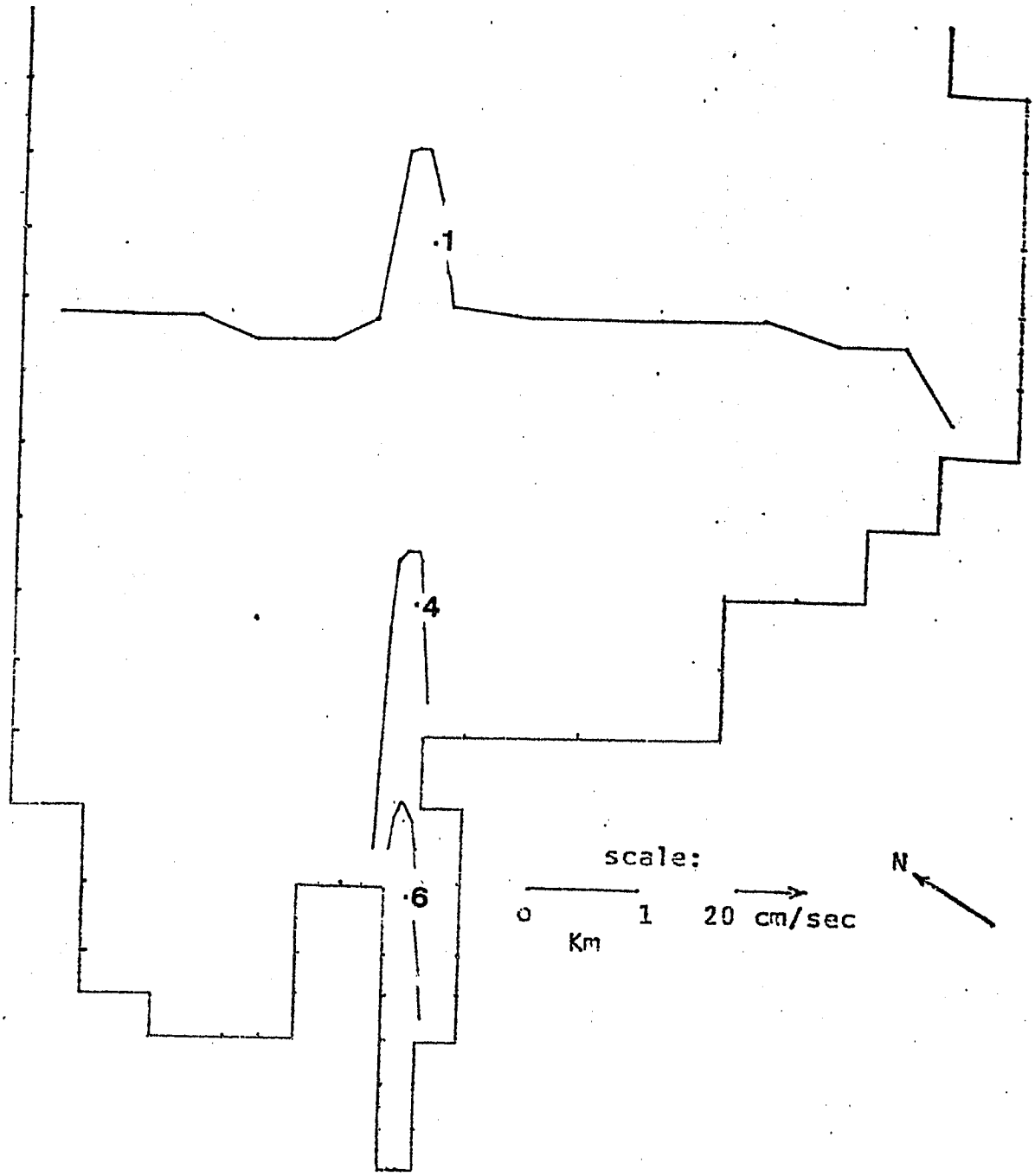

Figure 32. SGS model concentration profile for absorbing bottom and particle sinking velocity of 0.788 cm/s.

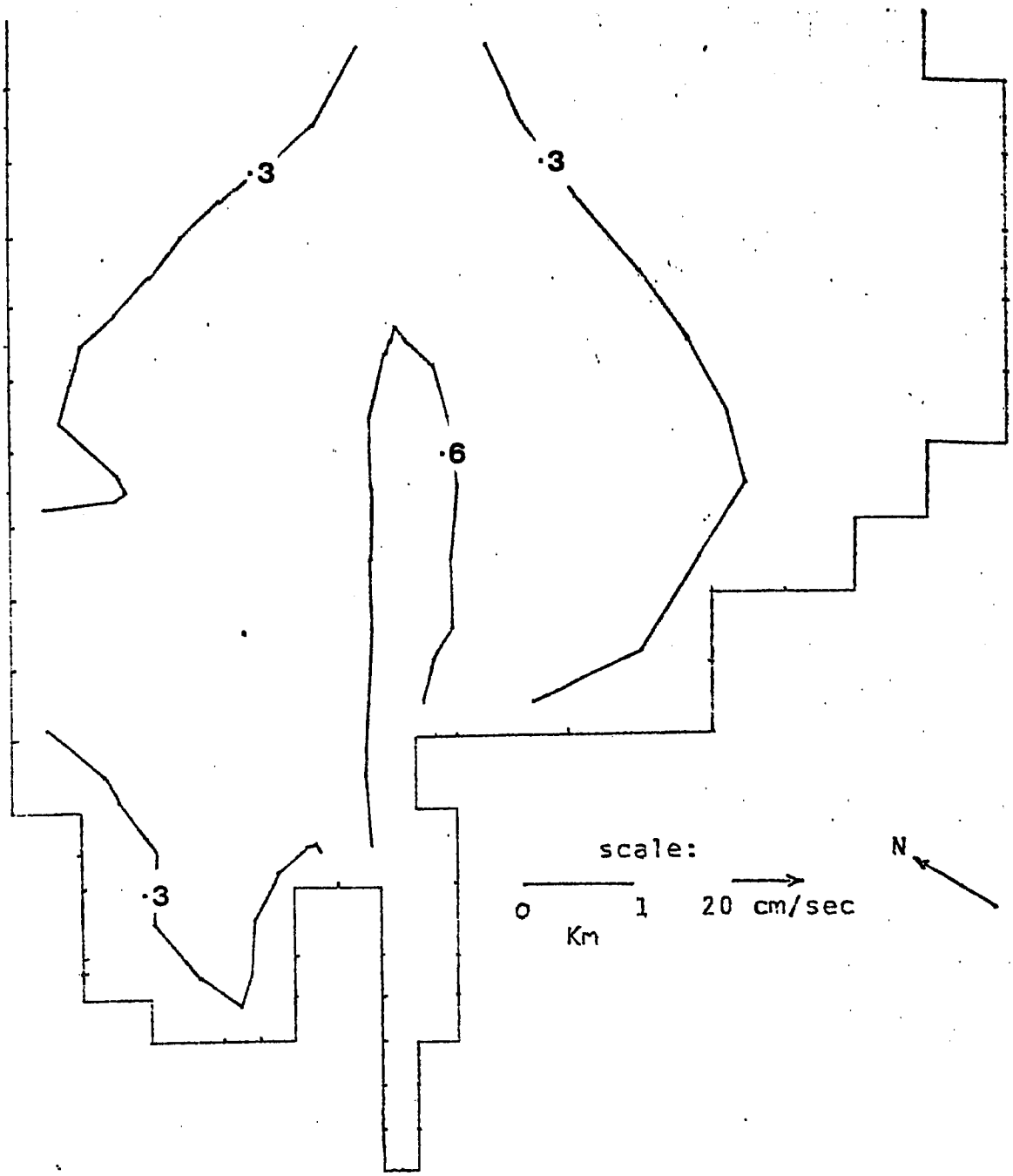

Figure 33. SGS model concentration profile for reflecting bottom and profile sinking velocity of 0.788 cm/s.

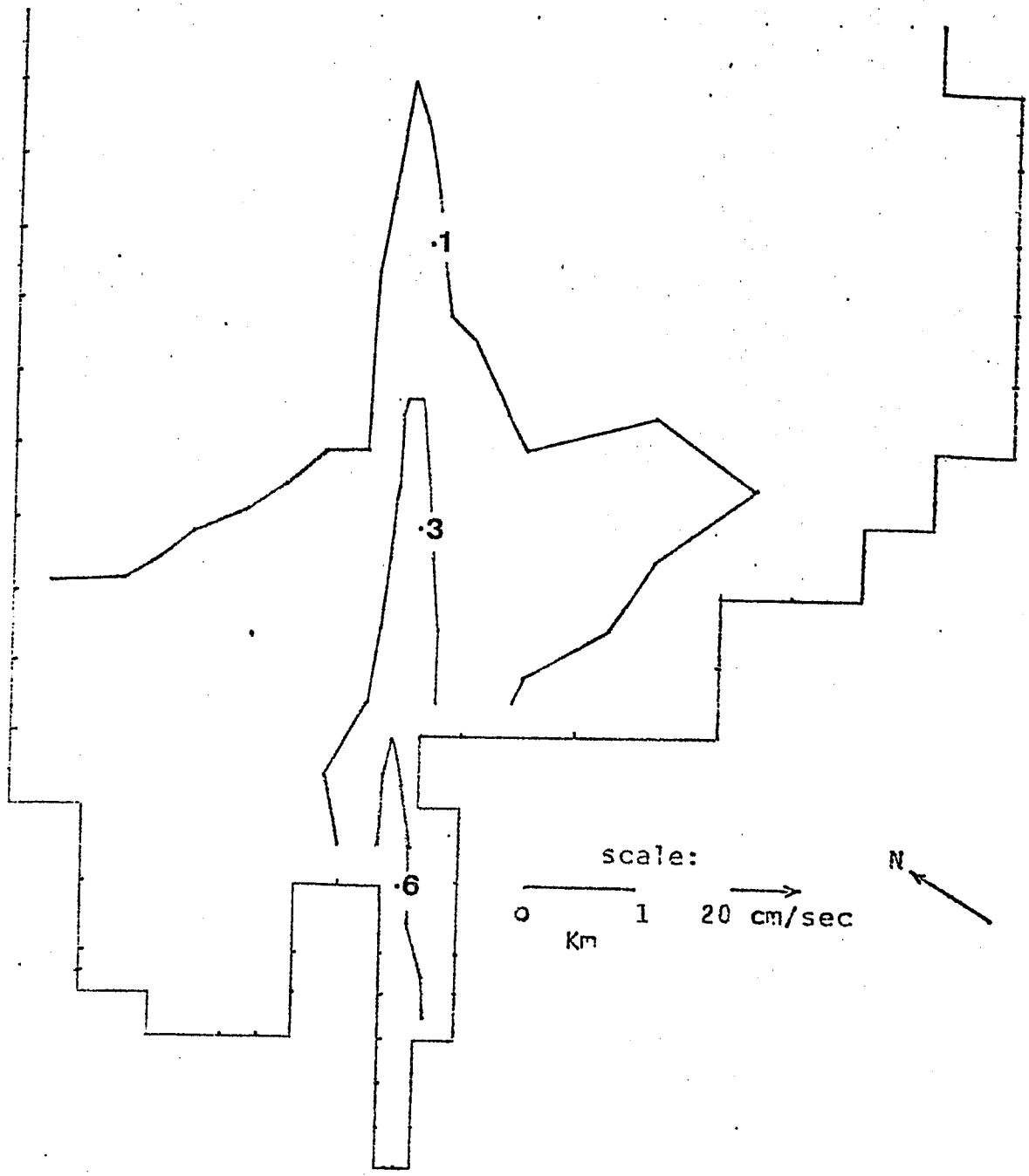

Figure 34. SGS concentration profile for absorbing bottom and particle sinking velocity of 0.0008 cm/s.

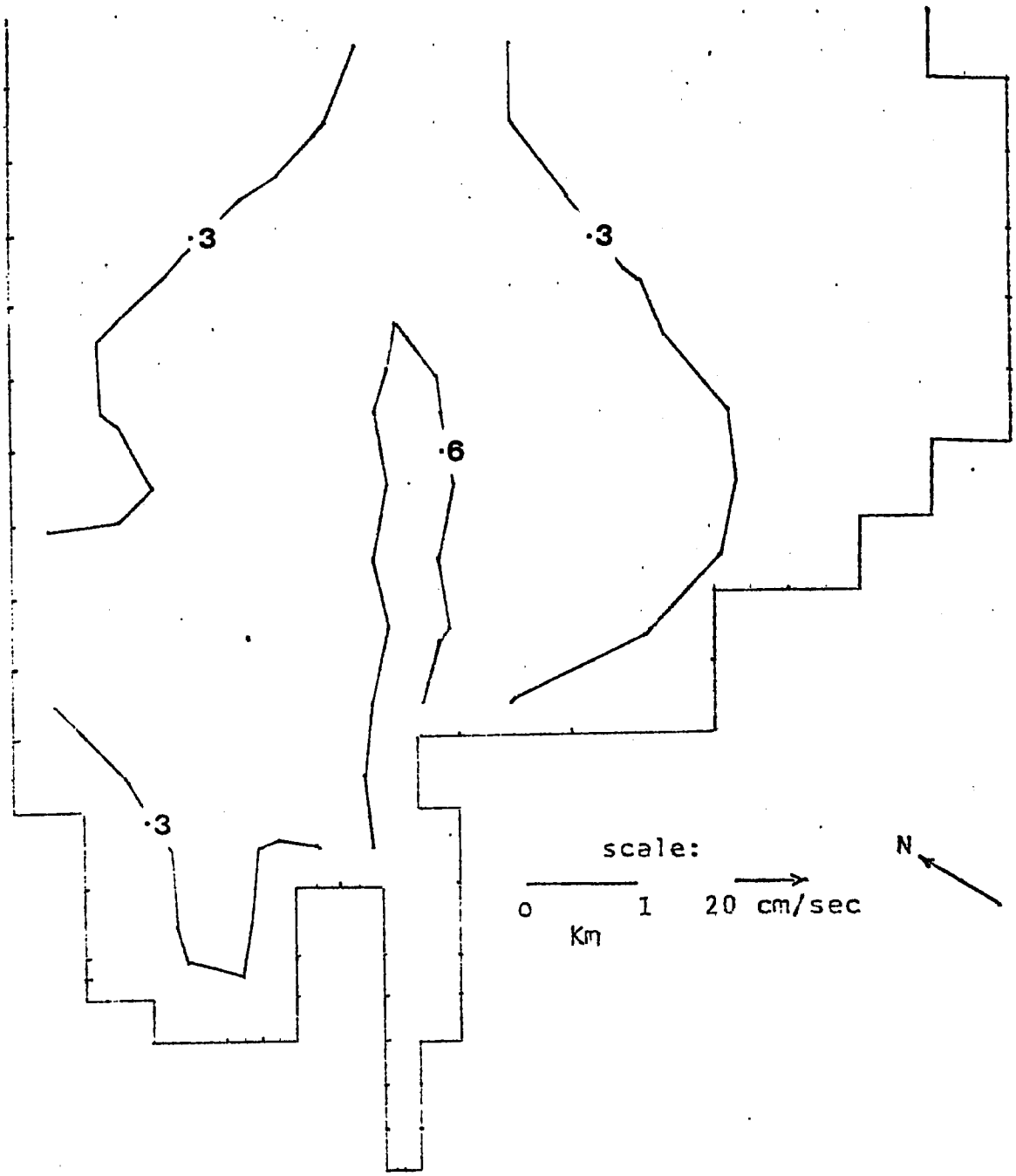

Figure 35. SGS model concentration profile for reflecting bottom and particle sinking velocity of 0.0008 cm/s.

system. It was found that about 6% and 93% of the lighter sediment coming into the Bay was transported out of the Bay for the absorbing and reflecting boundary conditions respectively. But for the heavier particle the quantities going in and out of the Bay remained the same as the particle size of 1/64 mm.

For all future calculations the design particle size of 1/64 mm with a sinking velocity of 0.0123 cm/s will be considered.

3. Horizontal Viscosities.

The effect of horizontal viscosities on the concentration contours was studied. The concentration contours for 1000 and 500,000 cm^2/s viscosities for the two bottom boundary conditions are shown in Figures 36 to 39. The geometry of Maumee Bay that is the bottom topography and the shoreline configuration is such that the horizontal viscosities introduce a flux opposing the convection flux. Hence it can be seen in the figures that the sediment is not transported further as the viscosities increase for both the reflecting and absorbing bottom boundary conditions.

D. Ottawa River Influence

Discharge information for Ottawa River was obtained from USGS station #04177000. From the sparse data available it was concluded a discharge of 200 cfs was reasonable. Since this is a small discharge it did not effect the flow field appreciably. The Ottawa River inlet was retained for future sediment calculations. No information is available for the sediment concentration in the Ottawa River.

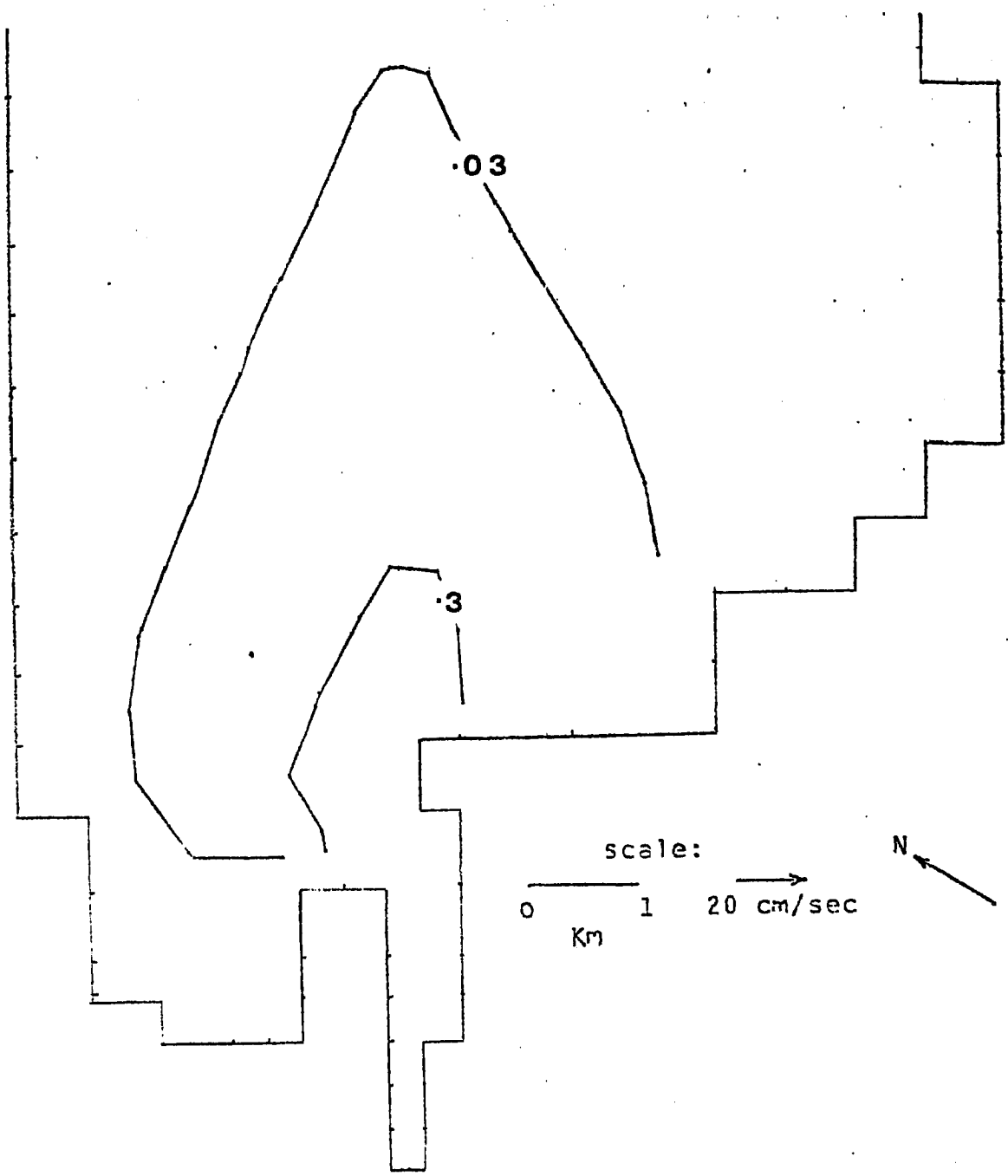

Figure 36. Concentration profile for absorbing bottom and 1000 cm^2/s viscosity.

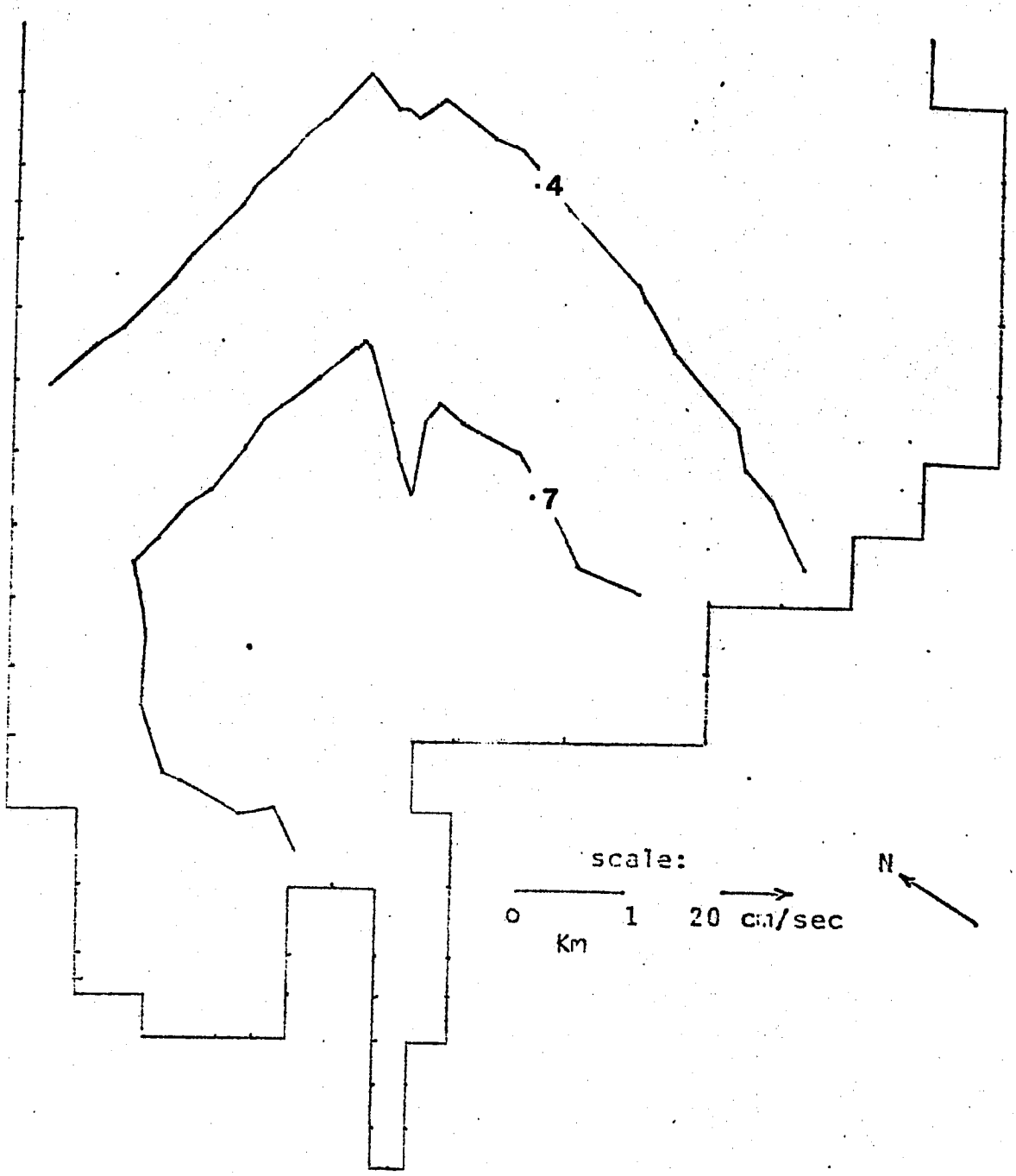

Figure 37. Concentration profile for reflecting bottom and 1000 cm^2/s viscosity.

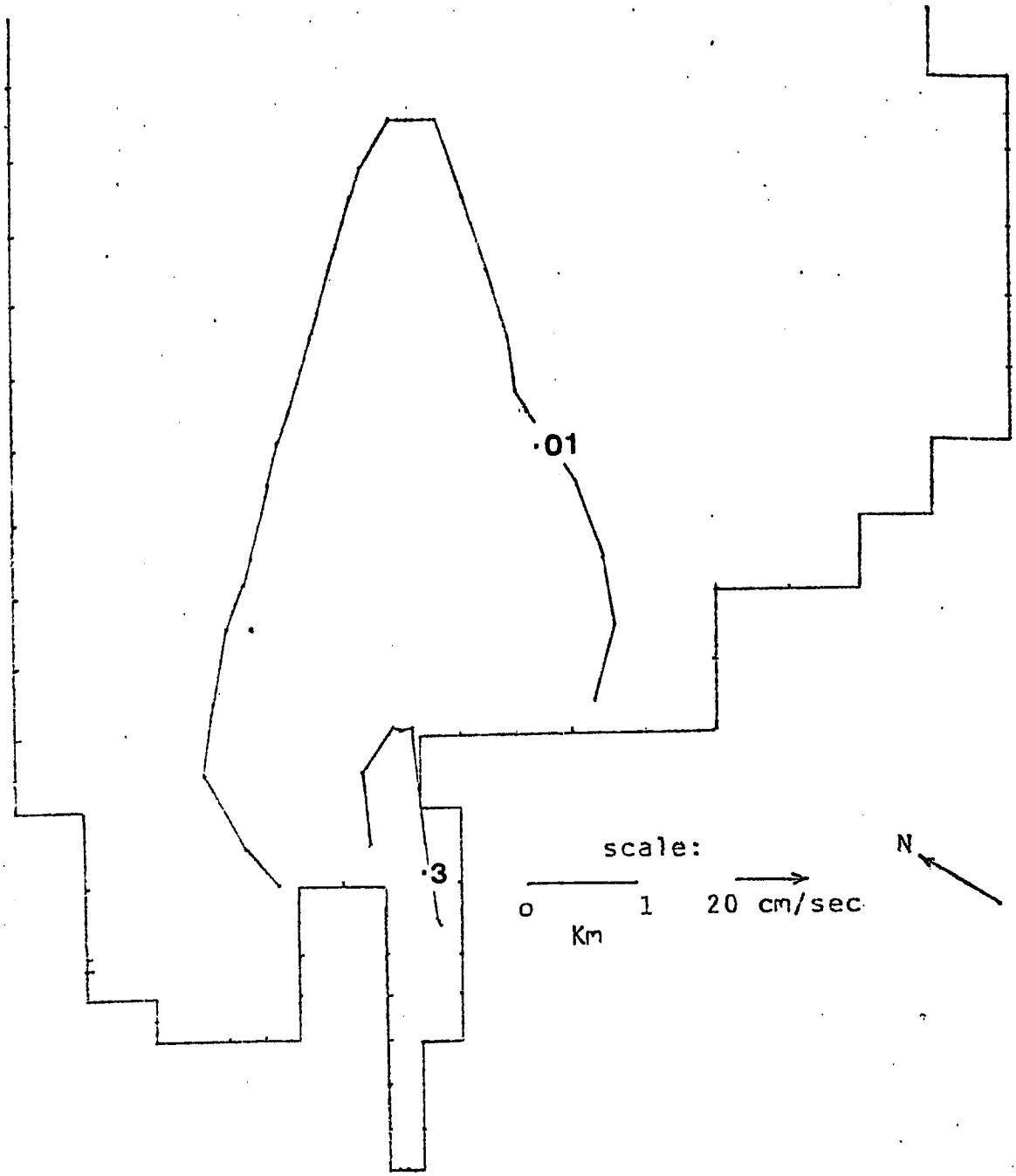

Figure 38. Concentration profiles for absorbing bottom and 500,000 cm^2/s viscosity.

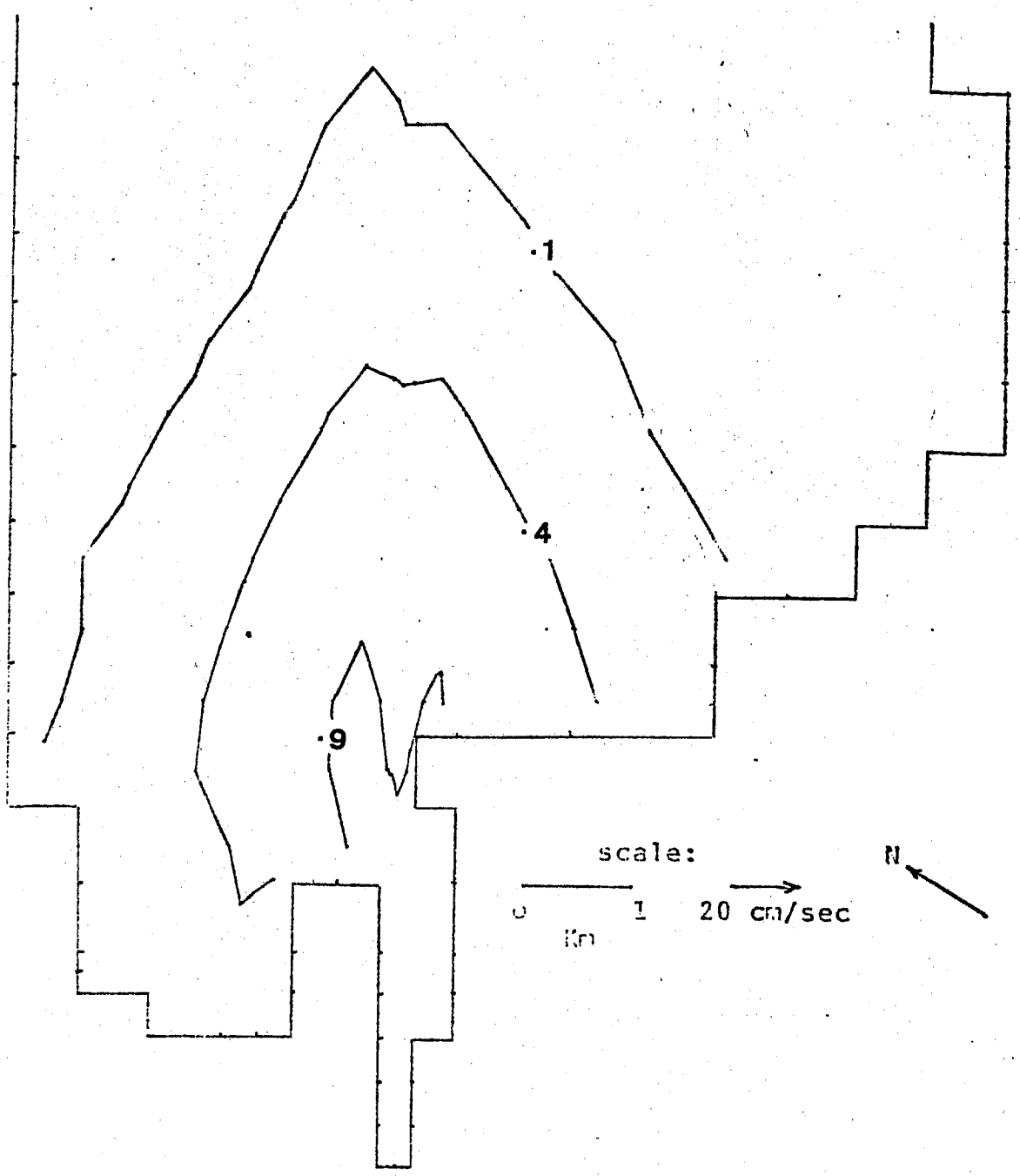

Figure 39. Concentration profile for reflecting bottom and 500,000 cm^2/s viscosity.

E. Wind Effects

The reaction of the Bay to wind influences was examined. For every wind direction and strength the results were obtained for two horizontal viscosities of 1000 and 50,000 cm^2/s to ascertain the effect of lateral spreading on the sediment. A design particle size of 1/64 mm with a sinking velocity of 0.0123 cm/s and the two boundary conditions discussed above were considered for all cases. This study concentrates on the three wind directions, southwest, northeast, and southeast as discussed in Chapter 2. The southwesterly and northeasterly winds blow parallel to the channel along the major axis of the Bay whereas the southeasterly winds blow along the minor axis.

The velocity profiles and the corresponding concentration contours for a southwest winds of 1 and 5 m/s are shown in Figures 40 to 48. For some cases the scale for the velocity profiles had to be changed because of larger velocities. The current speeds in the mid-channel were found to be considerably higher than the speeds near the channel edge. For the reflective bottom condition the lateral spreading and mixing for the higher viscosity of 50,000 cm^2/s can be seen. Whereas for the smaller viscosity of 1000 cm^2/s there was a strong current down the channel and the sediment in the channel is carried out of the Bay. About 17.8% and 100% of sediment introduced into the Bay was transported out for the absorbing and reflecting bottom respectively. When the wind speed is increased from 1 m/s to 5 m/s the sediment is transported further towards Lake Erie. The plume developed due to the inlet from Ottawa River can be seen for the reflective bottom condition. For the absorbing bottom the effect of Ottawa River is not

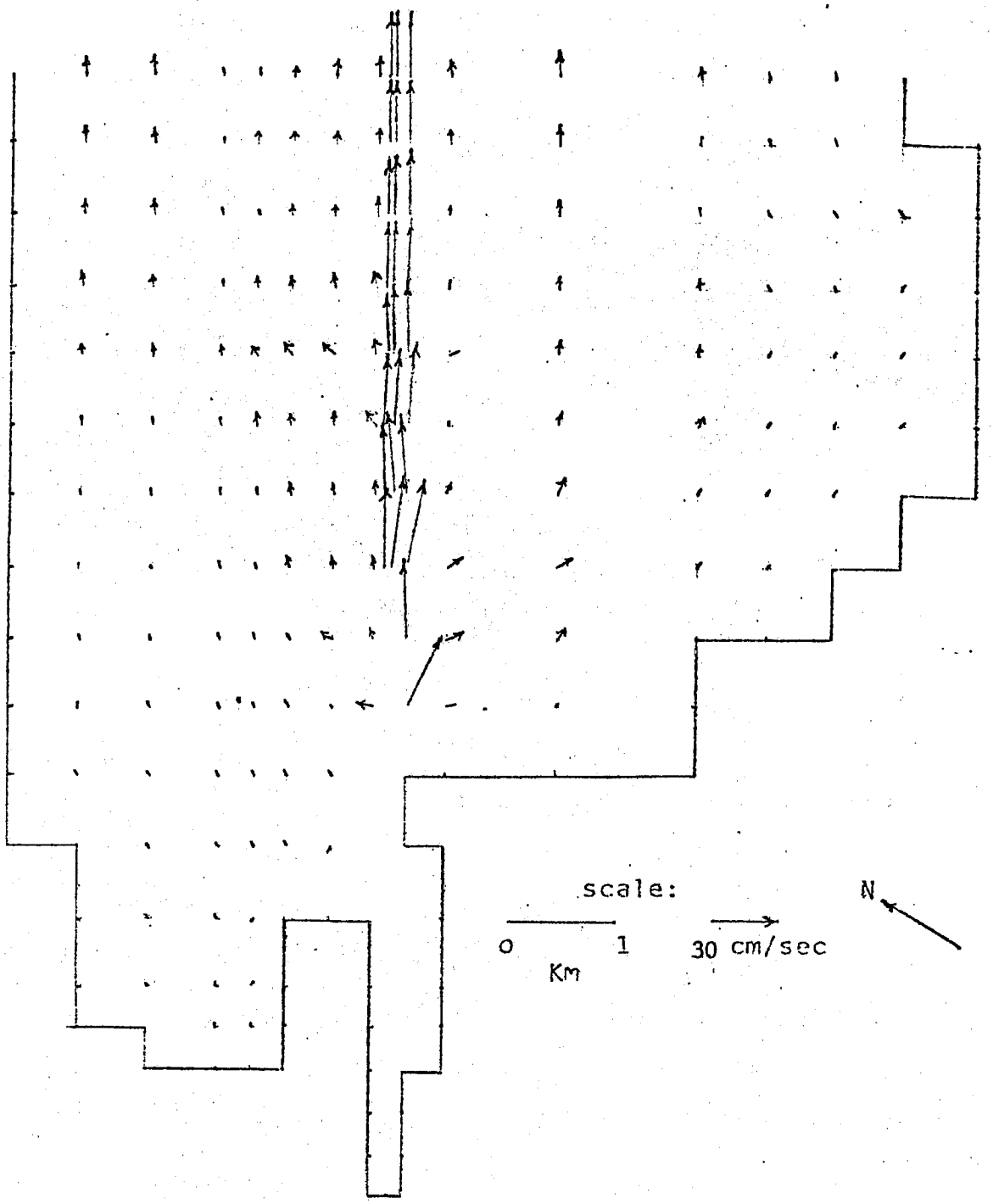

Figure 40. Surface velocities for SW wind of 1 m/s and 1000 cm^2/s viscosity.

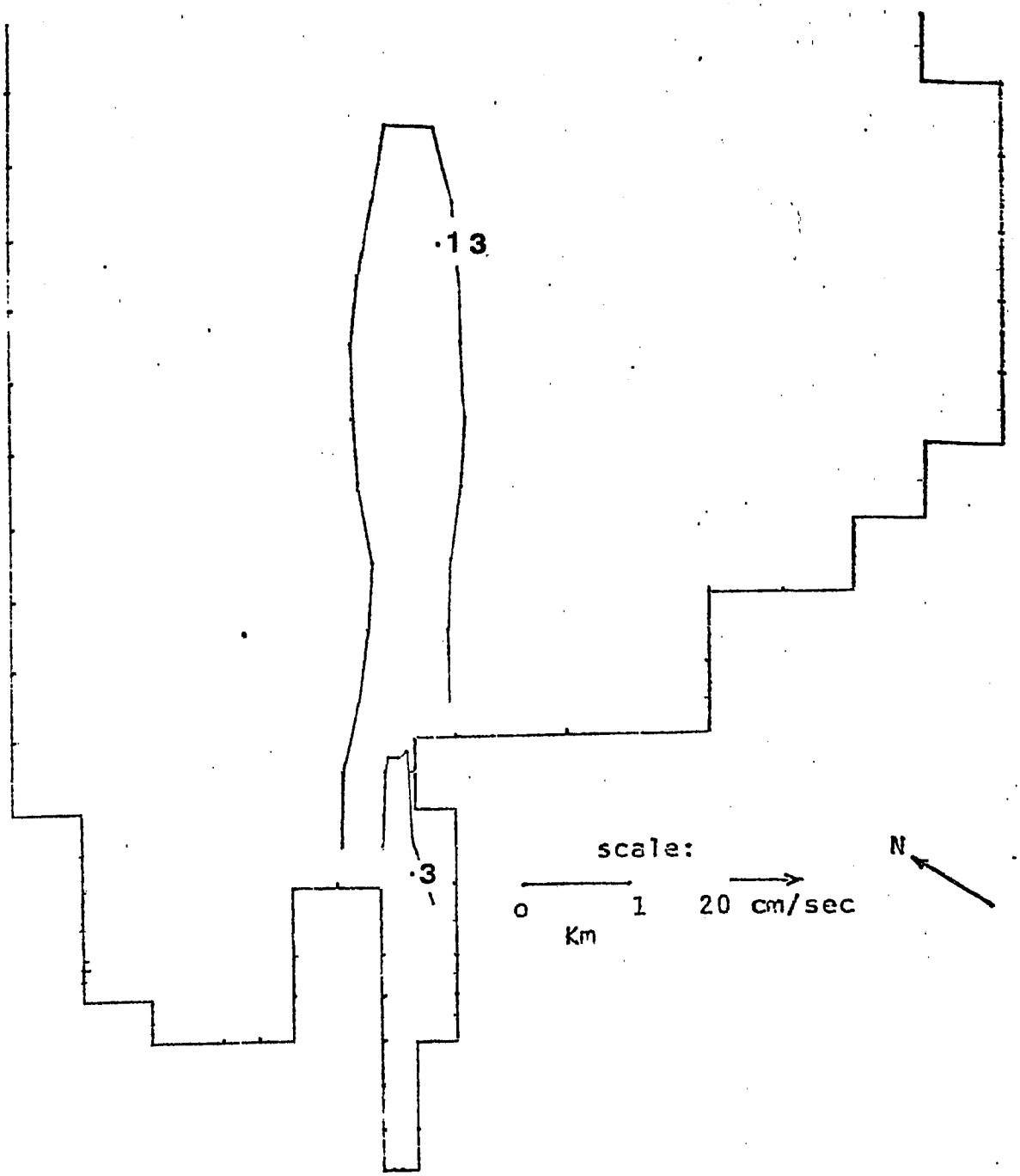

Figure 41. Concentration profile for SW wind of 1 m/s, absorbing bottom, and 1000 cm^2/s viscosity.

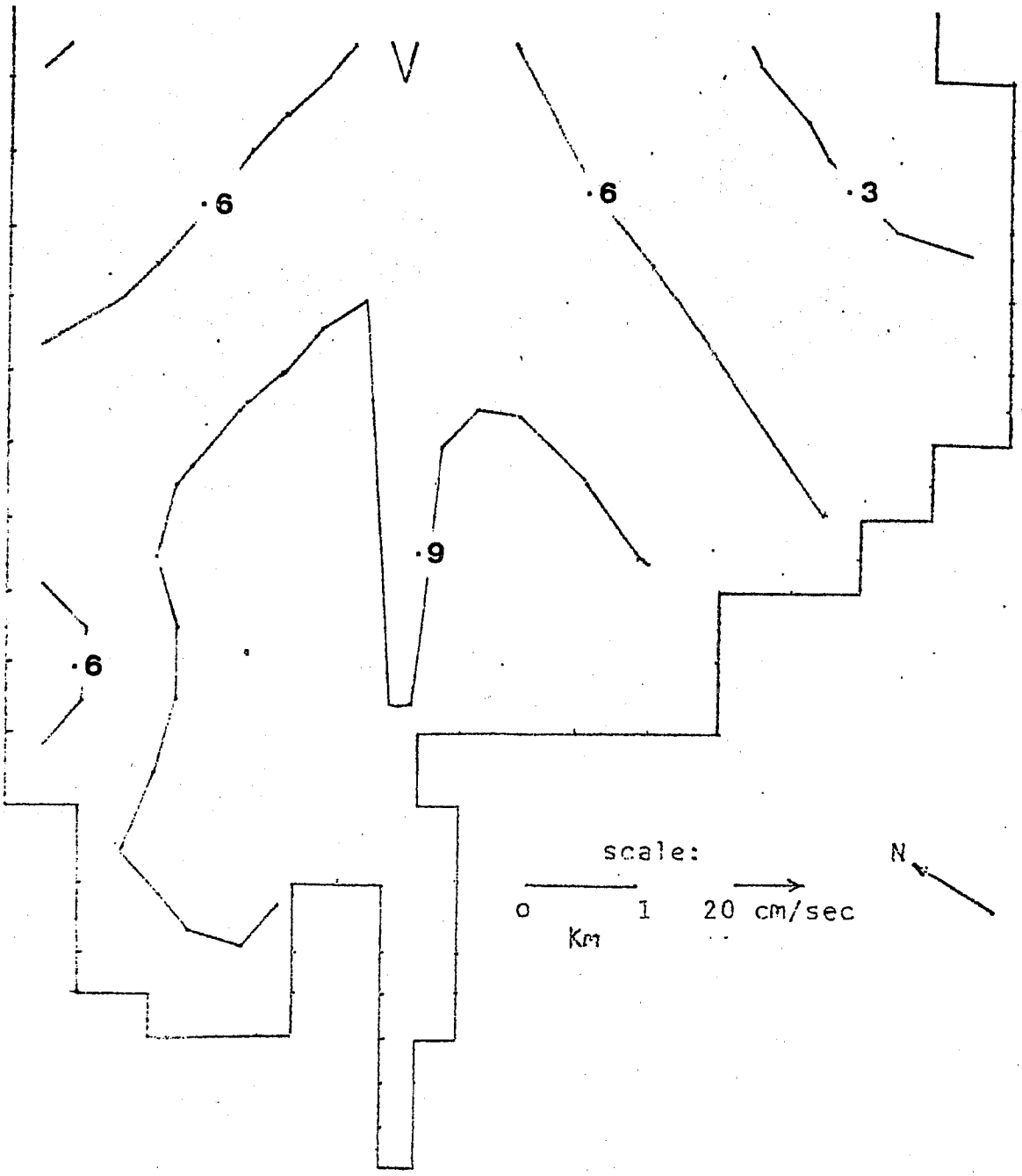

Figure 42. Concentration profile for SW wind of 1 m/s, reflecting bottom, and 1000 cm^2/s viscosity.

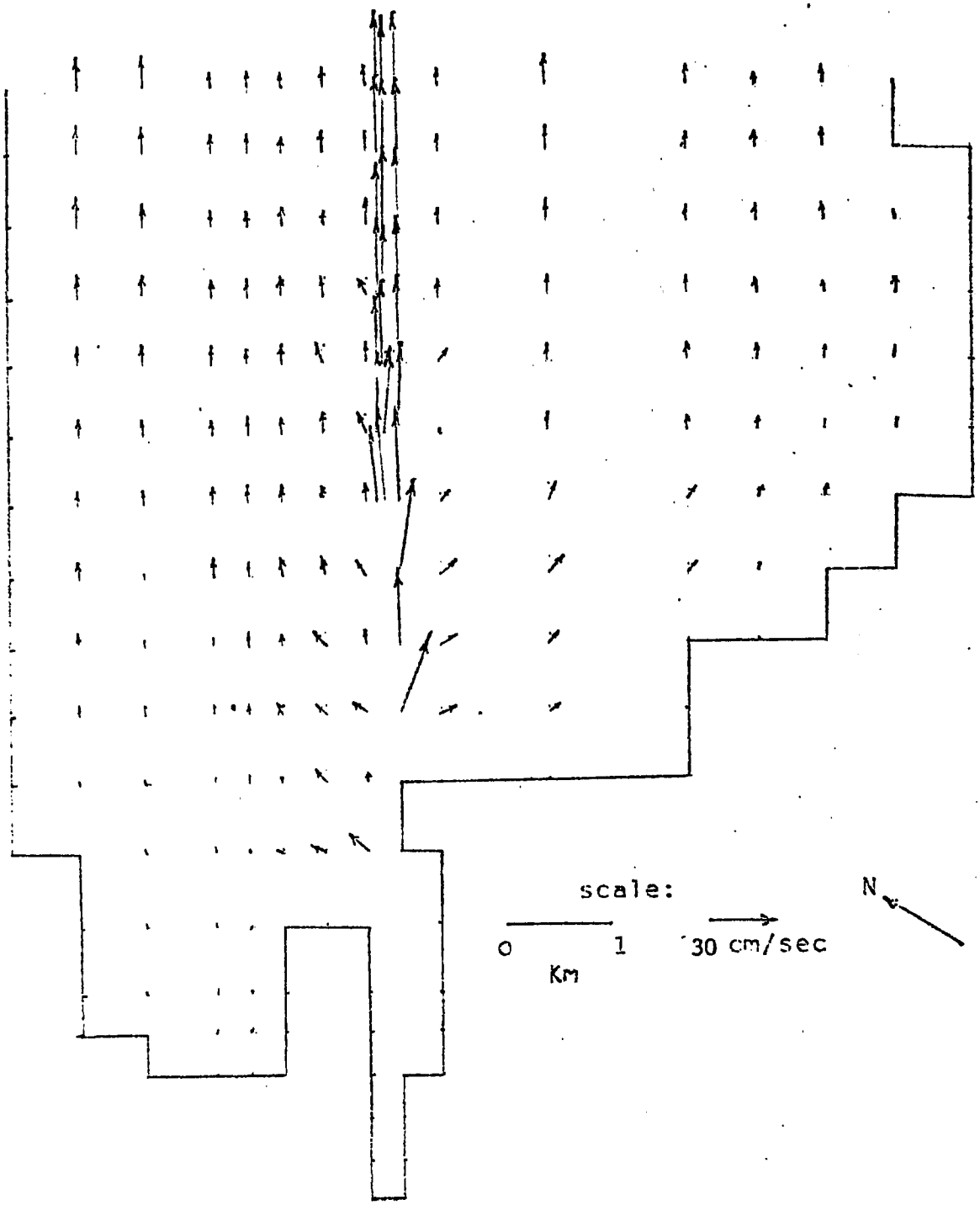

Figure 43. Surface velocities for SW wind of 5 m/s and 1000 cm^2/s viscosity.

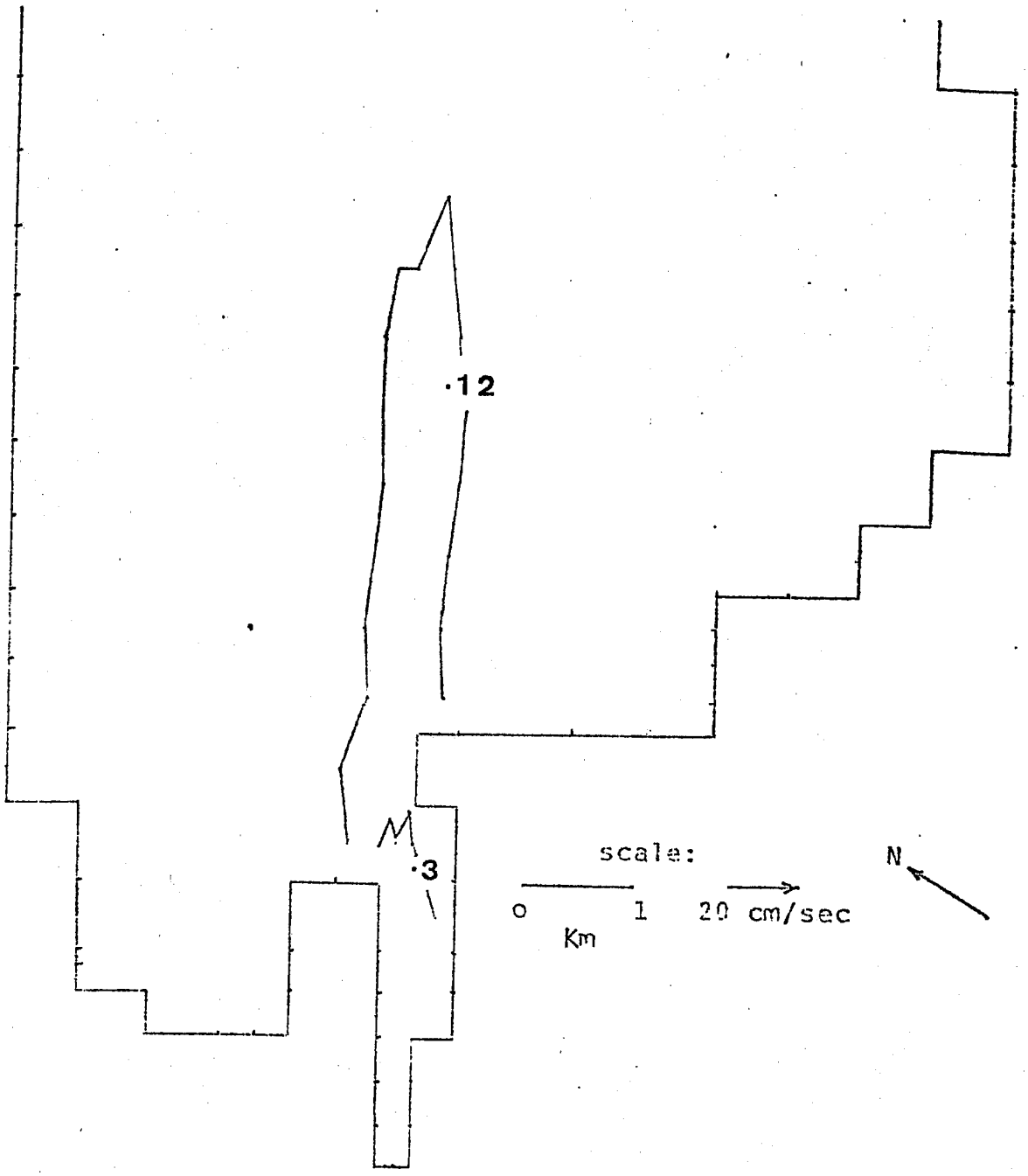

Figure 44. Concentration profile for SW wind of 5 m/s, absorbing bottom, and 1000 cm^2/s viscosity.

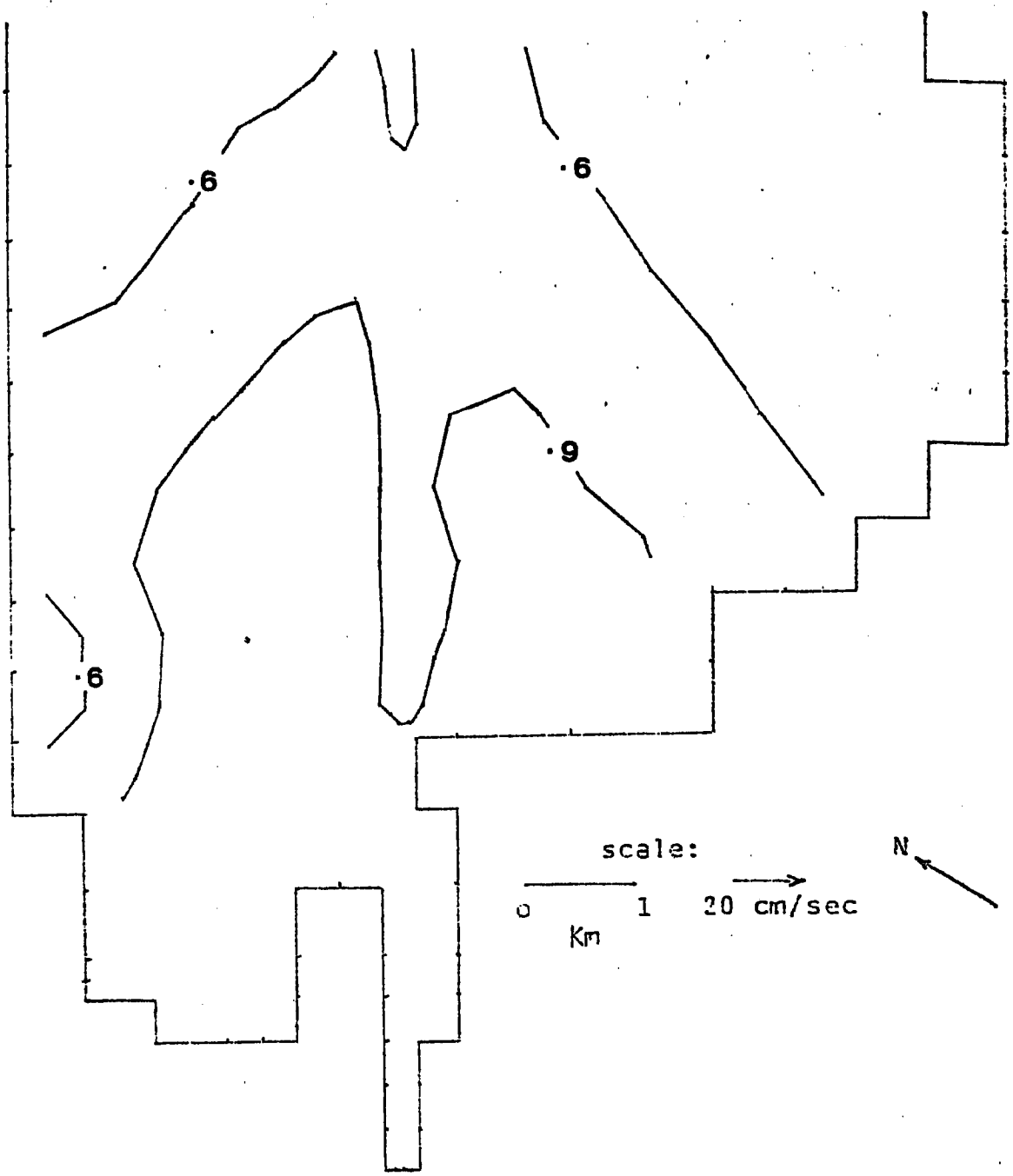

Figure 45. Concentration profile for SW wind of 5 m/s, reflecting bottom, and 1000 cm^2/s viscosity.

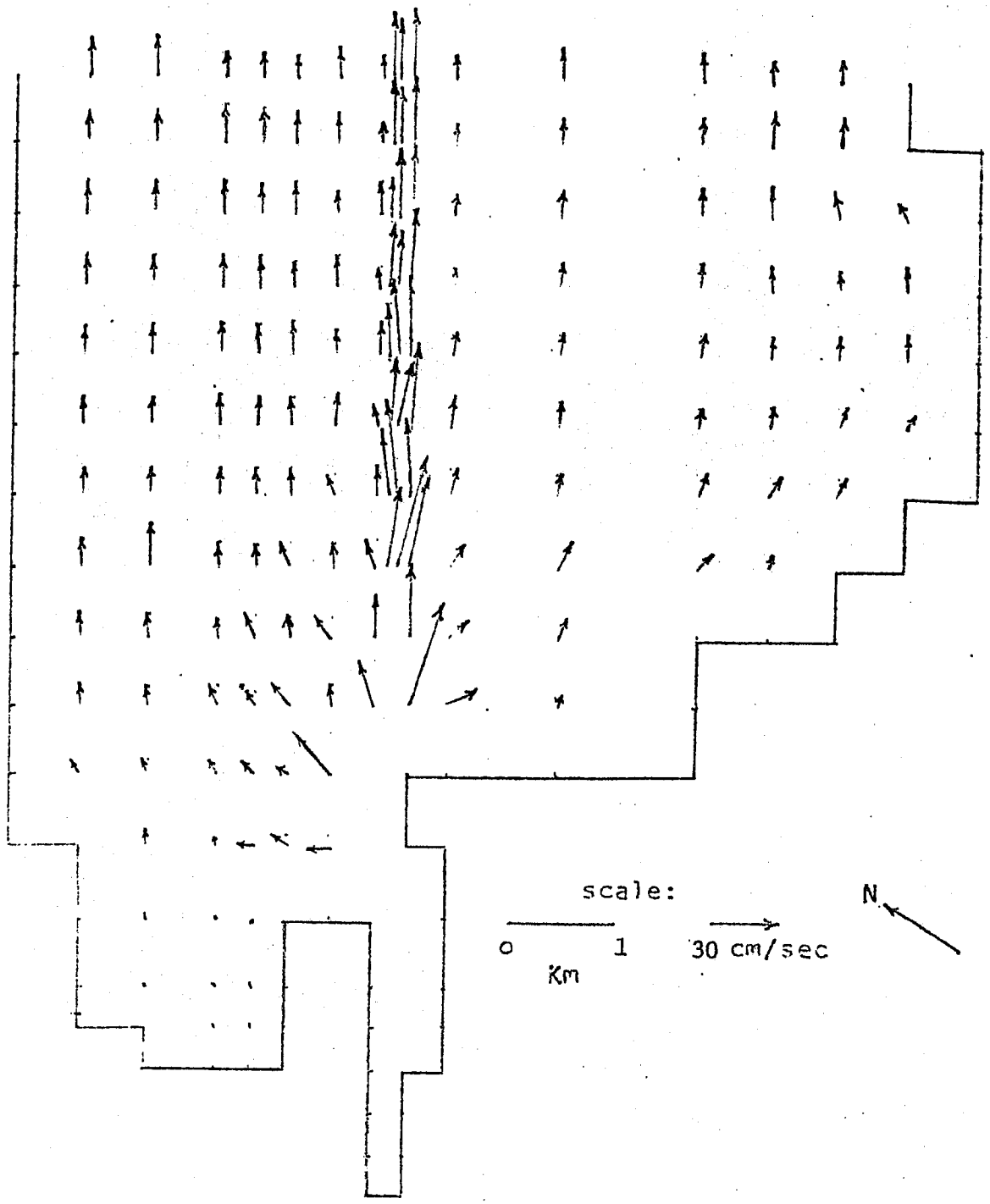

Figure 46. Surface velocities for SW wind of 5 m/s and 50,000 cm^2/s viscosity.

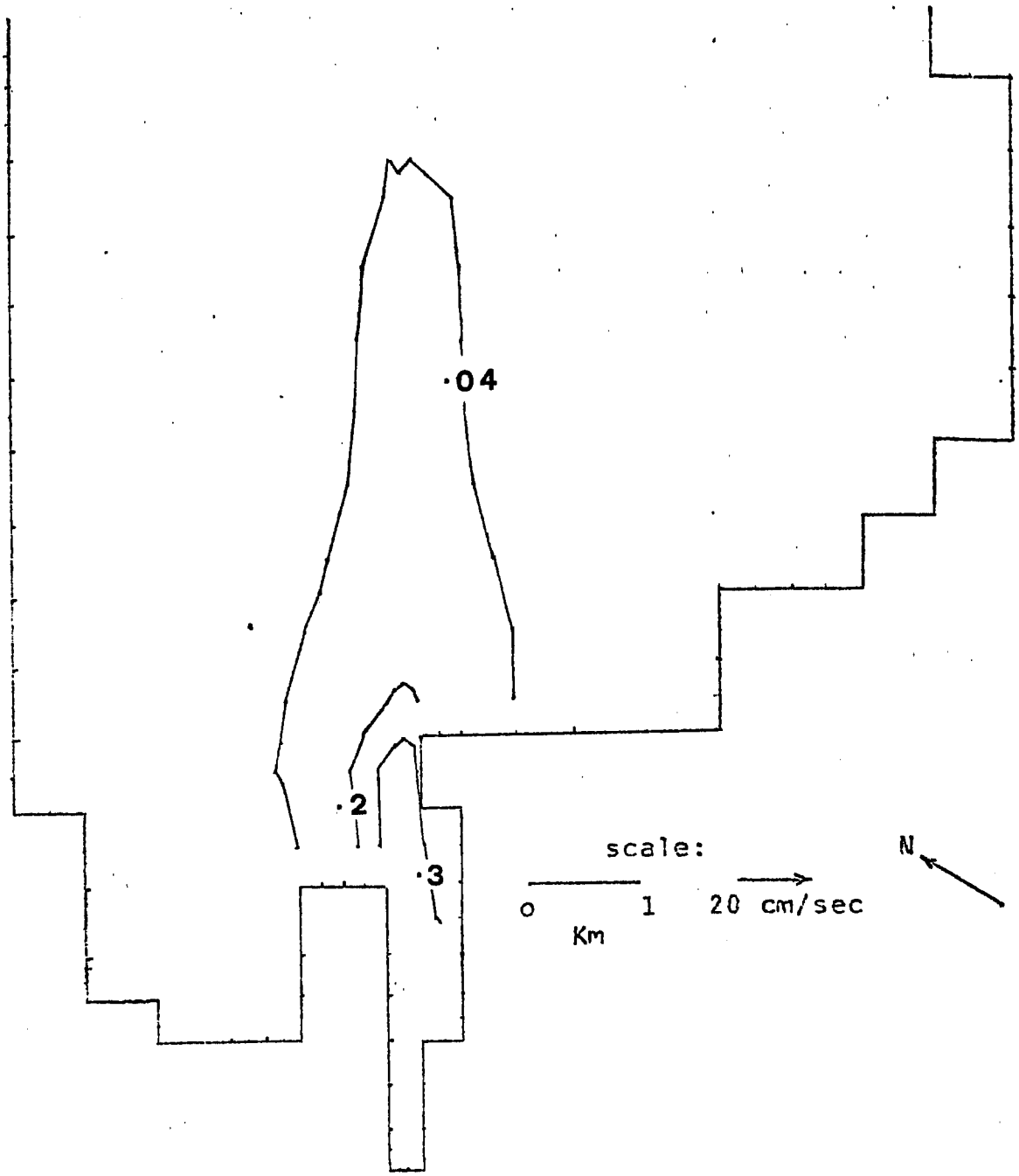

Figure 47. Concentration profile for SW wind of 5 m/s, absorbing bottom, and 50,000 cm2/s viscosity.

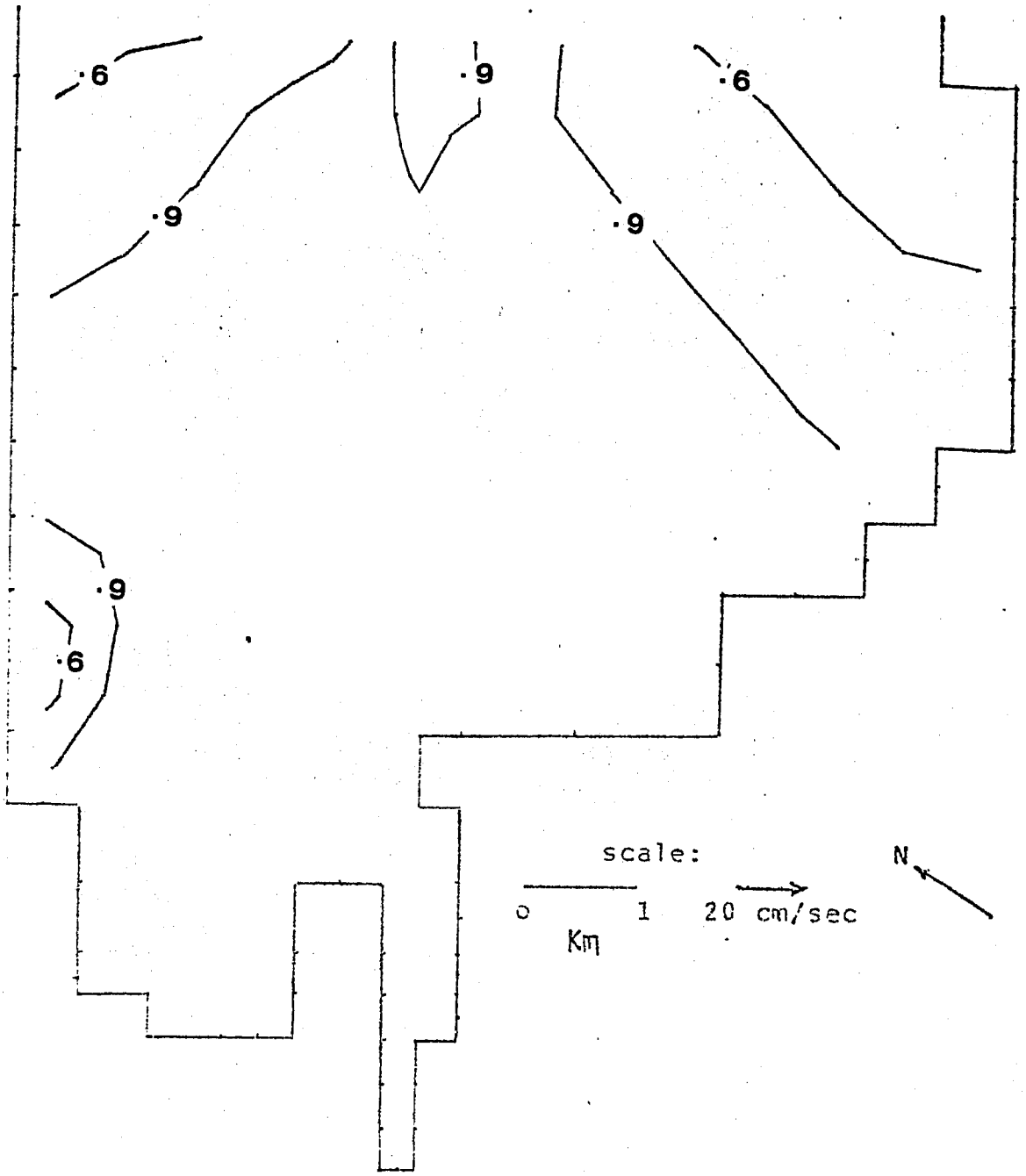

Figure 48. Concentration profile for SW wind of 5 m/s, reflecting bottom, and 50,000 cm^2/s viscosity.

apparent because the sediment coming into the Bay from Maumee River settles out close to the mouth. The vertical velocities for the SW wind were not insignificant outside the channel. There was a general downwelling at the outer boundary and upwelling at the inlet ignoring the local effects. Whereas in the channel the vertical velocities were downward.

The velocity profiles and the surface concentration contours for the northeast winds of 5 and 8 m/s are shown in Figures 49 to 58. The flow in the shallow regions of the Bay was reversed but the forward flow in the channel was maintained due to the large inflow from the Maumee River. Comparing Figures 44 and 50 for the absorbing boundary condition it can be seen that the SW wind pushes the sediment out of the Bay much faster since the NE wind tends to push the sediment back to the inlet. But for reflecting boundary condition almost 100% of the sediment introduced into the Bay is transported out for all cases. It can be seen that when the wind strength is increased from 5 m/s to 8 m/s the sediment is still further pushed back towards the inlet. The vertical velocities for the NE winds were the opposite of the vertical velocities for the SW wind. Again ignoring the local effects there was a general upwelling at the outer boundary and a general downwelling near the inlet. There was not any pattern for the vertical velocity in the channel.

Finally the surface velocity profiles and the concentration contours for the southeast winds of 5 and 8 m/s are presented in Figures 59 to 67. There was a strong flow towards NNE when the SE wind was applied to the Maumee Bay. Changing the horizontal viscosities from 1000 to 50,000 cm^2/s did not seem to influence the concentration

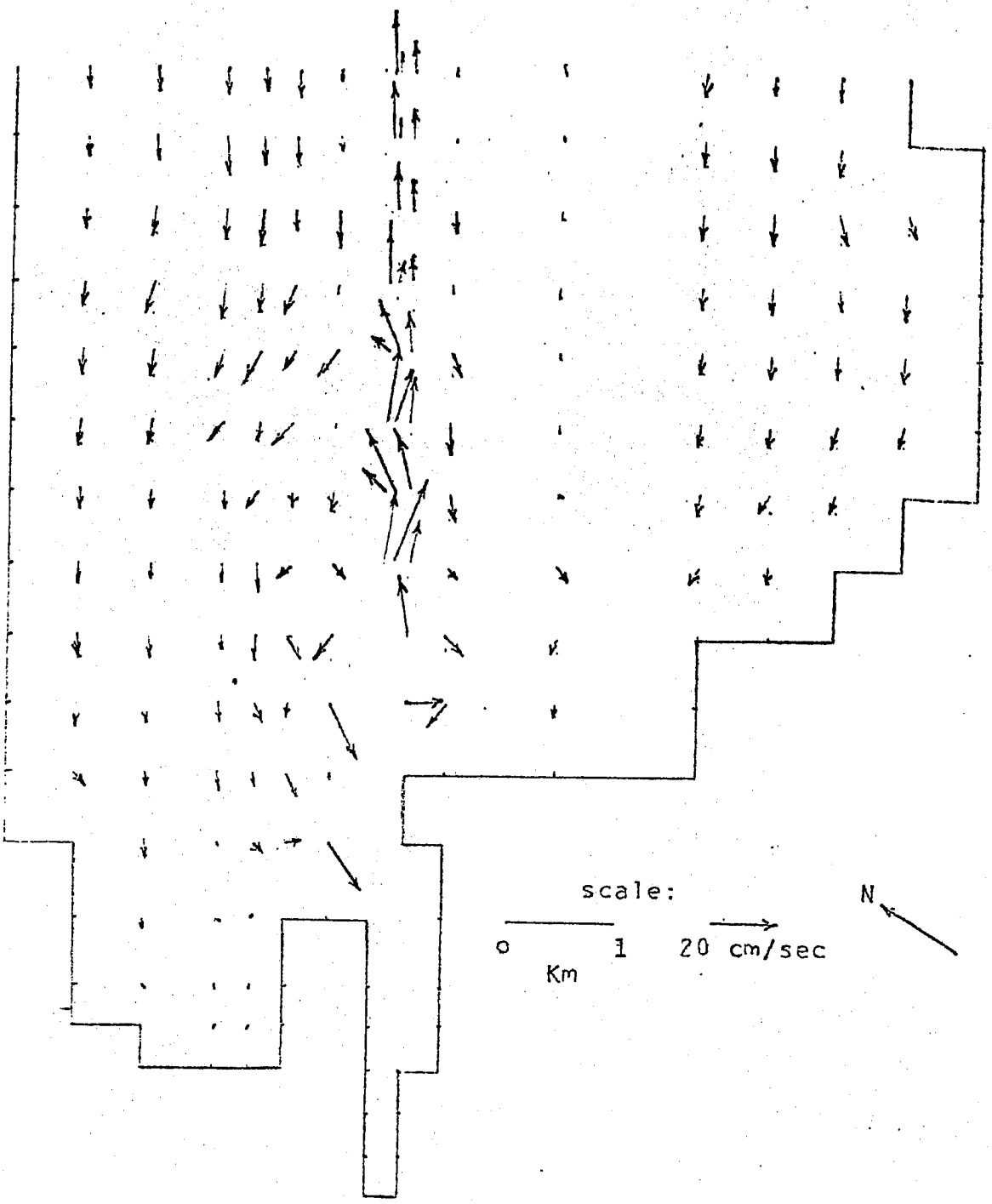

Figure 49. Surface velocities for NE wind of 5 m/s and 1000 cm^2/s viscosity.

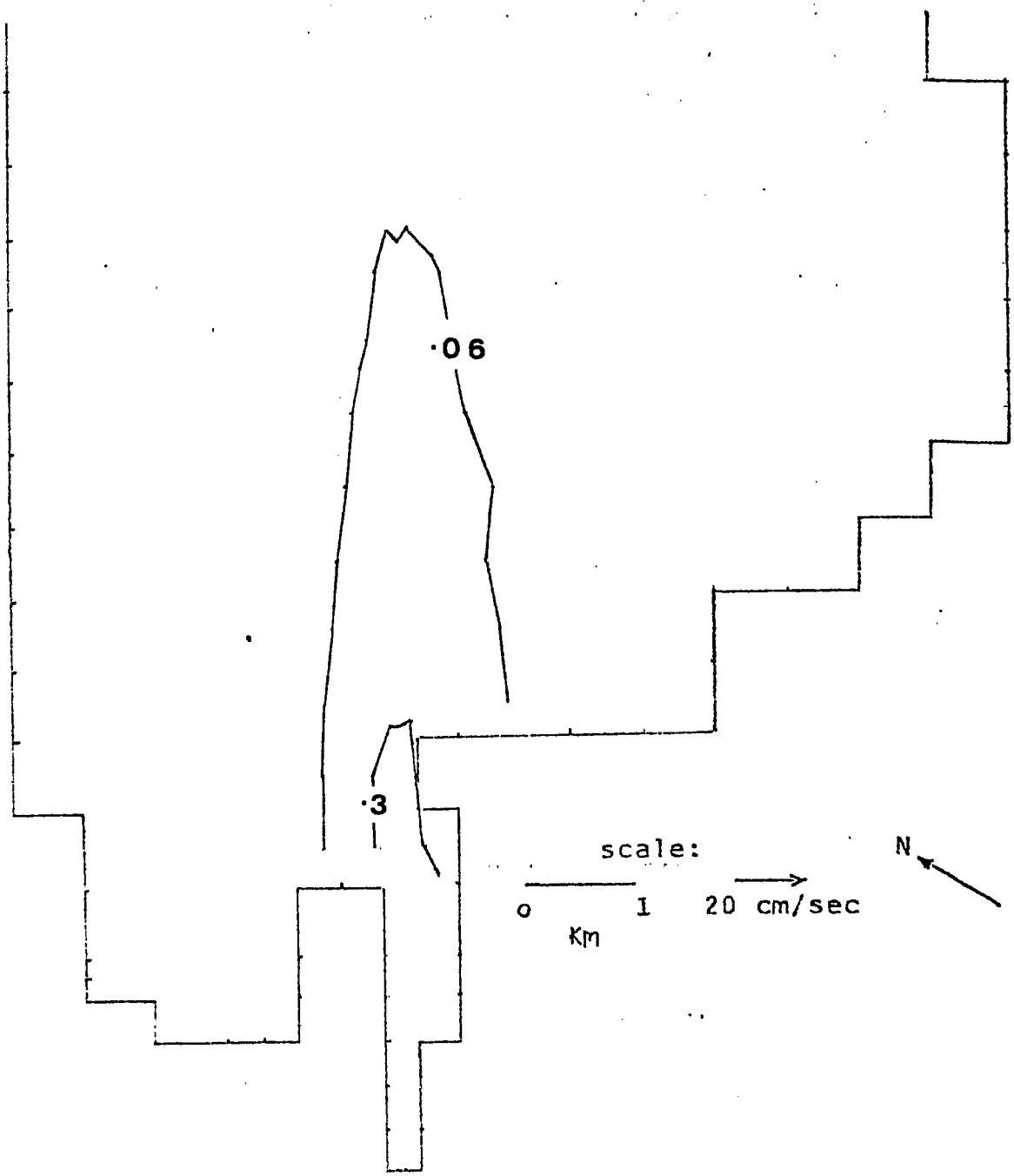

Figure 50. Concentration profile for NE wind of 5 m/s, absorbing bottom, and 1000 cm^2/s viscosity.

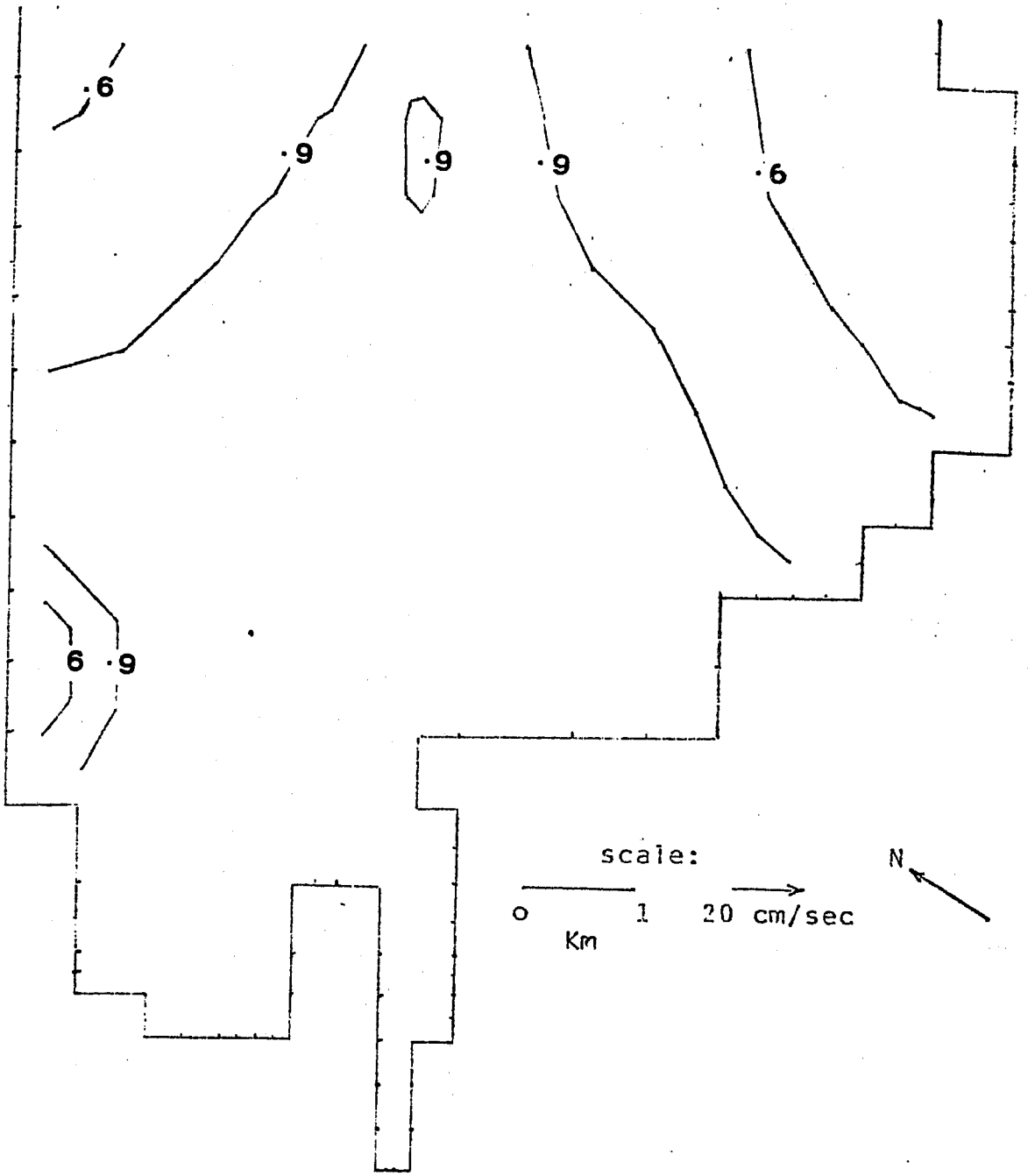

Figure 51. Concentration profile for NE wind of 5 m/s, reflecting bottom, and 1000 cm^2/s viscosity.

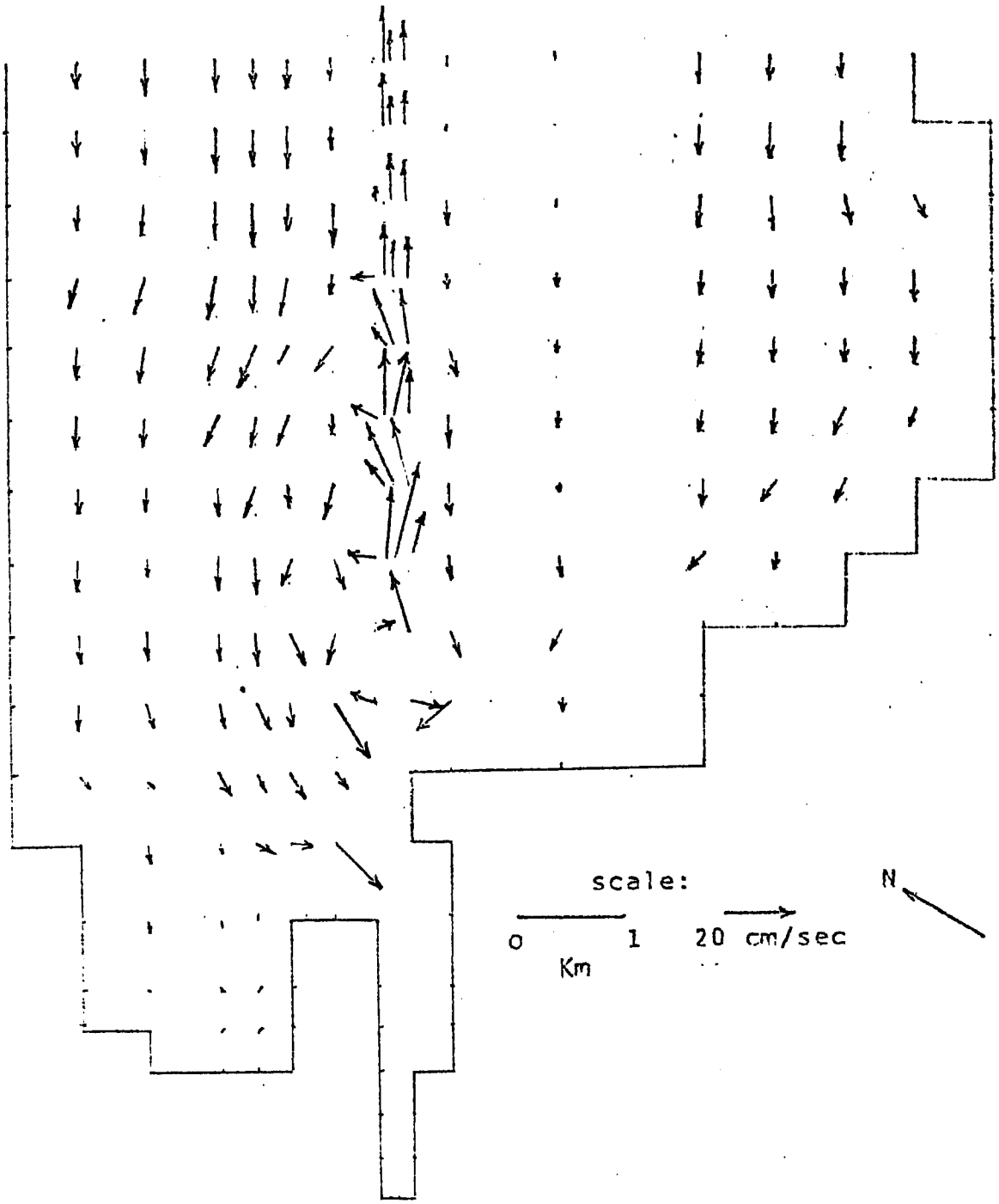

Figure 52. Surface velocities for NE wind of 5 m/s and 50,000 cm^2/s viscosity.

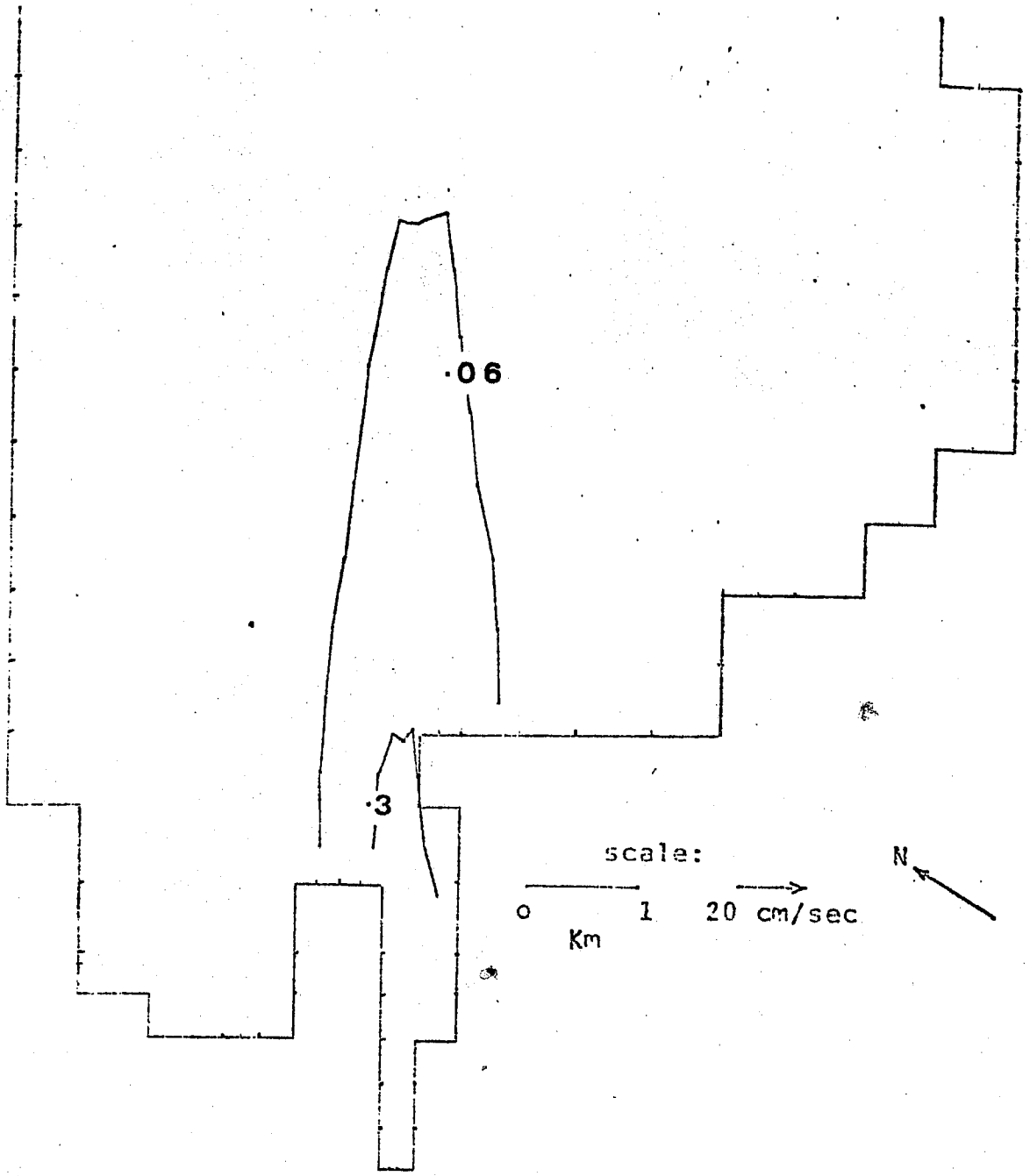

Figure 53. Concentration profile for NE wind of 5 m/s, absorbing bottom, and 50,000 cm^2/s viscosity.

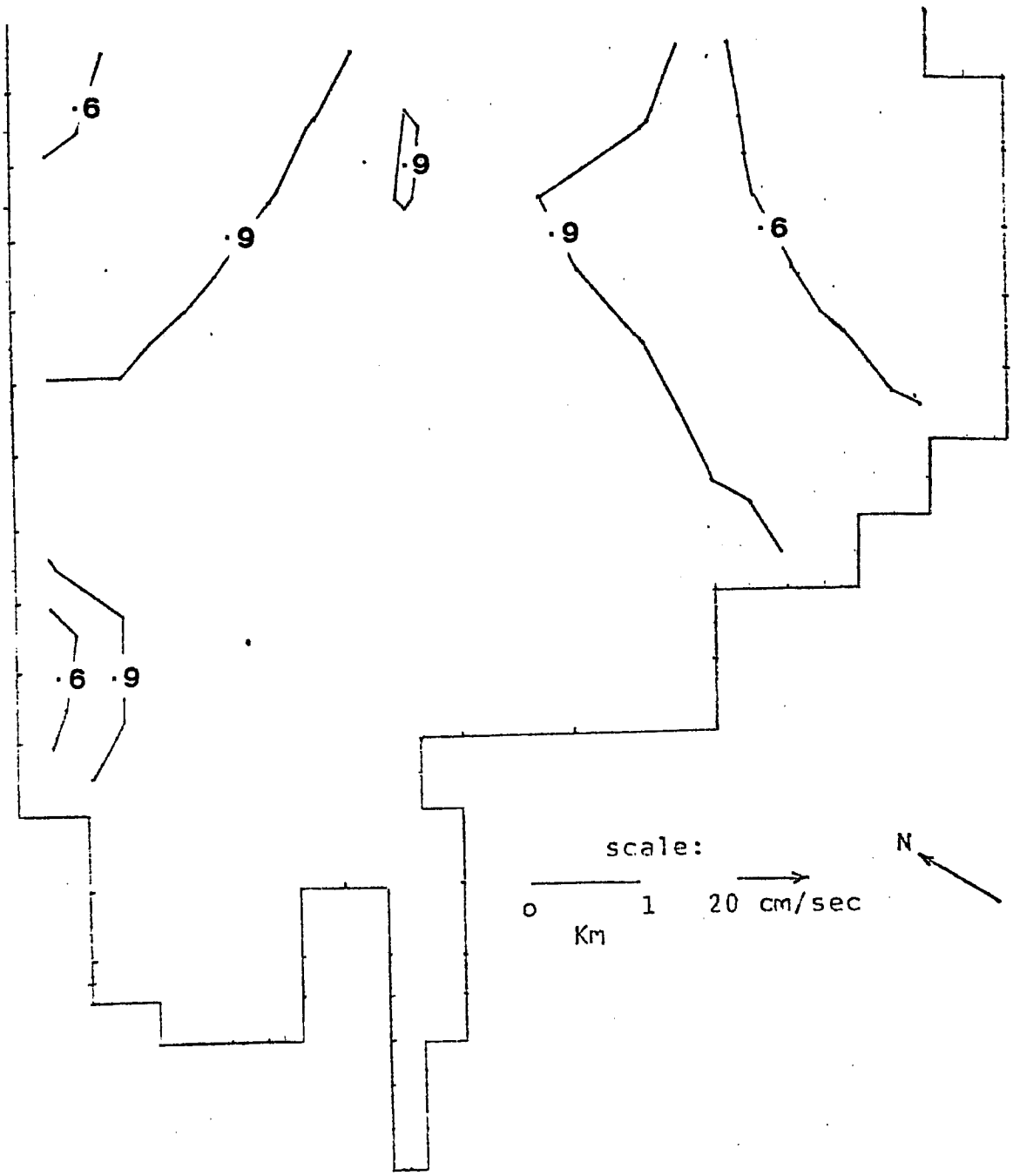

Figure 54. Concentration profile for NE wind of 5 m/s, reflecting bottom, and 50,000 cm^2/s viscosity.

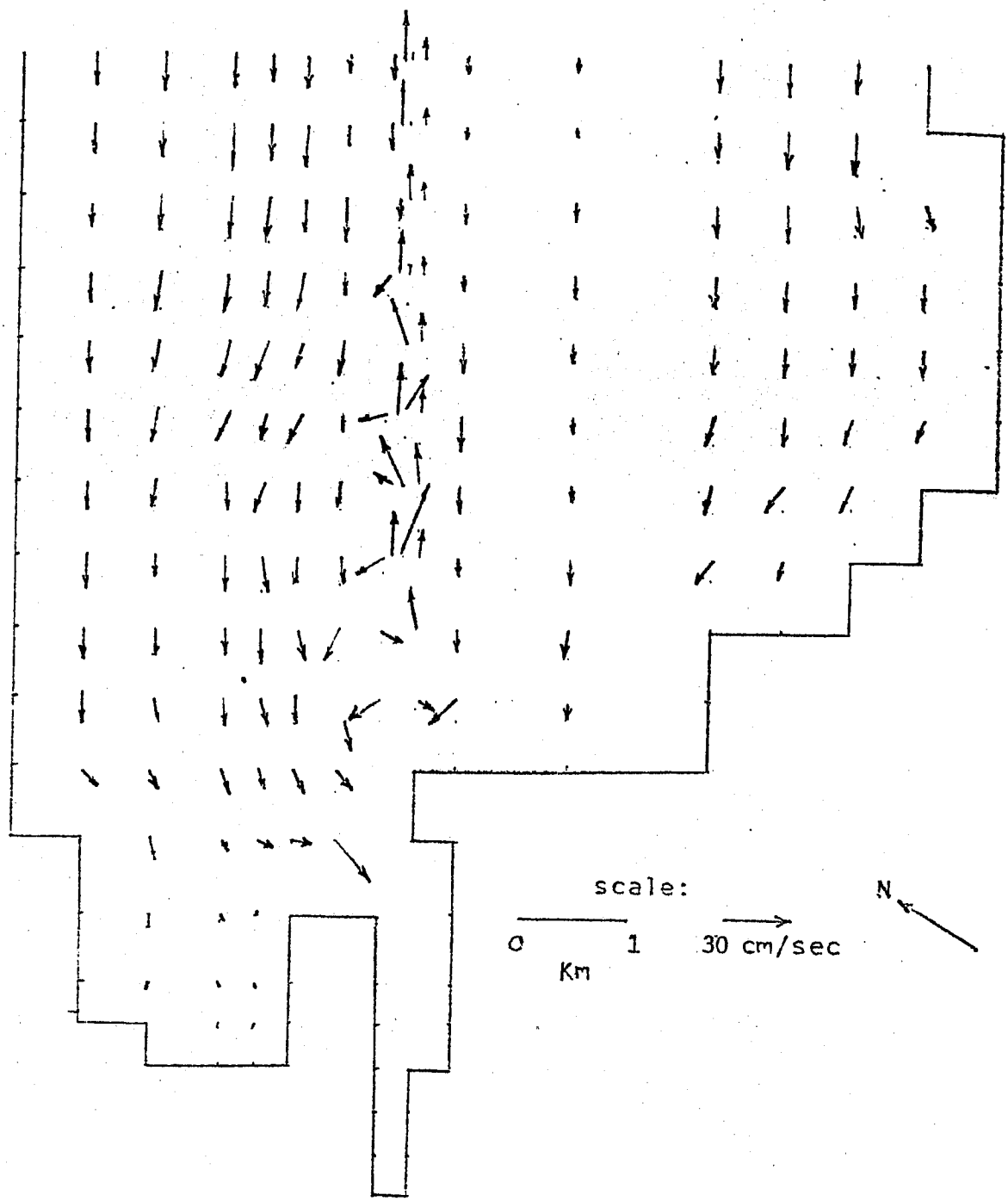

Figure 55. Surface velocities for NE wind of 8 m/s and 1000 cm^2/s viscosity.

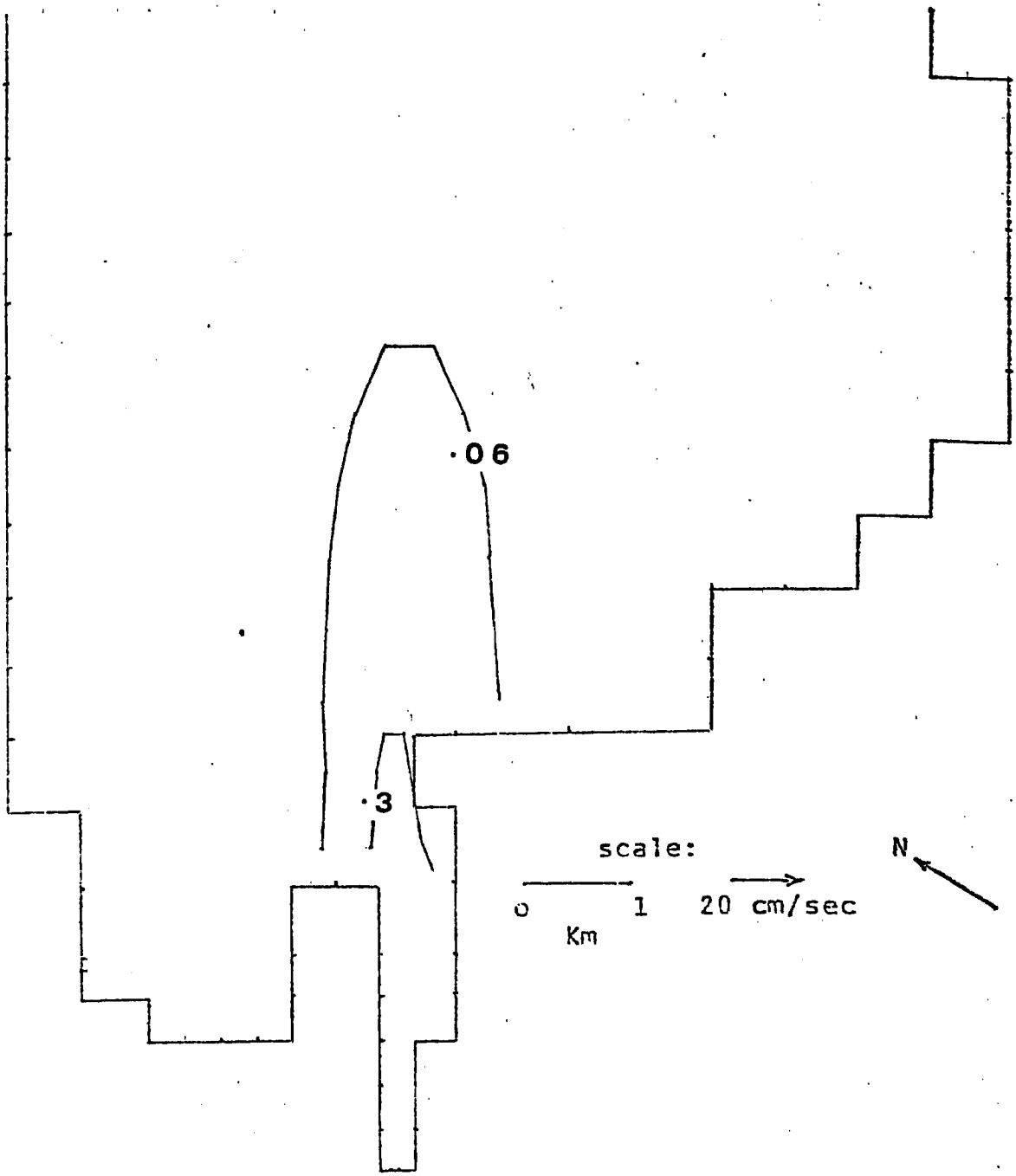

Figure 56. Concentration profile for NE wind of 8 m/s, absorbing bottom and 1000 cm^2/s viscosity.

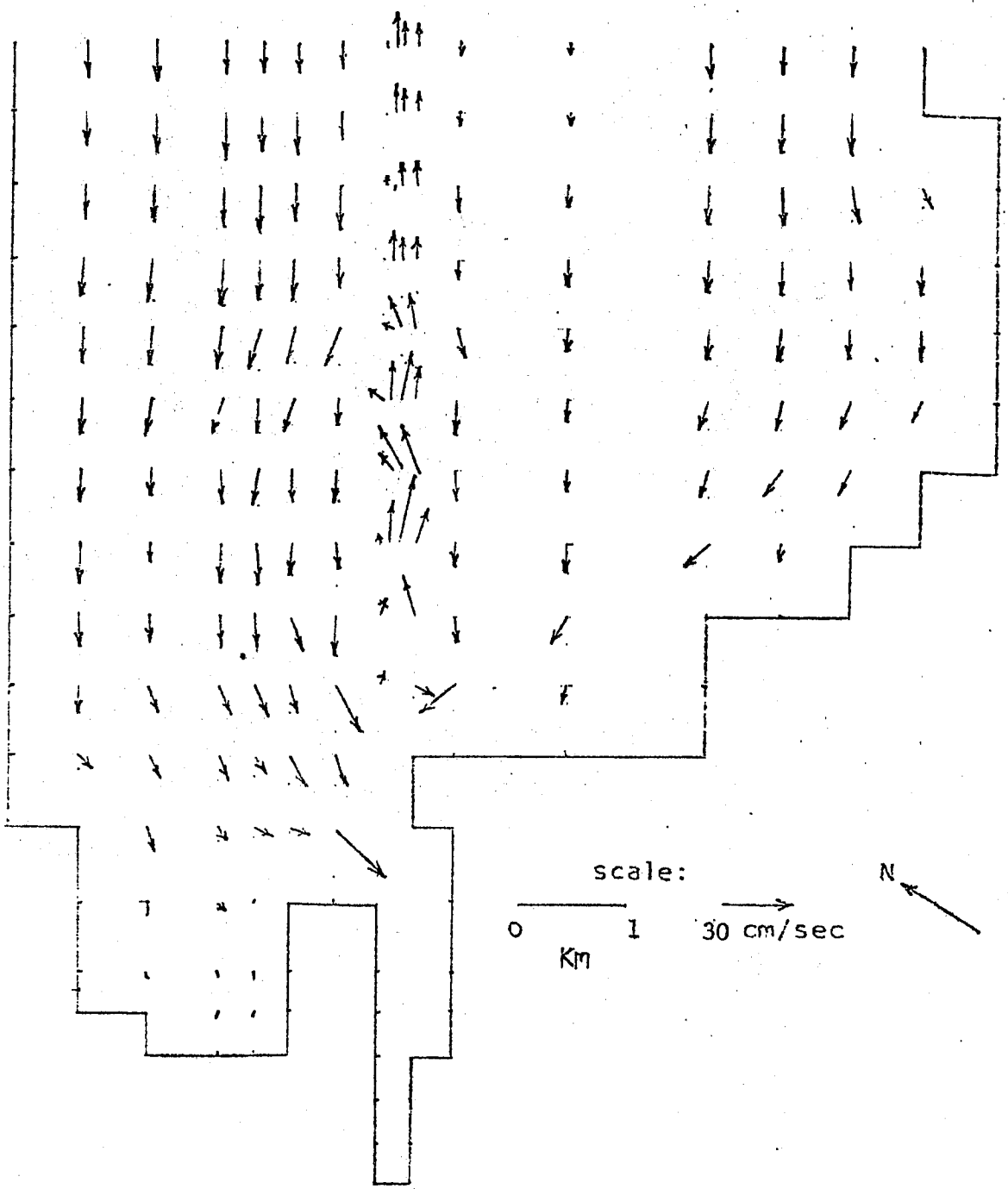

Figure 57. Surface velocities for NE wind of 8 m/s and 50,000 cm^2/s viscosity.

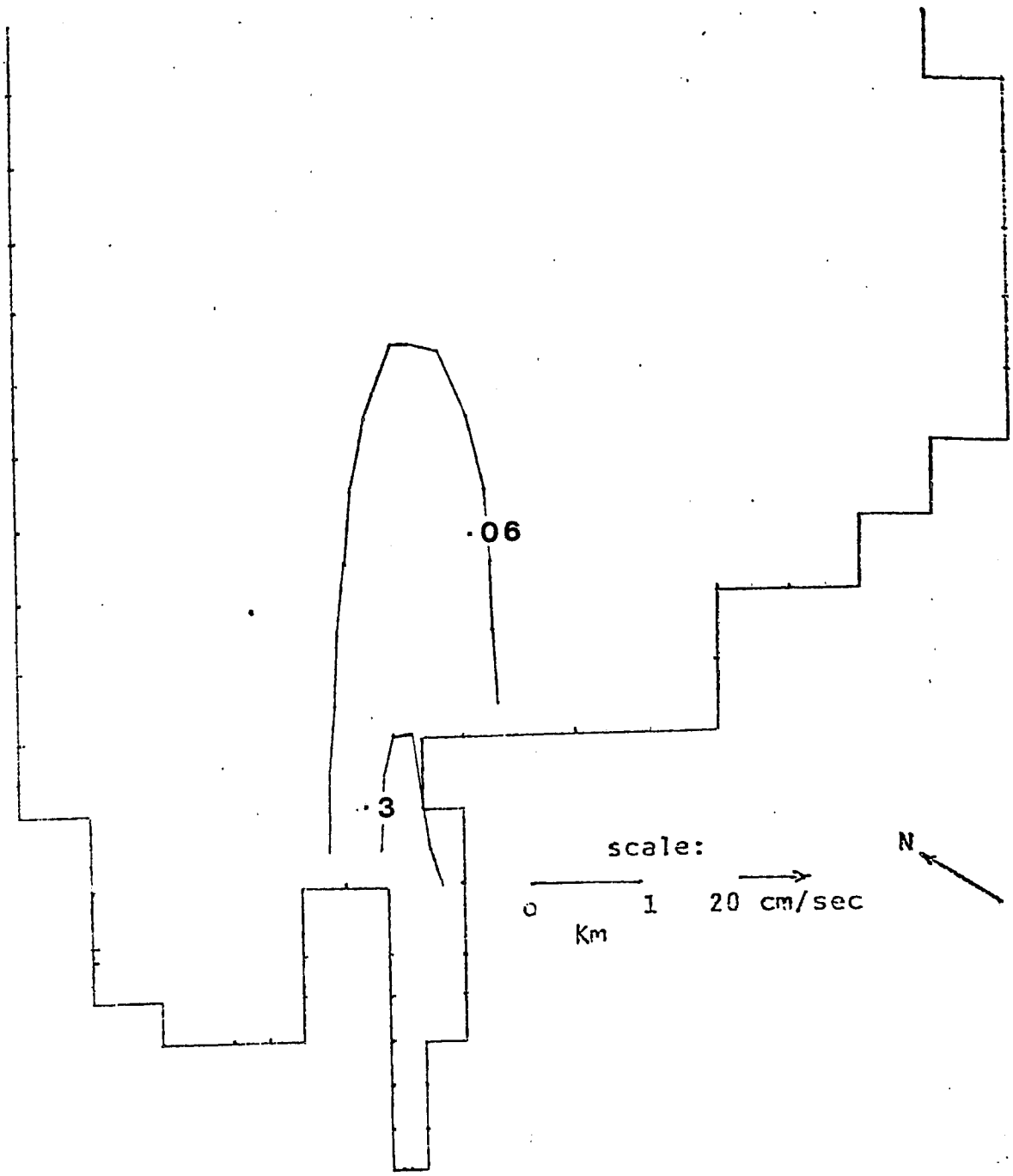

Figure 58. Concentration profile for NE wind of 8 m/s, absorbing bottom, and 50,000 cm^2/s viscosity.

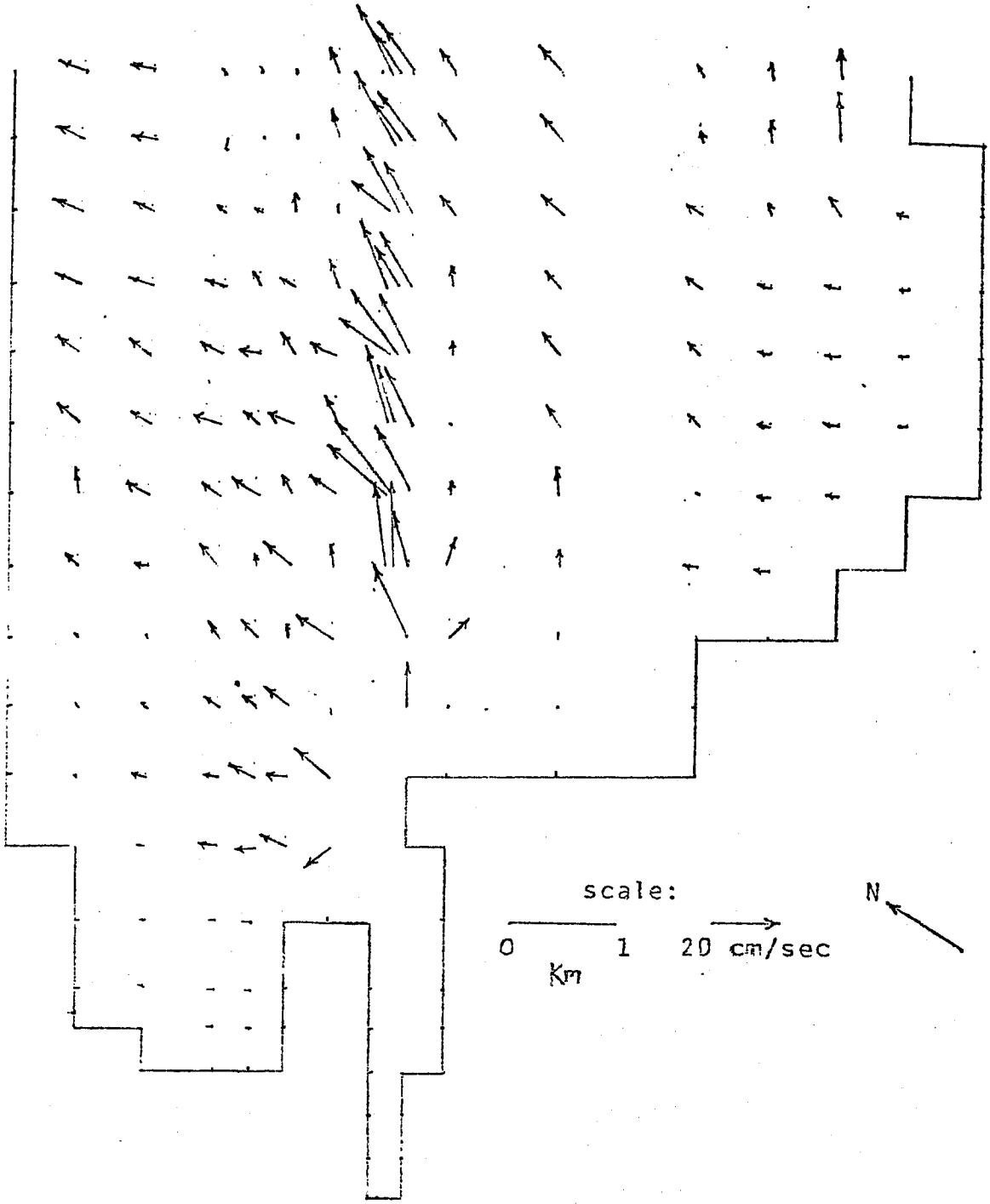

Figure 59. Surface velocities for SE wind of 5 m/s and 1000 cm^2/s viscosity.

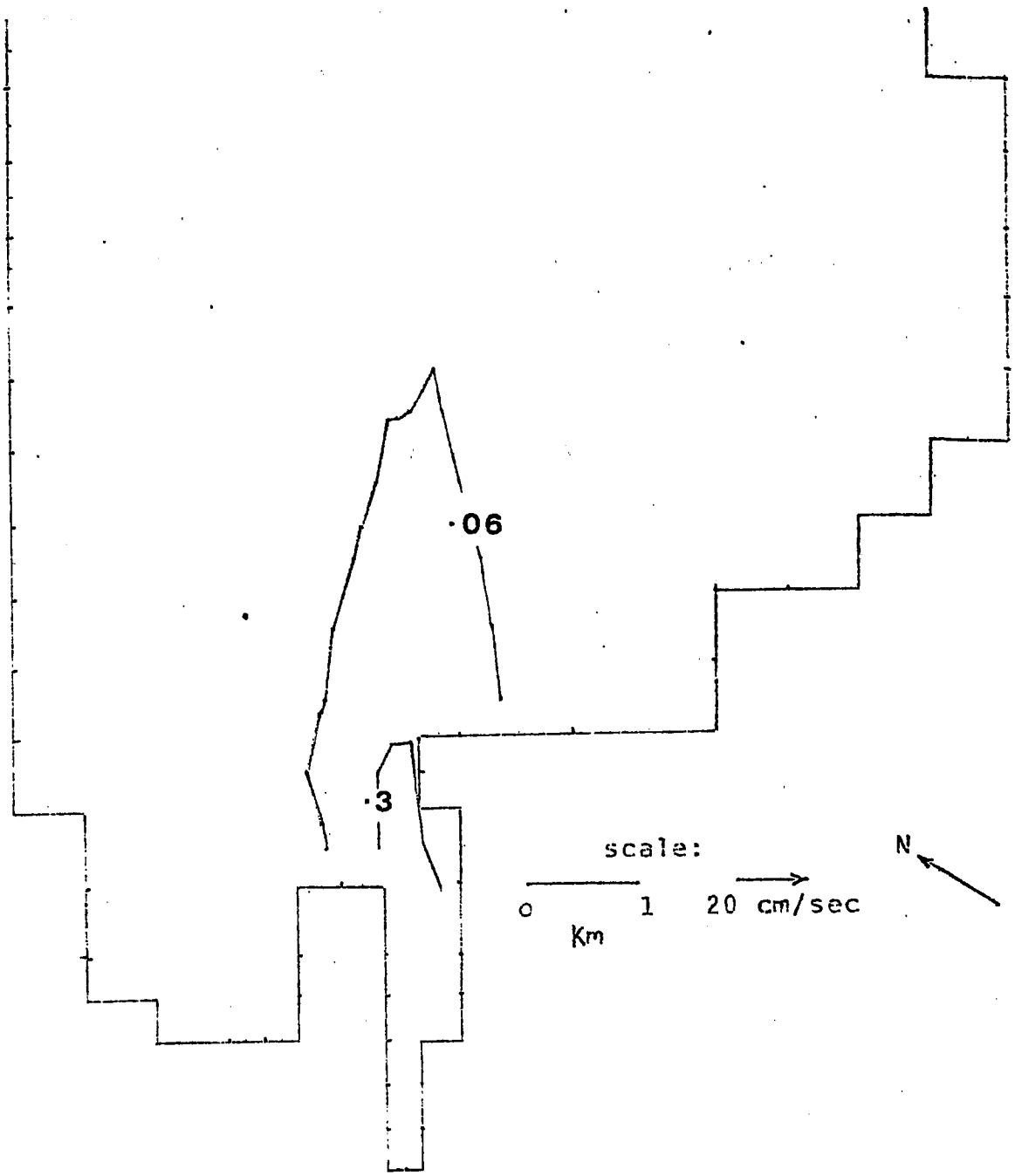

Figure 60. Concentration profile for SE wind of 5 m/s, absorbing bottom and 1000 cm^2/s viscosity.

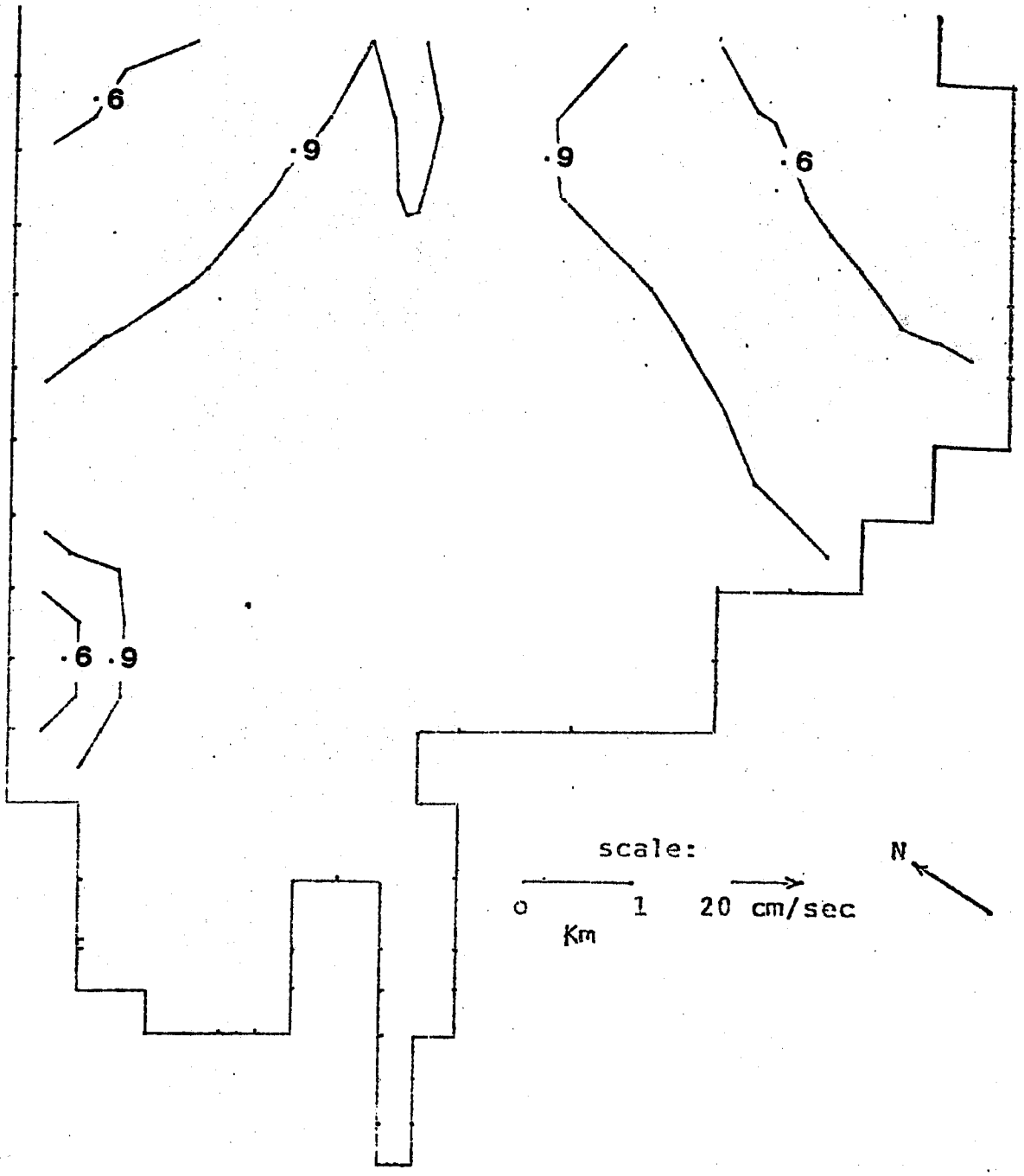

Figure 61. Concentration profile for SE wind of 5 m/s reflecting bottom and 1000 cm^2/s viscosity.

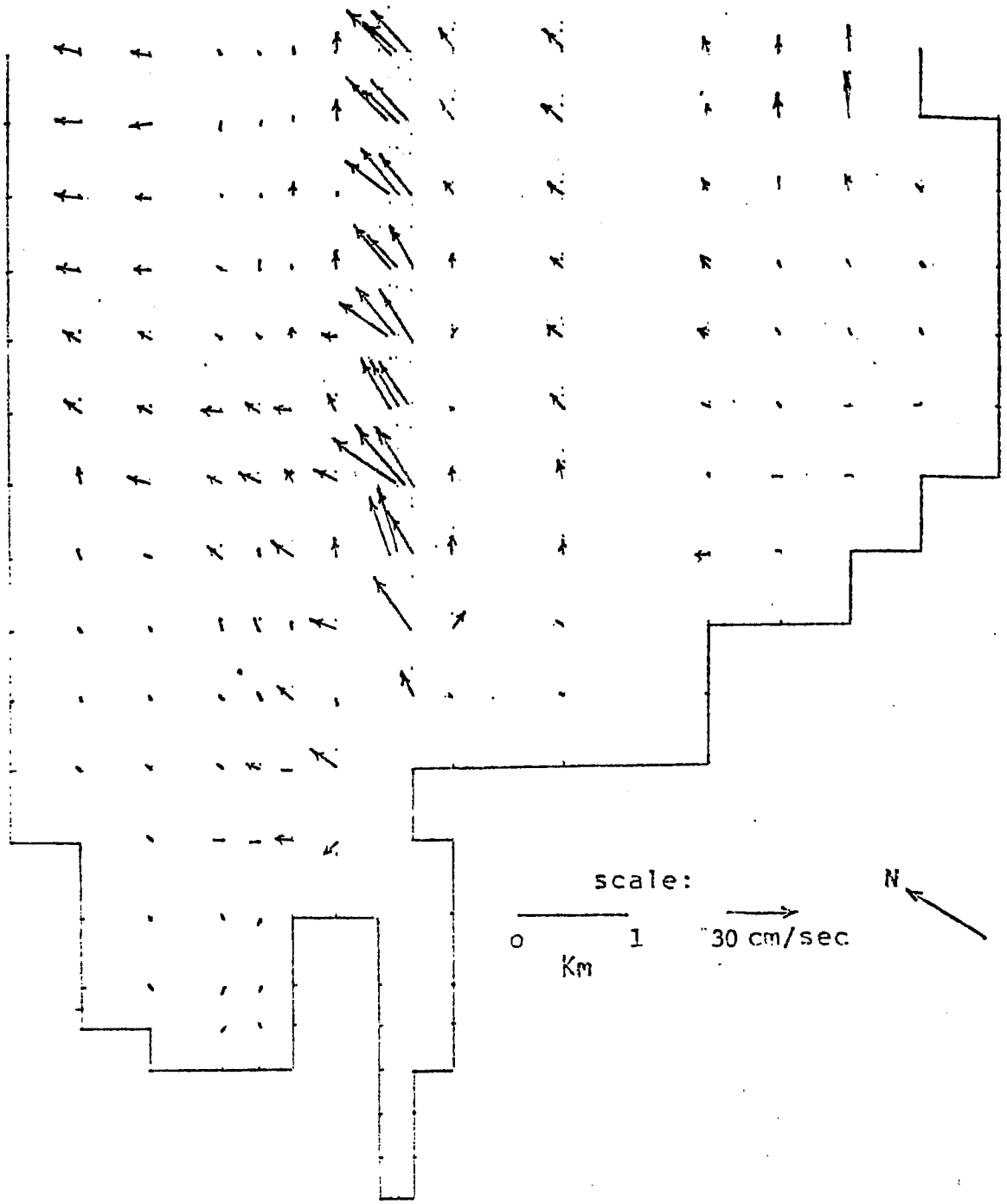

Figure 62. Surface velocities for SE wind of 5 m/s and 50,000 cm^2/s viscosity.

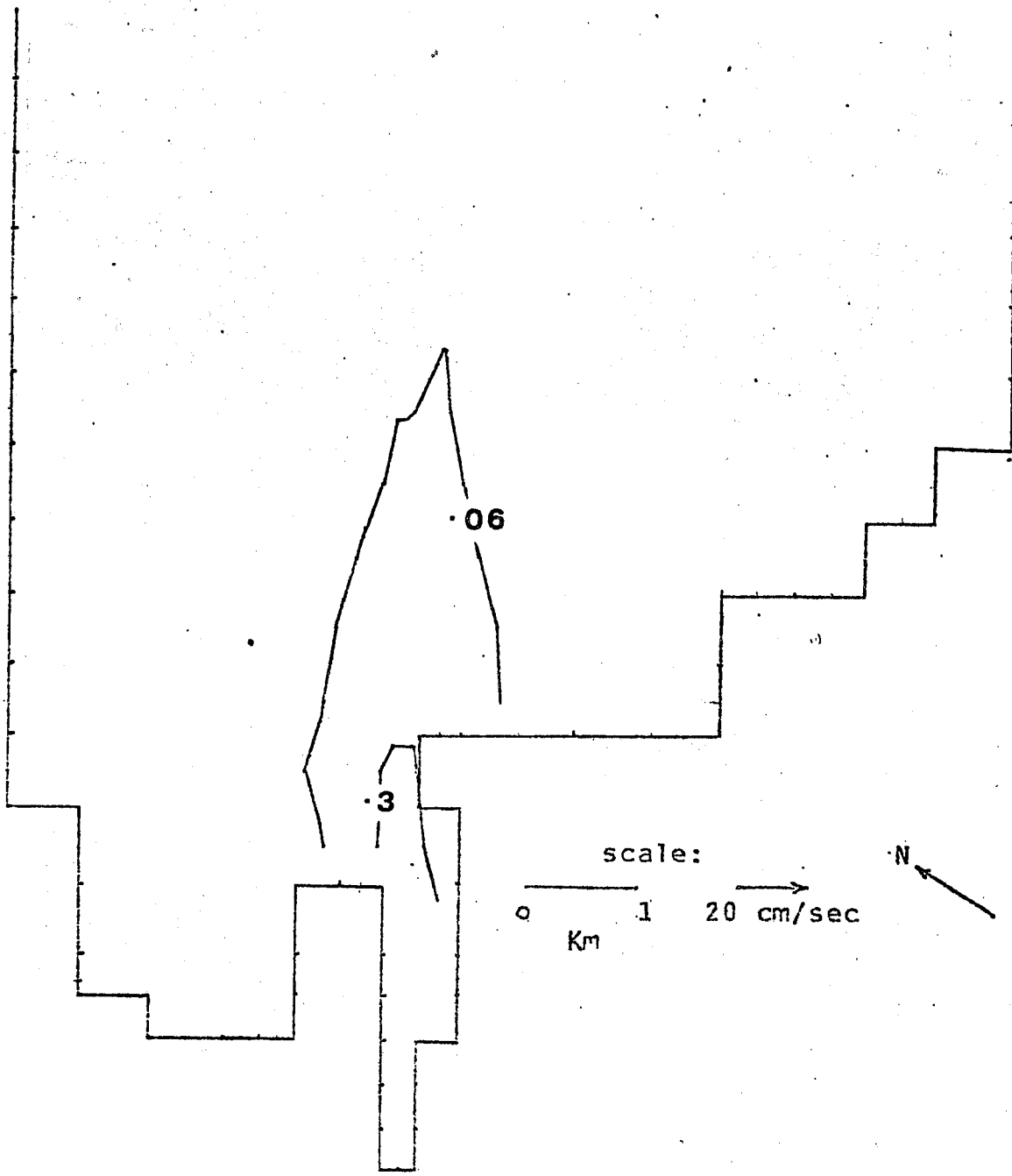

Figure 63. Concentration profile for SE wind of 5 m/s absorbing bottom and 50,000 cm^2/s viscosity.

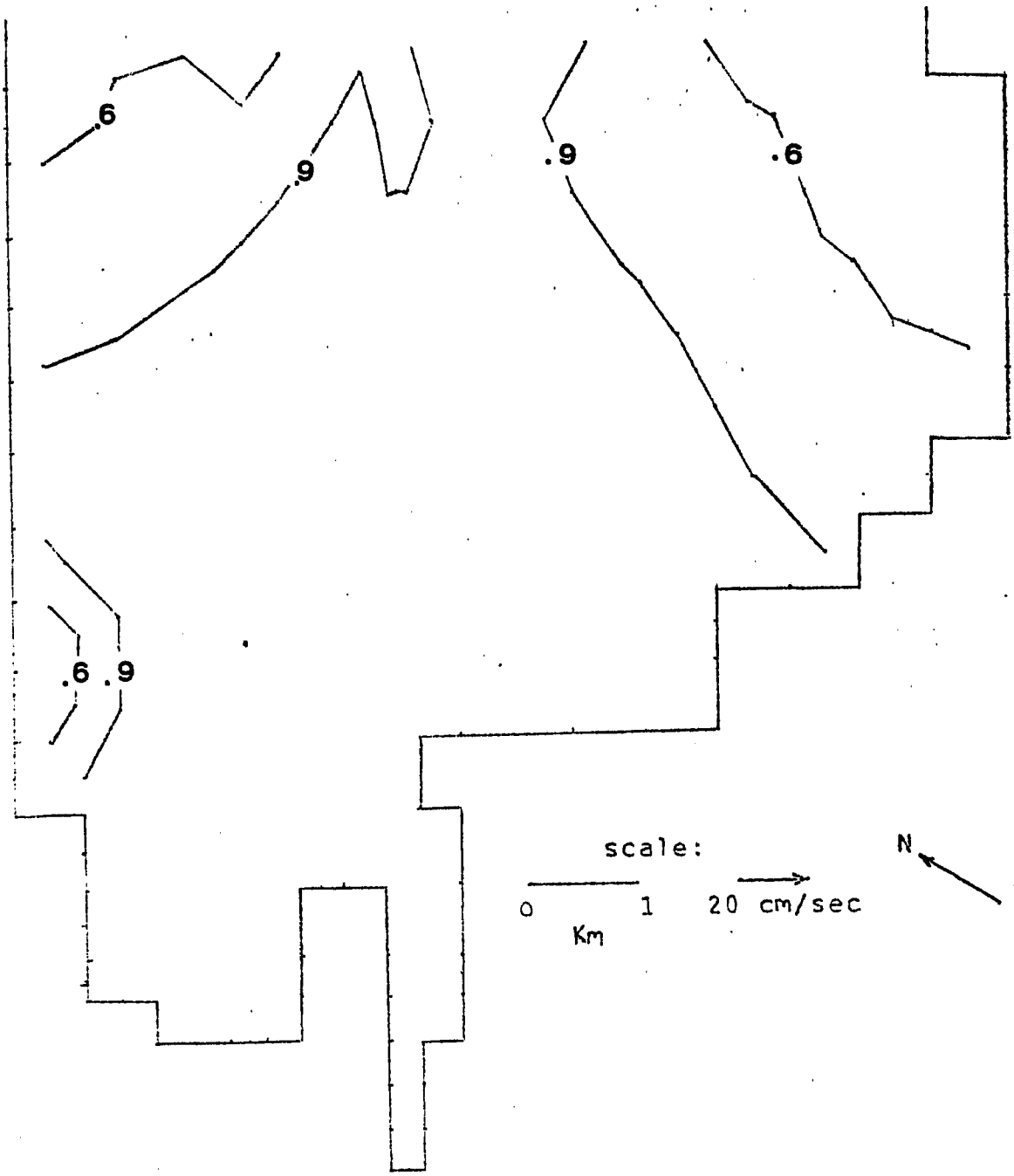

Figure 64. Concentration profile for SE wind of 5 m/s reflecting bottom and 50,000 cm^2/s viscosity.

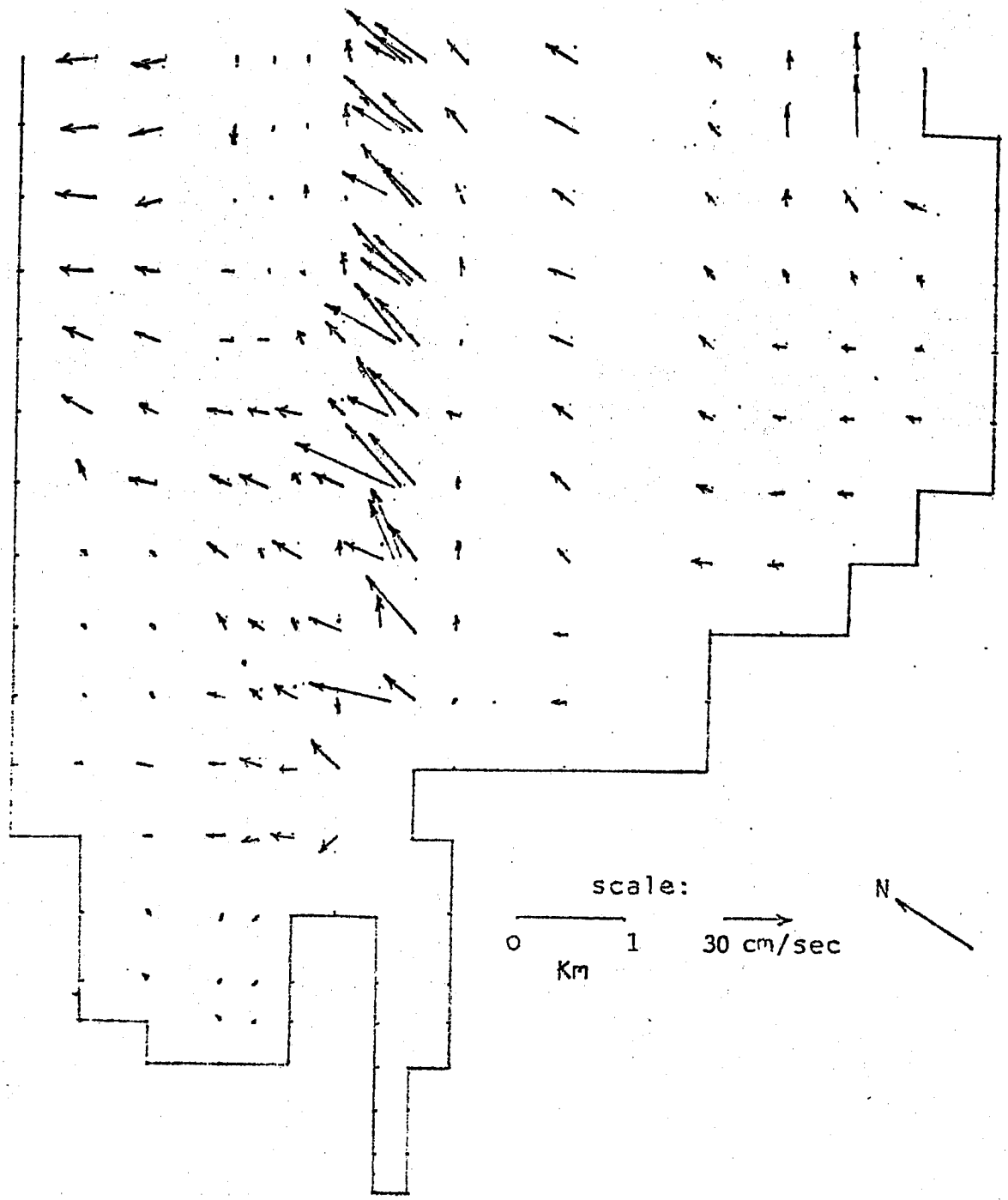

Figure 65. Surface velocities for SE wind of 8 m/s and 1000 cm^2/s viscosity.

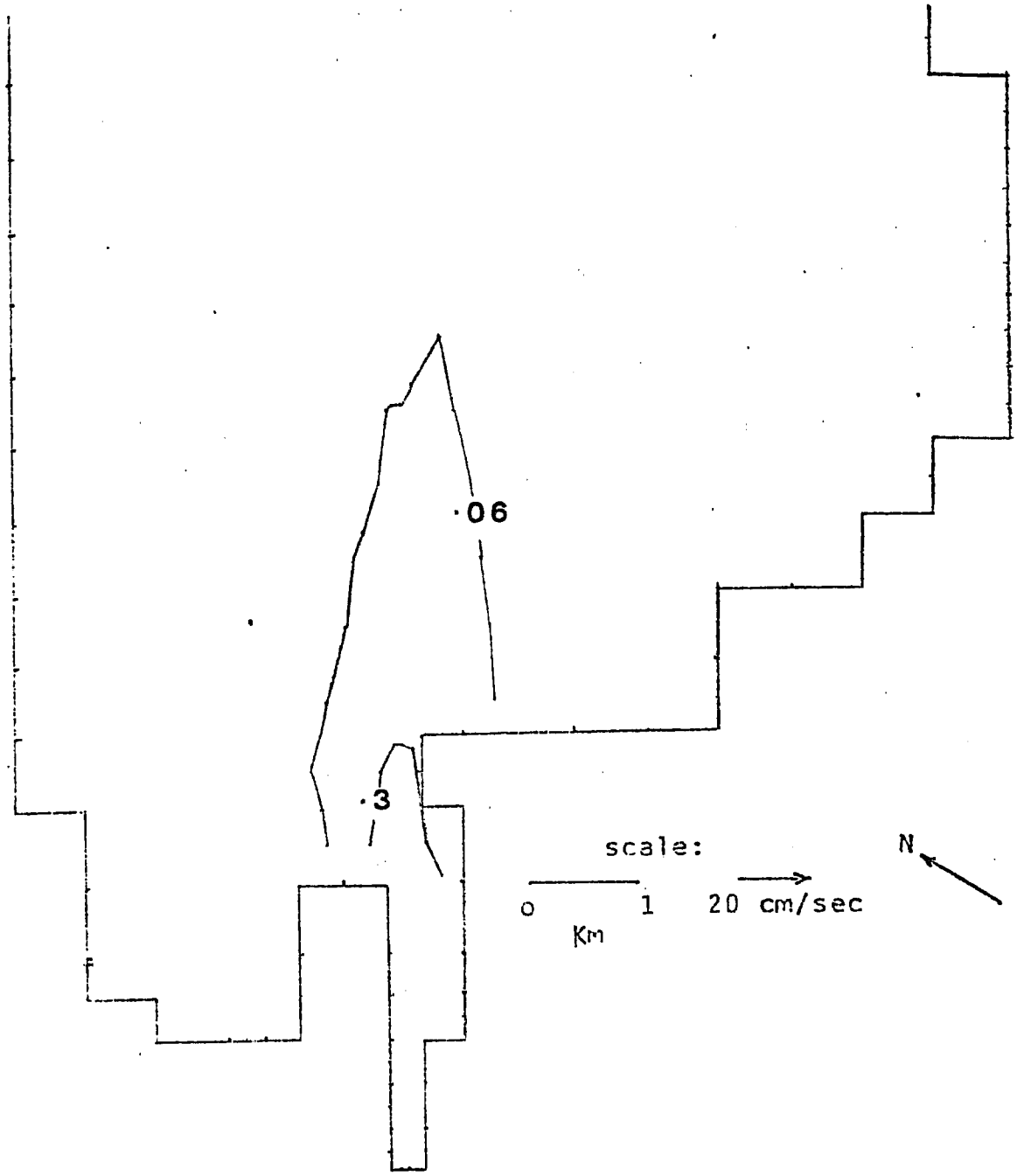

Figure 55. Concentration profile for SE wind of 8 m/s absorbing bottom and 1000 cm^2/s viscosity.

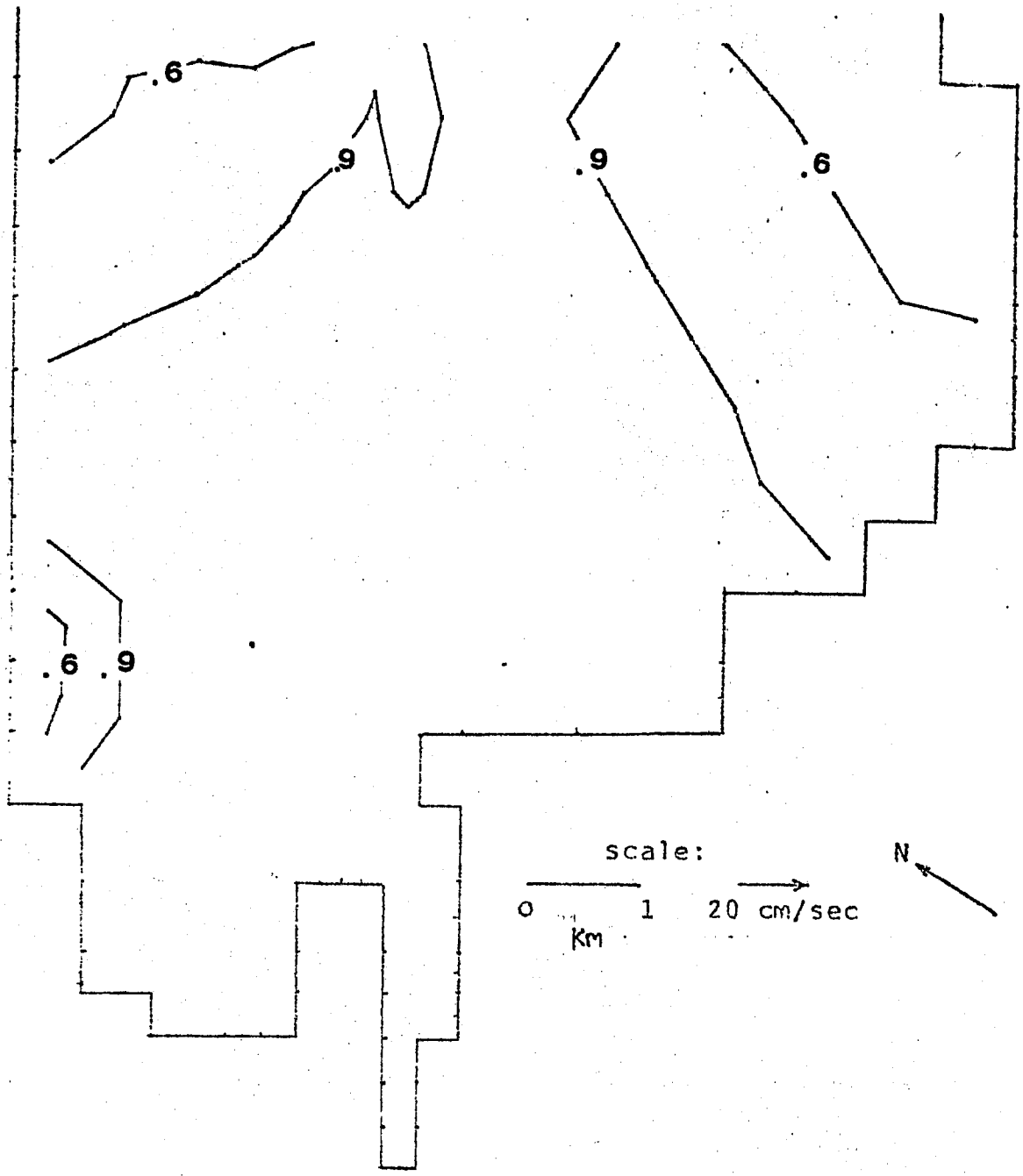

Figure 67. Concentration profile for SE wind of 8 m/s reflecting bottom and 1000 cm^2/s viscosity.

profiles a great deal. The sediment was carried further towards NNE when the SE wind strength was increased from 5 to 8 m/s. About 100% of the sediment is transported out of the Bay for the reflective bottom condition. There was a general downwelling on the left boundary or the windward side of the Bay and a general upwelling on the right boundary or leeward end of the Bay. The pattern was similar in the channel, there was downwelling on the left edge and upwelling on the right edge of the channel.

F. Computational Cost Analysis

The computation time and hence the cost is dependent upon the number of cells and the iterations required to solve the Poisson equation at each time step. Since the number of cells remain same the cost is directly proportional to the number of iterations. Initially the number of iterations required are large for convergence hence the cost is greater.

Table 6 shows the total number of iterations for the specified number of time steps and the cost for some typical runs. For the sediment concentration the velocities were not calculated but were assumed to be at steady state. Since the pressure equation was not solved at each time step the cost was reduced considerably for the sediment calculations.

Table 6. Cost Analysis

Run	Time Steps	Total Time (Sec)	No. of iterations	Time for iterations (Sec)	Cost $
60,000 cfs inlet, 10,000 cm^2/s viscosity, no wind	5	103.73	17500	89.93	19.32
60,000 cfs inlet, 50,000 cm^2/s viscosity, no wind	5	104.70	17500	92.34	20.01
SGS conc., no wind	100	28.83	--	--	7.59
Reflecting conc., 1000 cm^2/s viscosity	900	91.42	--	--	17.25
SW wind of 5 m/s	15	25.22	1376	--	7.59
SW wind conc.	400	43.60	--	--	10.35

CHAPTER SEVEN

CONCLUSIONS AND RECOMMENDATIONS

The wind driven circulation and dispersion of sediment in Maumee Bay was studied by modifying and adapting the three-dimensional numerical model developed by Paul and Lick (1973, 1976). The spatially varying grid system allowed a better resolution at the inlet and the channel. Because of this reduced cell size the time step was restricted. A vertical time splitting system, developed by Paul and Lick, was used to increase the time step. The deviations in bathymetry were incorporated by a stretched coordinate system. The stretched coordinate system was found to be effective both for the dredged channel and shallow areas.

Subgrid scale energy transfer was modeled adequately using an empirical model. The scaling parameter α for the SGS model was taken to be that developed by Spraggs and Street (1975). This method is an efficient way to isolate local phenomena as directly related to the grid size. The subgrid scale method introduced low effective diffusivities, hence the stabilizing effect of upwind differencing scheme was at times required. Though this method was found to be effective, more work needs to be done in order to predict turbulent transport with preserved statistical characteristics. A large number of iterations were needed for proper relaxation of the pressure equation

hence a direct solution for the Poisson equation is recommended in basins with this type of irregular topography.

River discharge, the navigational channel and wind were dominant transport influences during spring runoff. The relatively small scale of the Bay limits horizontal diffusion particularly lateral spreading, and therefore river discharge induced transport follows the channel. Evidence indicates that a wind induced secondary or rotary circulation exists in the channel in a plane perpendicular to the horizontal axis of the channel. This is definitely a source of some potential erosion as is the irregular velocity field surrounding the side dumped dredged spoils. Except for the channel there was no significant vertical velocity profile developed in the bay by the river discharge. But a definite vertical boundary layer structure persisted both in the channel and the surrounding bay. Also when only Maumee river inflow without wind or Ottawa river effects was considered, the flow tends to be greater on the Michigan side of the channel.

It was found that most of the particles which are less than 1/100 mm are transported out of the Bay. Changes in sediment loadings require approximately 1 to 1.5 days to be entirely propagated through the system. Two boundary conditions were utilized for all sediment transport calculations. Some combination of reflective and absorbing bottom boundary conditions is necessary for Maumee Bay. A combined effort of field observation, laboratory work, and numerical experiment is required to achieve this.

Coriolis force and Ottawa river influences, though present, are insignificant in altering the Bay sediment transport pattern.

Wind effects are a second dominant transport mechanism in the Bay. Moderate to heavy winds from the SW introduce a secondary circulation and the surface velocities together with the bottom shear are highly increased. Winds from the NE cause surface flow reversals near the channel, but even for strong winds river discharge dominates during spring runoff. Southeasterly winds introduce very active surface currents which again create well mixed channel plumes and shoreline regions of less sediment concentration. All plumes were guided by the channel and no significant cross flow deviation was observed.

REFERENCES

1. Bedford, K.W. and I.S. Rai, "An efficient rigid lid solution for circulation prediction".

2. Benson, D.J. "Maumee Bay erosion and sedimentation", U.S. Army Corps of Engineers, Draft Rept. Contract DACW 35-75-C-0038 (1975)

3. Bird, R.S., W.E. Stewart and E.N. Lightfoot, Transport Phenomena, J. Wiley and Sons (1964).

4. Bryan, K. "A numerical method for the study of the circulation of the world ocean", Journal of Comp. Physics, Vol. 4(1969)

5. Carnahan, B., H.A. Luther and J.O. Wilkes. Applied Numerical Methods, J. Wiley and Sons (1969).

6. Crowley, W.P. "A global numerical ocean model, Part I", Journal of Comp. Physics, Vol. 3(1968).

7. Deardorff, J.W. "A numerical study of three-dimensional turbulent channel flow at large Reynolds numbers", Journal of Fluid Mechanics, Vol. 41, Part 2(1969).

8. Gedney, R.T. and W. Lick. "Wind-driven currents in Lake Erie", J. Geophysical Research, Vol. 77(1972).

9. Graf, W.H. Hydraulics of Sediment Transport

10. Hag, A. and W. Lick. "On time dependent flow in a lake", J. Geophysical Research, Vol. 80(1975).

11. Herdendorf, C.E. "Sand and gravel resources of the Maumee River Estuary, Toledo to Perrysburg, Ohio", Ohio Dept. Nat. Resources, Div. Geological Survey Rept. Invest. 76(1970).

12. Herdendorf, C.E. and C.L. Cooper. "Environmental impact assessment of commercial sand and gravel dredging in Maumee River and Maumee Bay of Lake Erie", CLEAR Technical report No. 41 (1975).

13. Herdendorf, C.E. and J.E. Zapotosky. "Effect of tributary loading to Western Lake Erie during spring runoff events", CLEAR, Ohio State University (1977).

14. Hirt, C.W. and F.H. Harlow. "A general corrective procedure for the numerical solution of initial value problem", J. of Computational Physics, Vol. 2(1967).

15. Horowitz, J., J.R. Adams and L.A. Bazel. "Water polution investigation:Maumee River and Toledo area", U.S. Environmental Protection Agency, EPA-905/9-74-018(1975).

16. Kemp, A.L.W., R.L. Thomas, C.I. Dere, and J.M. Jaquet. "Cultural impact on the geochemistry of sediments in Lake Erie", J. Fisheries Res. Board Can., Vol. 33(1976).

17. Leendertse, J.J. "A water quality simulation model for well mixed estuaries and coastal seas, Vol. 1, Principles of computation", Rand Corp. (1975).

18. Lick, W. Numerical models of lake currents, U.S. EPA Ecological Res. Series Dept. EPA-600/3-76-020(1976).

19. Liggett, J.A. "A cell method for computing lake circulation", J. Hydraulics Division, ASCE, Vol. 96, No. HY3(1970).

20. Lilly, D.K. "A representation of small-scale turbulence in numerical simulation experiments", Proc. IBM Scientific Computing Syposium on Environmental Sciences (1967).

21. Monin, A.S. and A.M. Yaglom. Statistical Fluid Mechanics, MIT Press(1971).

22. Murray, S.P. "Settling velocities and vertical diffusion of particles in turbulent water", J. Geophysical Res., Vol. 75, No. 9(1970).

23. Neumann, G. and W.J. Pierson, Jr. Principles of Physical Oceanography, Prentice-Hall Inc.(1966).

24. Paul, J.F. and W. Lick. "Lake Erie international jetport model feasibility investigation", Lake Erie Regional Transportation Authority, Report 17-6(1975,1976).

25. Paul, J.F. and W. Lick. "A numerical model for a three-dimensional, variable density jet", Proc. 16th Conf. Great Lakes Res., IAGLR(1973).

26. Phillips, N.A. "A co-ordinate system having some special advantages for numerical forecasting", J. Meteorology, Vol 14(1957).

27. Pinsak, A.P. and T.L. Meyer. "Baseline reference for Maumee Bay, Maumee River basin level B study", Great Lakes Basin Comm. (1975,1976).

28. Pollution of Lake Erie, Lake Ontario and the International section of the St. Lawrence River., International Joint Commission(1970).

29. Pritchard, D.W. "Estuarine modeling:An assessment", U.S.EPA Water Pollution Control Res. Series, 16070DZV-02/71.

30. Reynolds, Osborne. "On the dynamical theory of incompressible viscous fluids and the determination of the criterium", Phil. Trans. Roy. Soc., Vol. 186(1884).

31. Roache, P.J. "Computation Fluid Dynamics", Hermosa Publishers(1976).

32. Schlichting, H. "Boundary Layer Theory", McGraw Hill Book Co.(1968).

33. Sheng, Y.P. and W. Lick. "The wind driven currents and contaminant dispersion in the near-shore of large lakes", Lake Erie Regional Transportation Authority, Report 17-5(1975).

34. Smagorinsky, J., S. Manabe and J.L. Holloway. "Numerical results from a nine-level general circulation model of the atmosphere", Monthly Weather Review, Vol. 93(1965).

35. Spraggs, L.D. and R.L. Street. "Three-dimensional simulation of thermally-influenced hydrodynamic flows, Stanford University, Tech. Dept. No. 190(1975).

36. U.S. Department of Commerce, Chart No. 370. West End of Lake Erie.

37. Vanoni, V.A., Sedimentation Engineering. ASCE(1975).

38. Waldrop, W.R. and R.C. Farmer. "Three-dimensional flow and sediment transport at river mouths", Tech. Rept. No. 150, Coastal Studies Institute, Louisiana State University(1973).

39. Water inventory of the Maumee River Basin, Dept. of Nat. Resources (Ohio).

40. Water resources data for Ohio. Water year 1976. USGS.

41. Wilson, B.W. "Note on surface wind stress over water on low and high speeds", J. Geophysical Res., Vol. 65(1960).

42. Yalin, M.S. Sediment Transport, Pergamon Press(1977).